

IMPERIAL COLLEGE LONDON

SCHOOL OF PUBLIC HEALTH

Calibration of a Dense Low-Cost Sensor Network for Urban Temperature Monitoring in London

Name: Parivrudh Sharma
(06025134)

Submitted in partial fulfillment of the requirements for the MSc degree in Health Data Analytics and Machine Learning of Imperial College London

25th August 2025

Word Count: 8,863

Contents

Contents	1
1 Abstract	3
2 Background and Literature Review	5
2.1 Urban Climate and Health	5
2.2 Importance of Dense Environmental Sensor Networks	6
2.3 The Calibration Challenge in Low-Cost Sensor Networks	6
2.4 London as a Case Study	8
2.5 Breathe London Sensor Nodes	8
2.6 Aims and Research Objectives	9
3 Methods	10
3.1 Data Sources	10
3.2 Data Pre-processing	10
3.3 Exploratory Analysis	11
3.4 First Stage Calibration	11
3.5 Coefficient Stability	12
3.6 Second Stage Calibration	13
3.7 Network-wide Calibration and External Validation	14
3.8 Spatial Interpolation	14
3.9 Software and Statistical Environment	16
4 Results	17
4.1 Exploratory Analysis	17
4.2 First Stage Calibration	21
4.3 Coefficient Stability	23
4.4 Second Stage Calibration	25
4.5 External Validation	28
4.6 Spatial Interpolation	31
5 Discussion	37
5.1 Summary of Findings	37
5.2 Calibration Performance	37
5.3 Spatial Interpolation	39

5.4 Limitations	41
5.5 Conclusion	41
6 Acknowledgments	42
7 Bibliography	43
8 Supplementary Materials	48

Abstract

Background

Urbanisation heightens heat-related risks through urban heat islands, making calibrated low-cost sensor networks essential for accurate monitoring. The Breathe London network provides an opportunity for high-resolution temperature monitoring, with over 600 low-cost sensor nodes distributed across the city.

Aims and Objectives

This study aims to establish a calibration framework for this sensor network to enhance the accuracy of its temperature measurements. The objectives are to improve sensor reliability through systematic calibration and drift correction, to benchmark performance against independent references, and to generate high-resolution spatial maps that reveal patterns of intra-urban temperature variability across London.

Methods

Co-location data for each node was used to construct linear regression models for first stage calibration. Two permanently co-located nodes supported the development of daily, weekly, and monthly calibration models, and were evaluated using blocking time-series split. The best-performing approach was then extended across the network. A Reference site was used for external validation on a susbet of sensors, and interpolated temperature maps were generated via a Bayesian approach.

Results

First stage calibration achieved an average R^2 value 0.93 across all nodes. In the second stage, weekly models produced the lowest RMSE at 0.95°C. External validation reduced errors by an average of 0.66°C root mean squared error. Spatial interpolation of the calibrated dataset revealed intra-urban variation in temperature.

Conclusions

This study delivers the first city-wide calibration of a low-cost temperature sensor network in London, demonstrating that a two stage calibration with Bayesian spatial interpolation can capture intra-urban temperature variability and provide evidence to inform targeted climate adaptation.

Background and Literature Review

2.1 Urban Climate and Health

Urbanisation is set to continue its rapid expansion through the 21st century.[1] It is estimated that 2.5 billion more individuals will be living in urban areas globally by 2050 alone. As urban areas expand, they will require substantial new infrastructure, and their larger populations will face increased vulnerability to stresses such as extreme heat.[2] The environmental consequences of this development include direct changes to the city's climate, which are most notably manifested in the urban heat island (UHI) phenomenon.[1] The UHI effect is defined as the rise in air and surface temperatures within a city compared to its surrounding areas. The effect specifically results from physical changes to the surface energy balance of the land where the city is built and is further driven by heat sources such as buildings and transportation.

It is important to distinguish the UHI effect, which is a localized heat accumulation phenomenon, from the broader temperature changes caused by global climate change.[1, 3] The latter is primarily driven by global greenhouse gas emissions and large-scale land-cover changes. Cities across the planet have witnessed a significant rise in the number of heatwaves since the 1980s.[4] This combination of increasing global temperature and the heat accumulation effect from UHIs can lead to an amplified effect on urban temperature, which has been noted to lead to negative health outcomes for urban citizens.[1, 5]

A 2017 review on the health implications of UHI, reported that exposure to heat is associated with exacerbation of pre-existing health conditions alongside an increased risk of hospitalisation and death.[6] Additionally, this review reported that high night-time temperatures are a key effect of UHI and were directly associated with increased mortality during the 2003 Paris heatwave. In terms of spatial differences, research has shown that urban areas also exhibit significant temperature variations within the city itself.[7] Temperatures are often highest in city centers, which are frequently home to more socially-disadvantaged individuals, while wealthier neighborhoods tend to experience cooler temperatures.[6] Considering the temperature variations within urban areas, their associated health effects, and the disproportionate impact on lower socio-economic individuals, research into the spatial and temporal temperature patterns of individual cities is essential. The data collected from such research can directly inform policy interventions in local cities, with the aim of protecting residents from high temperatures. A notable example of such an intervention is the development of cooling centers and cool routes in cities like Toronto.[8] Cooling

centers are designated public or private spaces, such as libraries, museums, or parks, which provide individuals with a cool shelter during heatwaves. Cool routes, on the other hand, are shaded walkways that offer pedestrians a cooler, more comfortable path in the city.

2.2 Importance of Dense Environmental Sensor Networks

Techniques for mapping a city's heat exposure typically involve climate modeling, satellite imagery, or interpolated observations to characterise urban temperature variations.[6] Air temperature can be accurately assessed by meteorological stations, such as UK Met Office (UKMO) weather stations, however the low density of such sites is their main limitation.[9] For example, the presence of only 25 weather stations in London, according to the UKMO, is insufficient for providing the detailed, street-level data required for effective urban planning across the city, and in turn also makes accurate interpolation difficult.[9, 10] Satellite-derived land surface temperature is another approach which can offer extensive spatial coverage and can reveal broad patterns of urban heat, however they have important disadvantages when used as a proxy for air temperature.[11] Cloud cover is a major limitation, as thermal infrared sensors cannot penetrate clouds, and therefore even partial coverage can render an image unusable. Consequently, detailed time-series data for temperature across a city is difficult to produce with satellite-based methods.

A recent advancement for mapping urban temperature variation with high spatial and temporal resolution involves using low-cost sensor networks (LCSNs).[12] An advantage of using LCSNs is their relatively low cost and lightweight build, which allows for the deployment of a high density of sensor nodes across a wide area. These nodes overcome many of the disadvantages of satellite-based approaches, allowing for the collection of a dataset that is rich in both temporal and spatial detail across an urban landscape due to continuous monitoring. However, due to their low cost, there is a compromise in the accuracy of their measurements.[12, 13] This, in turn, has required environmental researchers to develop specific calibration protocols for these sensors. Moreover, research has shown that even with initial calibration, these low-cost sensors are prone to a drift in their temperature measurements over time and may require regular re-calibration.[14] Nevertheless, these networks are widely used for urban environmental research, with the Birmingham Urban Climate Laboratory serving as a strong example.[15] This laboratory operates a LSCN that includes both weather stations and over 80 wireless Aginova Sentinel Micro air temperature sensors spread around Birmingham.

2.3 The Calibration Challenge in Low-Cost Sensor Networks

While LCSNs offer many potential benefits, improper calibration of individual sensor nodes can introduce significant errors into the data, which may lead to flawed analysis and the creation of ineffective urban policies.[16] Due to this, an effective data-driven calibration protocol is vital for using the data generated by LCSNs. A recent systematic review from 2021 described multiple different sensor calibration approaches for air pollution measure-

ments found in the literature.[16] The calibration strategies described in this review, although focused on air pollution, can also be applied to temperature sensors. The review reported that a common strategy for assessing the performance of low-cost sensors in real-world conditions is to co-locate them with a high-quality regulatory monitor. This method allows researchers to use the co-located data to improve sensor accuracy through various calibration techniques. These techniques range from physical mechanism-based and parametric models, such as linear regression, to more advanced non-parametric approaches, such as machine learning algorithms involving Random Forest and Gradient Boosting. Ultimately, the review concluded that machine learning approaches generally provide the most stable performance, however no approach is perfect for every situation. It is important to note that this review focused on initial calibration prior to deployment, and did not address re-calibration strategies for sensors already in the field.

Another research article in 2017 utilised a machine learning-based approach to calibrate low-cost air temperature sensors using long-term datasets and multiple environmental covariates.[13] Three sensors were deployed, two in an urban setting and one in a rural location, each co-located with a high-accuracy reference. Over 305 days of hourly measurements, a three-layer neural network was trained for each of the three sensors and compared against a linear regression approach, with both methods evaluated using 10-fold cross-validation. The neural network consistently outperformed regression, when a model was trained and tested on data from the same location. However, when a model trained on one site was applied to data from another site, performance was less reliable, and regression occasionally performed better, likely due to overfitting to site-specific environmental conditions. Once again, a key limitation was the absence of any consideration of temporal sensor drift, which is a known issue for low-cost devices and could affect long-term reliability.[17]

Building on the theme of maintaining sensor accuracy over time, a research paper from 2018 focused on a repeated in-field calibration strategy for wireless distributed air pollution sensors.[17] Their goal was to reduce the logistical burden and data loss caused by relocating all sensors to an Air Quality Monitoring station for direct calibration. The proposed node-to-node method directly calibrated only one sensor in a chain against the reference, with the remaining sensors calibrated sequentially against each other while deployed and co-located in pairs. In addition to evaluating the feasibility and accuracy of this approach, the authors investigated how long calibrations remained valid in the field. They found a calibration persistence time of approximately six weeks for their low-cost pollution sensors, based on continuous monitoring over five months. Specifically, the mean absolute error (MAE) became three times larger over the course of six weeks. These results demonstrate the need for frequent re-calibration in order to mitigate sensor drift and preserve long-term measurement reliability. Although dynamic calibration has been recognised as necessary due to sensor drift over time, a recent systematic review identified very limited evidence of dynamic or repeated recalibration protocols for low-cost temperature sensors.[18] This highlights a gap in the literature, underscoring the need to evaluate appropriate dynamic calibration time periods.

2.4 London as a Case Study

Given these calibration challenges, the application of LCSN in a city such as London requires careful consideration. London comprises of a complex thermal landscape due to its strong UHI effect, heterogeneous land, and large gradients in green space distribution between boroughs.[19, 20] Existing high-quality temperature monitoring infrastructure in the city, such as UKMO weather stations, is sparse, with only a few sites across London.[10] To counteract this, a recent study utilised a dense network of 490 Netatmo personal weather stations, supplemented by a small number of UKMO stations, to examine the effect of tree canopy coverage on near-surface air temperature and heat-related mortality in London over the period October 2015 to September 2022.[21] A strength of this study is the large volume of temperature sensors utilised which provide dense spatial coverage. However, a key trade-off is that the accuracy of these low-cost stations is lower than that of official meteorological instruments. No calibration or co-location of the Netatmo devices against reference-grade sensors were undertaken to offset this, suggesting that uncorrected instrumental biases and long-term sensor drift may have contributed to their measurement errors and influenced the reliability of their conclusions.[16, 17, 21]

2.5 Breathe London Sensor Nodes

Building on the need for high density and temporal resolution temperature monitoring in London, the present study makes use of data from the Breathe London network, which is a coordinated system of fixed environmental sensor nodes managed by the Environmental Research Group at Imperial College London.[22] This LCSN was established in 2020 with an initial deployment of 136 nodes, and since has expanded to over 600 locations across the city. Although its primary purpose is to measure air pollution, each node also records hourly air temperature and humidity data. These meteorological variables are currently solely used to correct air pollutant measurements. However, given the network's density and spatial distribution, the temperature data collected by this LCSN has significant potential for mapping fine-scale thermal patterns across London. The Breathe London operational nodes are Clarity Node-S air quality sensor instruments (Clarity Movement Co., Berkeley, USA), which integrate air pollutant and meteorological sensing capabilities within a compact, low-maintenance unit.[23]

As with other low-cost sensor networks, individual nodes within the Breathe London system are subject to measurement variability of an unknown magnitude relative to reference-grade instruments, making calibration essential to ensure data quality. In practice, calibration in this network is challenging because each node is deployed to a part of London where there is no reference temperature available. To address this, all nodes underwent an initial co-location period prior to deployment, during which they are temporarily stationed at Honor Oak Park. This site is equipped with a reference-grade temperature monitor as part of the London Air Quality Network.[24] This period enables the characterisation and correction of sensor-specific biases before field deployment. However, the network is dynamic as nodes are added and removed over time, and their duration in the field can

vary. Some nodes may be deployed for a significant period of time, increasing the likelihood of long-term sensor drift.[17] To mitigate this, two nodes are permanently stationed at Honor Oak Park alongside the reference monitor and are referenced to as the golden nodes. These golden nodes serve as a continuous benchmark for assessing sensor drift over time and provide a basis for potentially recalibrating the wider network. Another study has similarly recommended maintaining a small number of “gold standard” nodes permanently co-located with regulatory-grade instruments, which can then be used to generate generalisable calibration models for the wider network, although the optimal number of such nodes required to achieve sufficient robustness remains an open question.[25]

2.6 Aims and Research Objectives

This study aims to develop an interpretable calibration of the Breathe London LCSN to produce accurate, high-resolution air temperature data, and to generate an interpolation-based mapping of temperature across London to illustrate spatial and temporal thermal variation. The objectives of this study include:

1. To perform and evaluate per-node linear regression calibrations using pre-deployment co-location data.
2. To quantify and correct temporal sensor drift using two permanently co-located golden nodes.
3. To identify sensor nodes located in proximity to a reference site and assess their performance before and after calibration steps.
4. To apply the calibrated dataset to generate interpolated temperature maps of London, highlighting intra-urban temperature variability.

Methods

3.1 Data Sources

The primary data set comprises hourly air temperature records between 2021 and 2025, with associated date and time stamps, from Clarity Node-S units. This dataset includes two types of site codes for sensor nodes: CLCA, which are nodes stationed at Honor Oak Park during their co-location period prior to deployment, and CLDP, which are the subsequent deployed versions of CLCA nodes, to fixed locations across London. Two of the nodes, referred to as golden nodes (AFZHPFH3 and ARNKZ5XY), are permanently located at Honor Oak Park. Two additional datasets provide metadata for these nodes: the CLCA metadata specify the start and end dates of the co-location period for each device, while the CLDP metadata provides the deployed location's address, along with the longitude and latitude coordinates of each site. A separate lookup table links each CLDP site to its corresponding CLCA co-location record and device code, noting that a single site may host multiple devices over time. Reference temperature data at Honor Oak Park for calibration is provided by the London Air Quality Network, with the dataset containing recorded temperature values at 15-minute intervals. Additional UKMO reference site data from across London was obtained via the `worlmet` R package.[26]

3.2 Data Pre-processing

The primary dataset containing hourly temperature records was split into two datasets, one for CLCA nodes and one for CLDP nodes. Metadata tables were reviewed for structural consistency and alignment errors, with discrepancies in field placement corrected to ensure accurate mapping between variables.

For CLCA nodes, metadata start and end dates for co-location were used as the ground truth, replacing the start and end dates derived from the CLCA dataset itself. The discrepancy between the dates in these two datasets for each node likely stems from the fact that a node could have started recording temperature when it was first turned on in an indoor setting prior to placement at Honor Oak Park. In turn, these indoor temperature measurements cannot be used for calibration against the temperature available at Honor Oak Park. Faulty date ranges, including cases where the end date preceded the start date, were corrected by referencing the CLCA dataset. Where multiple co-location periods existed for a node, only the most recent period was retained. CLCA nodes with missing start or end

dates were removed, along with their corresponding CLDP nodes. CLCA nodes without corresponding CLDP nodes, and vice versa, were also removed. Co-location times were rounded to the nearest full hour by rounding start times up and end times down to match the hourly measurement resolution of the CLCA dataset. Using the corrected co-location metadata, a new dataset for CLCA nodes was generated containing only hourly measurements within each node's co-location period. The two golden nodes were excluded from this dataset, as their measurements were recorded solely in the CLDP dataset.

Reference temperature data from the London Air Quality Network at Honor Oak Park, recorded at 15-minute intervals, were aggregated to hourly values and matched to the newly-generated CLCA dataset by date-time. The resulting dataset contained the date, time, each node's temperature measurements, and matched reference temperatures, with all temperature values rounded to one decimal place. Finally, the two golden nodes were extracted from the CLDP dataset and compiled into a separate dataset containing their hourly temperature measurements and matched reference temperature values from Honor Oak Park.

3.3 Exploratory Analysis

All sensor node locations were plotted on a map of Greater London alongside UK Met Office reference sites obtained via the `worldmet` R package to visualise the spatial distribution of the network per year.[26] Each sensor's start and end co-location dates are displayed in table format. Missing co-location data was quantified by calculating, for each node, the total number of expected hourly measurements, and the corresponding percentage missing. An additional column recorded the number of matching ground truth temperature observations available for calibration. The distribution of the number of matching ground truth data points across nodes was visualised using a boxplot. The total number of co-location days for each node was also calculated and plotted as a boxplot.

The uncalibrated temperature ranges from each type of site code, CLCA, CLDP, the two golden nodes, and corresponding data from the reference site at Honor Oak Park, was plotted independently to assess the spread of uncalibrated temperature values across the network. For the CLDP site code, full uncalibrated time-series data were plotted to visualise temporal variation across the deployment period, and a separate time-series plot was produced for the two golden nodes alongside the reference temperature from Honor Oak Park. Moreover, missing data for the two golden nodes were quantified and displayed as a bar graph.

3.4 First Stage Calibration

Calibration was performed on each individual node using ordinary least squares (OLS) regression, with each device's temperature measurements regressed against ground truth observations from the Honor Oak Park reference site for its corresponding co-location period.

Separate linear regression models were fitted for each unique device code. For each node, residuals were assessed using residual-versus-fitted plots, at the aggregate level across all devices. Model performance was quantified using root mean squared error (RMSE), MAE, and coefficient of determination (R^2) for each node, and also as an aggregated summary for all nodes. Distributions of RMSE, MAE, and R^2 values were plotted separately for visual comparison.

The analysis did not formally test the full set of linear regression assumptions, as the primary aim of calibration was predictive accuracy rather than statistical inference. Residual-versus-fitted plots were inspected to assess heteroscedasticity, while other assumptions were not considered given the large sample sizes and the presence of temporal autocorrelation in the hourly data.[27] Cross-validation was not performed due to the highly variable co-location periods across nodes, as well as the presence of temporal autocorrelation in the hourly time-series data.[28] To assess potential improvements from modelling non-linear relationships, a quadratic term was added to the OLS models and performance was compared against the corresponding linear models through aggregated RMSE, MAE, and R^2 metrics. The final calibration approach for each node was selected based on comparative performance between the linear and quadratic specifications.

3.5 Coefficient Stability

To assess temporal stability in calibration parameters, weekly OLS regression models were fitted to the two golden nodes (AFZHPFH3 and ARNKZ5XY) over their entire deployment period. Each model used the golden node's hourly temperature measurements as the predictor and the Honor Oak Park reference temperature as the response. The slope and intercept from every model were saved, and their variation over time was visualised in time-series plots for each node.

As an exploratory analysis, the intercept for each regression was fixed to the median temperature from the reference site over the entire reference period. The median of the reference temperature distribution was selected as this provided a stable representation of the central tendency for the entire reference period while reducing sensitivity to outliers. This constraint was applied to remove baseline temperature shifts and to isolate changes in the slope coefficient, which reflects the proportional scaling of the sensor's readings relative to the reference. The temporal variation in slope under this fixed-intercept model was plotted to examine potential seasonal effects or long-term drift in sensor sensitivity. Variation in either coefficient over time would indicate that a one-off calibration is insufficient, and that a dynamic calibration strategy is likely required to maintain long-term measurement accuracy.

3.6 Second Stage Calibration

Following initial co-location calibration, a second calibration stage was implemented using the two golden nodes to quantify and correct for temporal drift in the deployed network. The first step involved estimating the median co-location duration derived from the exploratory analysis. For each golden node, an OLS regression was fitted using only the initial period equivalent to this median co-location duration, with the golden node's temperature measurements as the predictor and the Honor Oak Park reference temperatures as the response. Model performance for this initial calibration period was assessed through error metrics, such as RMSE, MAE, and R^2 , and visual inspection of the regression plots as per first stage calibration described earlier. The fitted calibration model was then applied to the remainder of the golden node's data to produce simulated first stage calibrated temperature time series. To assess how RMSE evolves over time following first stage calibration, both golden nodes' subsequent weekly RMSE were plotted for their entire duration. As the initial calibration of each golden node may have taken place in a specific season, the first stage calibration step for the golden nodes was repeated using data from an alternative season and compared to the results above. This allowed assessment of whether the timing of calibration influenced error metrics over subsequent years. Aggregate error metrics for uncalibrated temperature and first stage calibrated temperature for each golden node was also calculated.

Agreement between the two golden nodes was then evaluated to determine whether their calibration models could be pooled when applying second stage calibration to the wider network. Bland–Altman analysis, and the test's underlying assumptions, were used to assess systematic differences in temperature measurements between nodes.[29] Agreement between the two golden nodes was also assessed using a linear mixed-effects model (LMM). Hourly temperature differences between the two nodes were modelled with a fixed intercept and a random intercept for the grouping variable to account for temporal correlation within periods. The decision to pool data from both golden nodes was based on the absence of significant systematic differences in their behaviour.

A time-period evaluation was then conducted to identify the most effective temporal resolution for dynamic calibration updates. Calibration models were fitted at daily, weekly, and monthly aggregation levels to the golden nodes. These models were between the first stage calibrated temperature data from each golden node and the reference data at Honor Oak Park. To prevent temporal leakage, a time-series blocking approach was applied, using a 70-30 split between training and testing data within each aggregated period.[28] Due to this approach, yearly calibration was not evaluated to avoid strong seasonal bias in the test period. For each time period at every timescale, RMSE and MAE were calculated. Aggregate metrics were computed across all time periods within each timescale, and the best-performing timescale was selected for application to the wider sensor network. Finally, RMSE was calculated for uncalibrated node temperature, first stage calibrated temperature, and second stage calibrated temperature on a rolling weekly basis for each golden node across the full deployment period, and plotted separately to visualise changes and

improvement in accuracy over multiple years.

3.7 Network-wide Calibration and External Validation

Both the first and second stage calibration approaches were applied sequentially to all deployed nodes in the network to generate a two-staged calibrated temperature dataset. For independent evaluation, deployed nodes located in close proximity to UKMO reference sites were identified using metadata coordinates and reference station locations obtained via the `worldmert` R package.[26] Previous research has shown that the influence of land cover on near-surface air temperature is strongest at spatial extents of approximately 100 to 300 meters (m).[30] Accordingly, UKMO reference stations within 300m of a sensor node, and with comparable surrounding land cover, were chosen to provide external validation data. Missing data from either a deployed sensor node or from a reference station was quantified and removed. Performance of the uncalibrated, first stage calibrated, and second stage calibrated datasets were assessed against these reference measurements using RMSE and MAE. Aggregated performance metrics were computed for each node individually. Temporal variation in weekly RMSE for uncalibrated temperature, first stage calibration temperature, and second stage calibration temperature for all nodes involved in external validation were displayed graphically.

3.8 Spatial Interpolation

Initially, to visualise the spatio-temporal distribution of calibrated temperatures across London, yearly average temperatures for each CLDP sensor node was calculated. Sensor coordinates were recorded in latitude and longitude using the Global Positioning System and were therefore treated as WGS84.[31] To ensure spatial alignment, the Greater London Authority boundary shapefile, used as the underlying map of London, was reprojected to WGS84.[32] To enable direct comparison across years, a common colour scale was applied to all maps using the global minimum and maximum of yearly average temperatures. Separate maps were generated for each year between 2021 and 2025, however due to incomplete temporal coverage in 2021 and 2025, only the full years, 2022 to 2024, were retained for interpretation.

To capture the spatial structure of urban temperatures and account for areas of missing sensor coverage, a Bayesian spatial interpolation approach using the Stochastic Partial Differential Equation (SPDE) framework through Integrated Nested Laplace Approximation (INLA), as provided in the INLA R package, was implemented.[33, 34, 35] This approach has been shown to remain robust even when calibration datasets are relatively sparse, with accurate models reported using as few as 40 to 60 samples.[36] While the sensor network described in this study is considerably denser, it shares the challenge of uneven spatial coverage and large gaps between sites. The robustness of the INLA-SPDE approach to such irregular support makes it well suited to capturing London's heterogeneous urban temperature structure. A further strength of the Bayesian formulation is its ability to yield full

posterior distributions for both parameters and predictions, providing not only mean estimates but also quantification of uncertainty at each location. This is particularly valuable in areas of sparse coverage, where explicit uncertainty estimates are essential for interpreting interpolated fields.

Penalised Complexity (PC) priors were specified for the key hyperparameters, namely the spatial correlation range (ρ) and the marginal standard deviation (σ) of the spatial field. PC priors were chosen because they penalise unnecessary model complexity, shrinking the model towards a simpler baseline unless the data provide strong evidence for a more complex spatial structure.[37, 38] The observation model for each site s is given by:

$$y(s) = \mu + x(s) + \epsilon(s), \quad \epsilon(s) \sim \mathcal{N}(0, \sigma_\epsilon^2)$$

Here, $y(s)$ represents the observed yearly mean temperature, μ is the overall mean, $x(s)$ is the latent spatial field capturing spatial correlation across London, and $\epsilon(s)$ is an independent noise term.

The latent spatial field $x(s)$ was modelled as a Gaussian random field with Matérn covariance, parameterised by a correlation range ρ and a marginal standard deviation σ :

$$x(s) \sim \text{Matérn}(\rho, \sigma)$$

In this formulation, ρ controls the distance beyond which spatial correlation becomes negligible, and σ determines the overall amplitude of spatial variability.

PC priors were placed on these two hyperparameters:

$$\Pr(\rho < \rho_0) = \alpha, \quad \Pr(\sigma > \sigma_0) = \beta$$

These priors were chosen to regularise the model by shrinking towards smoother, low-variance surfaces unless the data provide evidence for shorter correlation ranges or larger variability.[39] The range prior (ρ) defines the expected distance over which temperatures remain correlated, with larger values implying smoother fields and smaller values allowing for more localised variability. The standard deviation prior (σ) specifies the expected magnitude of temperature contrasts across the city, with higher values permitting greater variability and lower values favouring more uniform fields. In this study, ρ_0 was set using empirical nearest-neighbour distances between sensors, while σ_0 was informed by the distribution of daily cross-city temperature variability. The ρ prior encodes the expectation that temperature fields should remain spatially smooth over at least the typical distance between sensors, which discourages the model from inferring unrealistically fine-scale variation. The σ prior represents the expectation that city-wide temperature contrasts are usually moderate, which discourages the model from attributing excessive variability to noise unless strongly supported by the data. This procedure ensured that priors reflected the expected scale of microclimatic variation while discouraging overfitting to noise. Both priors, and the resulting posteriors for ρ and σ , were examined to confirm appropriate behaviour of the model.

The SPDE mesh was constructed with a cutoff equal to the median nearest-neighbour spacing of the network from a year which had the most number of deployed nodes, preventing over-resolution in locally clustered areas. Maximum edge lengths were set to 1,500m within the domain and 4,000m outside the convex hull, providing sufficient resolution to capture sub-kilometre variability while maintaining computational efficiency and smooth boundary behaviour.

Model evaluation was carried out using the Deviance Information Criterion (DIC) and the Watanabe–Akaike Information Criterion (WAIC). These criteria are primarily designed for model comparison, where lower values indicate a better balance of fit and complexity.[40] In the absence of alternative models to benchmark against, these values were reported for completeness but were not interpreted in absolute terms. In addition, posterior prediction maps were generated for both the posterior mean and posterior standard deviation, which enable visualisation of the interpolated temperature surfaces alongside explicit representations of uncertainty. Mesh structures supporting the SPDE models were also plotted to illustrate the spatial subdivisions underlying the interpolation.

In addition to yearly averages, the same Bayesian SPDE-INLA framework was applied to seasonal subsets of the dataset, covering winter (December to February), spring (March to May), summer (June to August), and autumn (September to November), following the UKMO definitions.[41] Seasonal models were fitted across the full observation period to provide finer temporal resolution than yearly averages and to characterise intra-annual differences in the spatial temperature structure. Posterior mean temperature fields were standardised within each season by subtracting the London-wide seasonal mean and dividing by the corresponding seasonal standard deviation, thereby producing z-normalised anomaly maps that highlight relative spatial deviations independent of absolute seasonal differences. As with the yearly models, posterior mean and standard deviation maps were generated for each season, together with priors and posteriors for ρ and σ , and WAIC, and DIC for consistency across models.

3.9 Software and Statistical Environment

All analyses were conducted in R (version 4.4.2), which was used for statistical modelling, data processing, and visualisation. Core data manipulation and cleaning were performed using `dplyr`, `tidyr`, and `purrr`, while temporal variables were managed with `lubridate`. Spatial data handling, projection, and mapping were undertaken with `sf`, `terra`, `geosphere`, `ggspatial`, and `nngeo`. Visualisation was carried out primarily with `ggplot2`, complemented by `gridExtra`, `ggforce`, `viridis`, and `viridisLite` to improve graphical clarity. For statistical modelling and evaluation, `caret`, `Metrics`, `lmtest`, `lme4`, `INLA`, and `broom` were used to implement and summarise model fits. Domain-specific analyses were supported by `openair`, `worldmet`, and the `leaflet` packages which provide tools for handling atmospheric and meteorological datasets.[26]

Results

4.1 Exploratory Analysis

Following data cleaning, a total of 679 sensor nodes were retained for calibration and 616 unique CLDP site codes were identified. In some instances, a single deployed site code corresponded to multiple devices. Two golden nodes were also present in the dataset, AFZHPFH3 and ARNKZ5XY, but are not included in the above counts. The spatial distribution of deployed devices by year, alongside UKMO reference sites, is shown in Figure 1. Across the deployment period from 2021 to 2025, the number of active CLDP nodes varied by year, with 266 nodes in 2021, 353 in 2022, 517 in 2023, 467 in 2024, and 234 in 2025.

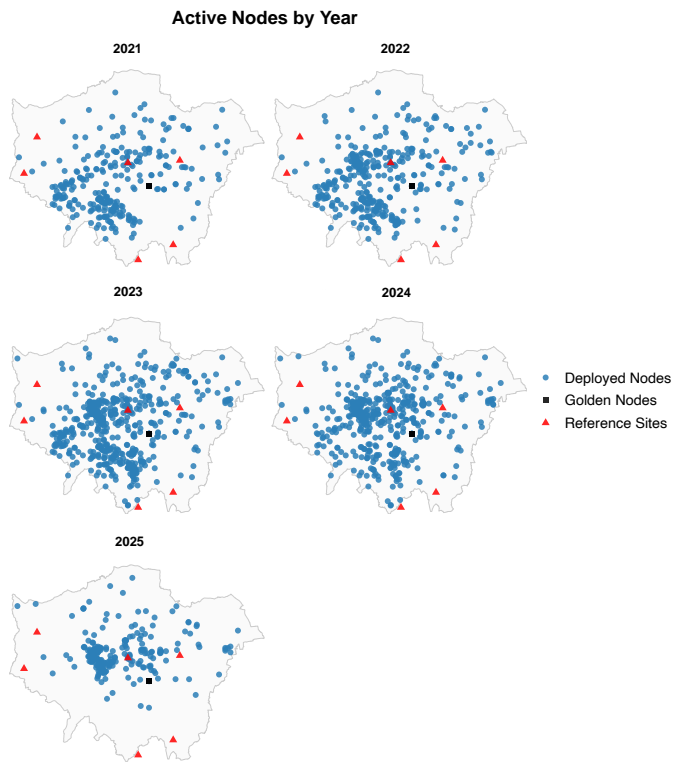


Figure 1: Active deployed sensor nodes by year in London between 2021 and 2025, alongside the two golden nodes in black, and reference temperature sites from the `worldmet` R package. The number of deployed nodes varied by year, with 266 nodes in 2021, 353 in 2022, 517 in 2023, 467 in 2024, and 234 in 2025.

Device level summaries containing co-location periods and corresponding missing data per node, are presented in Supplementary Materials 1. The distribution of the number of sensor-recorded temperature observations per node that had a corresponding reference temperature measurement during the co-location period is visualised in Supplementary Materials 2. A boxplot of the distribution of co-location days per node is shown in Figure 2, with the spread of all co-location temperature values from sensor nodes and from the reference site at Honor Oak Park presented in Supplementary Materials 3.

Across the deployment period from 2021 to 2025, a total of 12,267,466 hourly records were obtained from 679 unique nodes after pre-processing. The distribution of total observations per node is visualised in Figure 3. The spread of temperature values across all deployed nodes and the two golden nodes is presented in Supplementary Material 4. The spread of temperature values for each golden separately is presented in Supplementary Material 5. Temporal variation in uncalibrated node measurements is illustrated using a time-series plot in Figure 4.

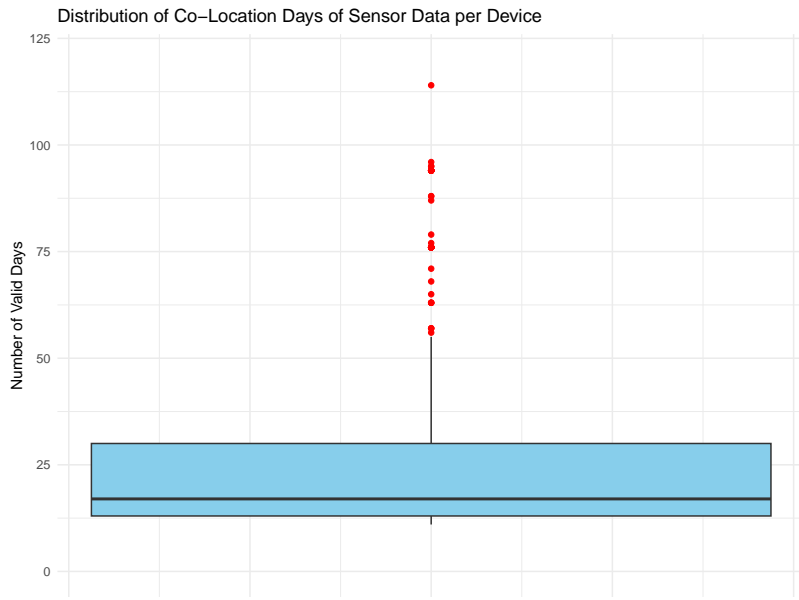


Figure 2: Distribution of valid co-location days per device, displayed as a boxplot with red markers indicating outliers. The median number of co-location days was 17.

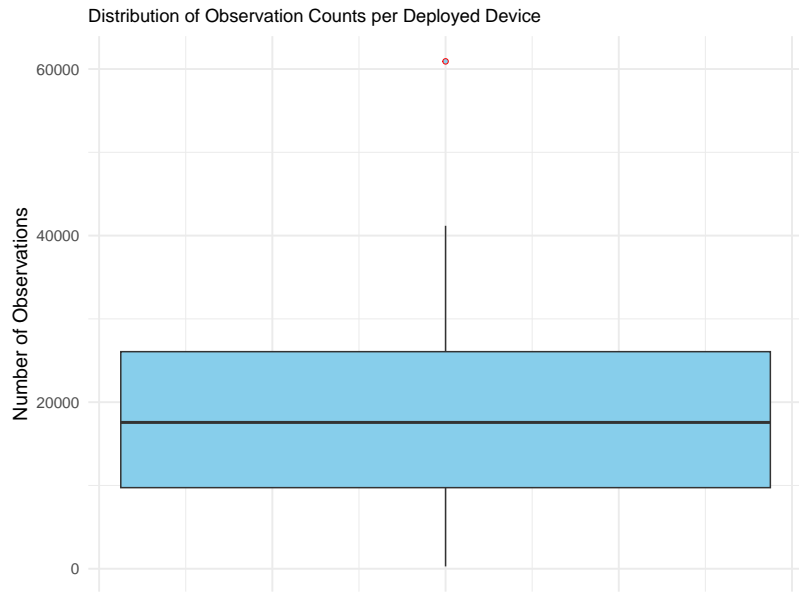


Figure 3: Boxplot showing the distribution of the number of recorded observations per device code across all deployed nodes in the study period.

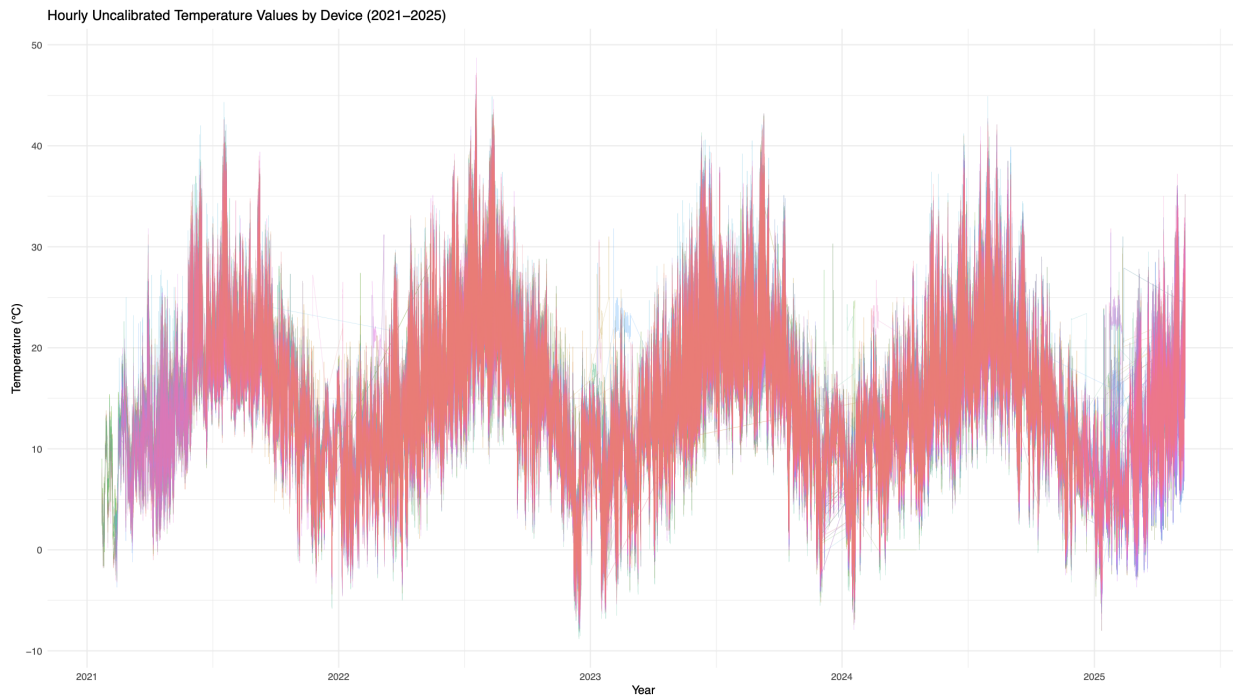


Figure 4: Time-series plot of hourly uncalibrated temperatures recorded by all deployed sensor nodes between 2021 and 2025. Each line represents a single device code, illustrating temporal variation and seasonal trends across the full deployment period. The legend is omitted due to the large number of devices.

Golden node AFZHPFH3 was active from 3 February 2021 at 02:00 until 12 May 2025 at 13:00, yielding 36,933 hourly observations. Golden node ARNKZ5XY was active from 17 April 2021 at 19:00 until 11 May 2025 at 22:00, yielding 35,527 hourly observations. Temporal variation in uncalibrated node measurements from the two golden nodes alongside reference temperature data from Honor Oak Park is illustrated using a time-series plot in Figure 5. Missing data across the lifetimes of the two Golden Nodes are shown in Supplementary Figure 6.

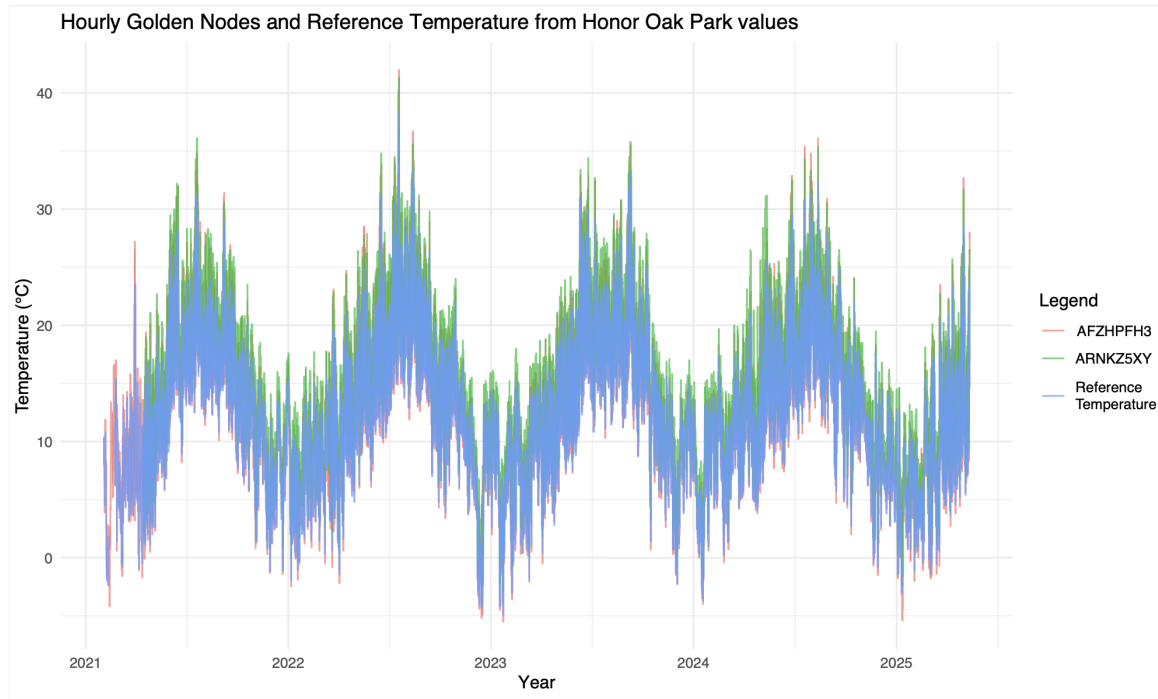


Figure 5: Time-series plot of uncalibrated temperature values from the two golden nodes and the corresponding reference temperature values, showing their trajectories over the study period.

4.2 First Stage Calibration

The average error metrics for all first stage calibration models included an MAE of 0.65, RMSE of 0.87, and an R^2 of 0.93. The distribution of these performance metrics across all devices is visualised in Figure 6 using boxplots. Two aggregated residual versus fitted plots for first stage calibration are shown in Figure 7 and 8.

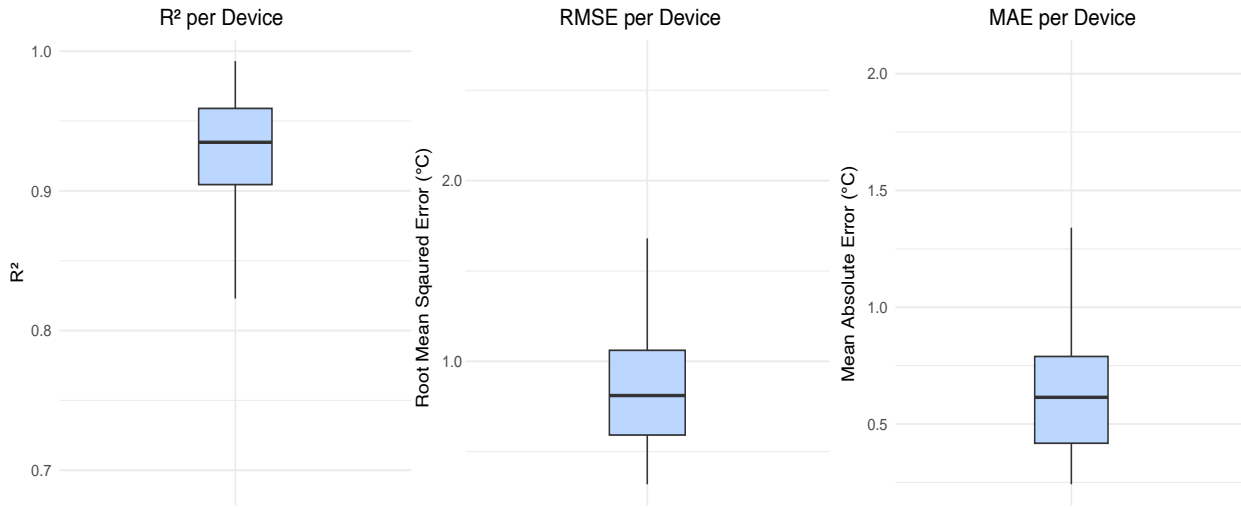


Figure 6: Boxplots showing the distribution of calibration performance metrics including R^2 , root mean squared error (RMSE), and mean absolute error (MAE) across all co-located devices.

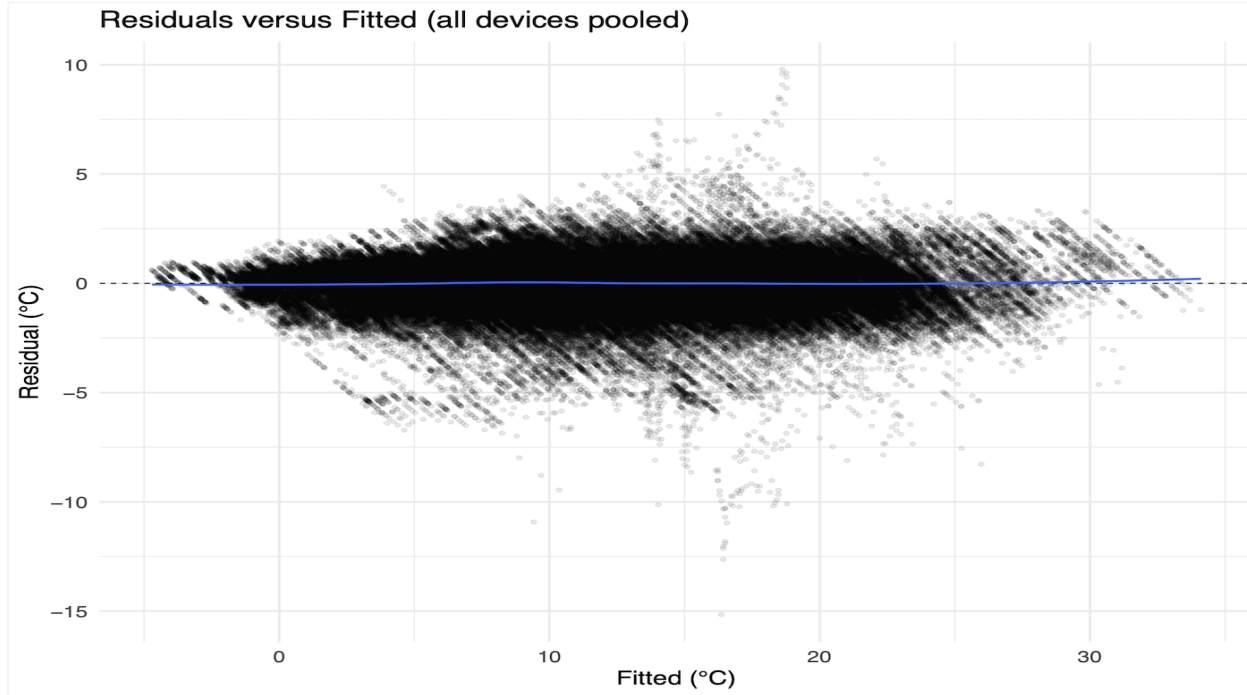


Figure 7: This is the aggregated residuals versus fitted values for all devices for the co-location period. Each point represents the residual error from an individual device-level first stage calibration model. The dashed line indicates zero residuals, while the smoothed blue curve highlights systematic deviations.

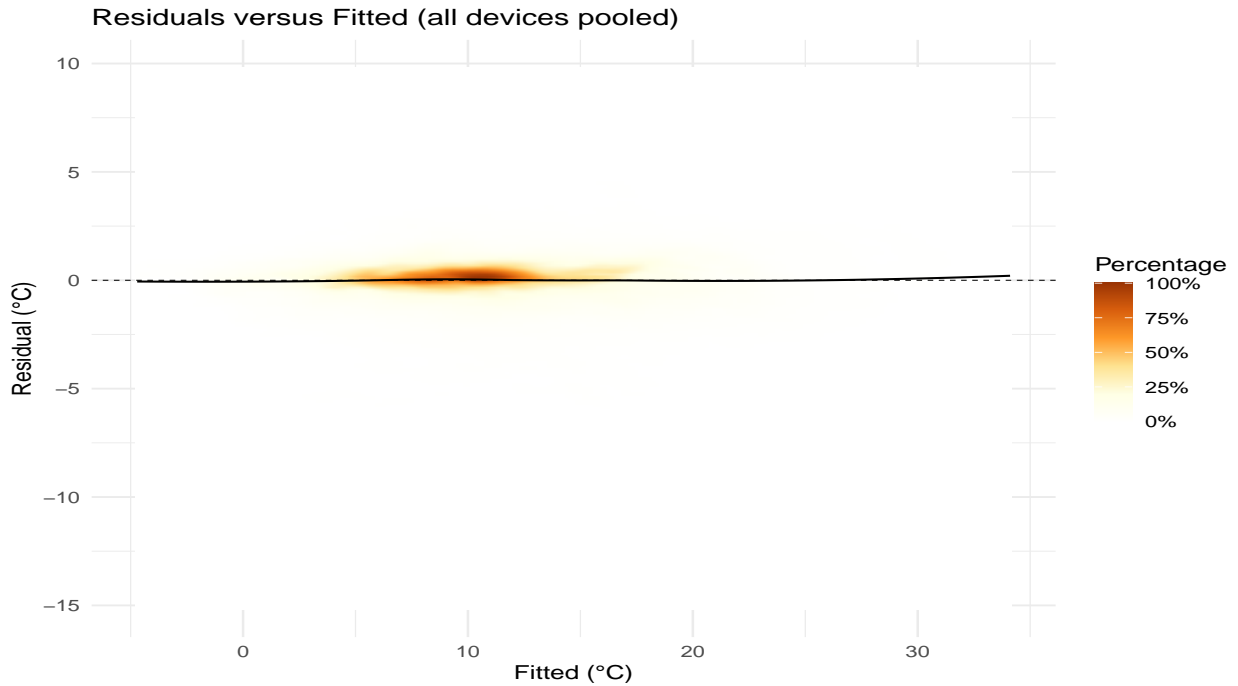


Figure 8: Heatmap of residuals versus fitted values for all devices pooled. The colour scale represents the relative density of observations, with darker regions indicating areas where residuals are most concentrated. The smoothed black curve highlights systematic deviations

For quadratic regression models, the overall average MAE was 0.64, RMSE was 0.86, and R^2 was 0.93. Following this, linear regression was chosen as the approach for first stage calibration.

4.3 Coefficient Stability

Time-series plots of the weekly regression intercept and slope coefficients for each golden node are presented in Figure 9. Results from the fixed-intercept exploratory analysis, showing variation in slope estimates only, are presented in Figure 10.

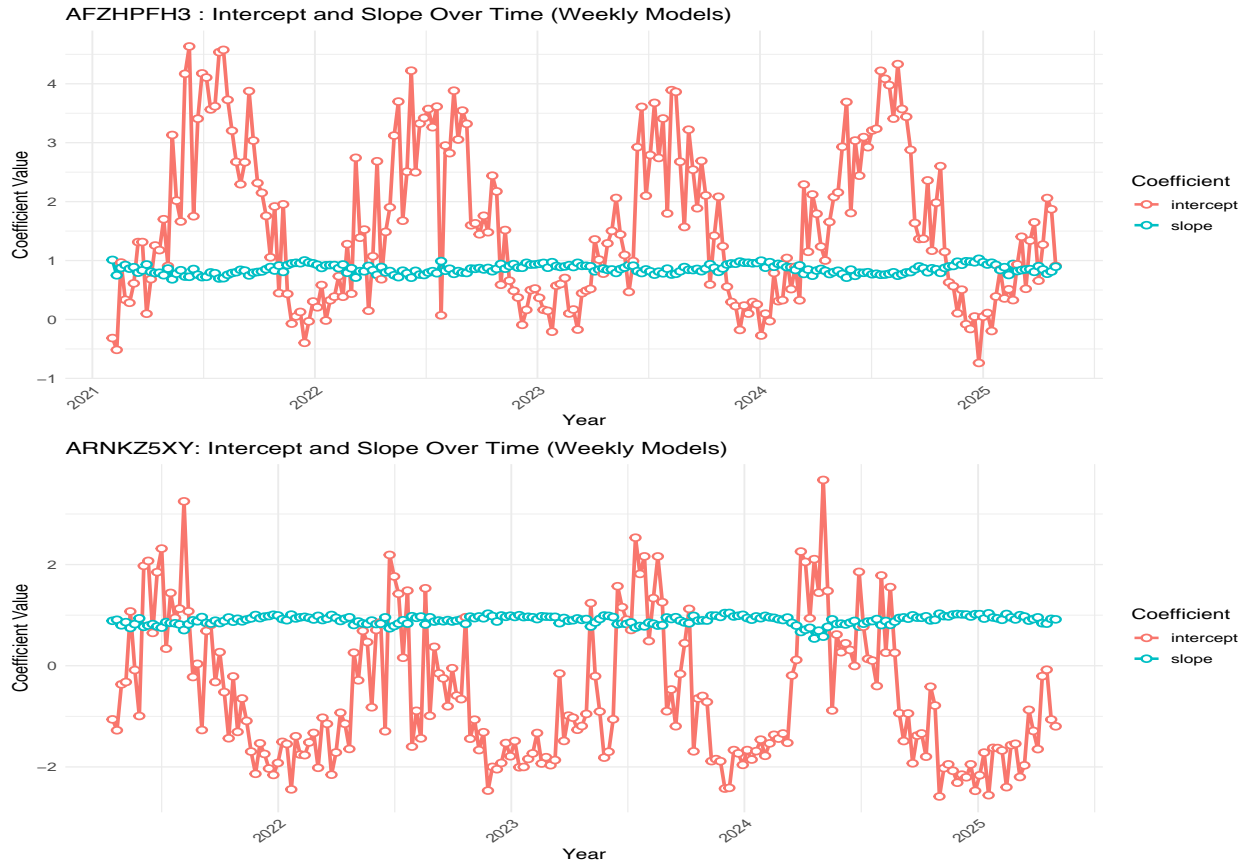


Figure 9: Weekly regression coefficients, intercept and slope, for the two golden nodes. Time-series plots display the estimated slope and intercept values for top, AFZHPFH3, and bottom, ARNKZ5XY, golden nodes with points representing individual weekly models.

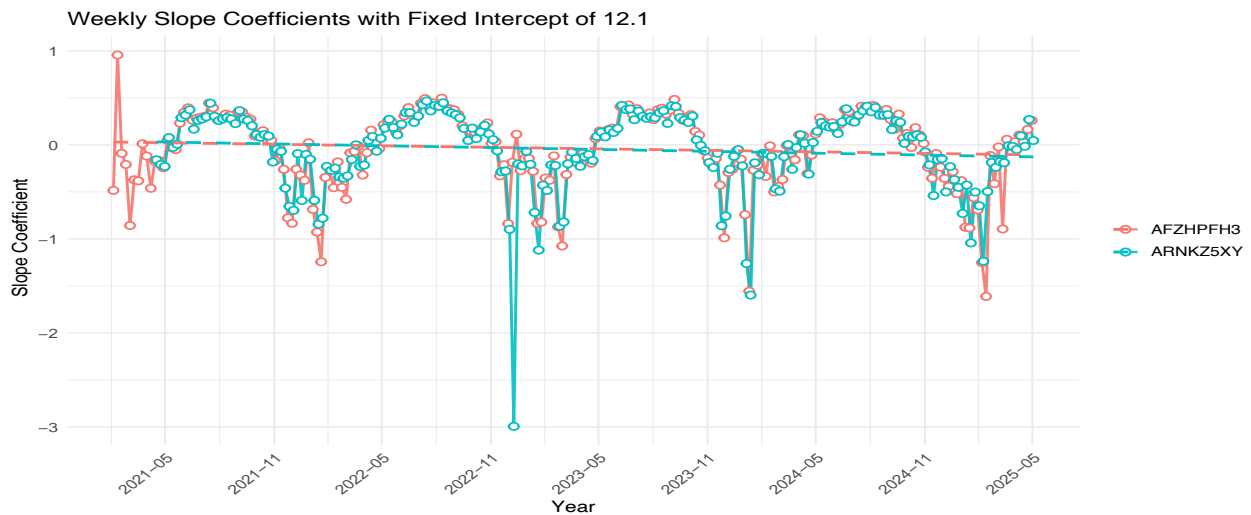


Figure 10: Weekly slope estimates with fixed intercept of 12.1°C , for the two golden nodes, AFZHPFH3 and ARNKZ5XY, over the study period. Trend lines are overlaid to illustrate long-term stability.

4.4 Second Stage Calibration

For the uncalibrated measurements for each of the golden nodes, AFZHPFH3 recorded an RMSE of 1.14°C and an MAE of 0.78°C, while ARNKZ5XY recorded an RMSE of 2.46°C and an MAE of 2.26°C.

The median co-location period for all sensor nodes was 17 days (Figure 2). first stage calibration was performed for each of the two golden nodes using their initial 17 days of data. For AFZHPFH3, the first stage calibration resulted in an RMSE of 0.51°C, MAE of 0.37°C, and R^2 of 0.99. For ARNKZ5XY, the corresponding values were an RMSE of 1.02°C, MAE of 0.80°C, and R^2 of 0.92. These models were fitted in February for AFZHPFH3, and April for ARNKZ5XY. The regression plots for both nodes are presented in Supplementary Materials 7. Rolling weekly RMSE for this first stage calibration are shown for each node in Figure 11. Over the full observation period, after first stage calibration AFZHPFH3 exhibited an RMSE of 0.99°C and an MAE of 0.73°C, while ARNKZ5XY exhibited an RMSE of 1.15°C and an MAE of 0.90°C.

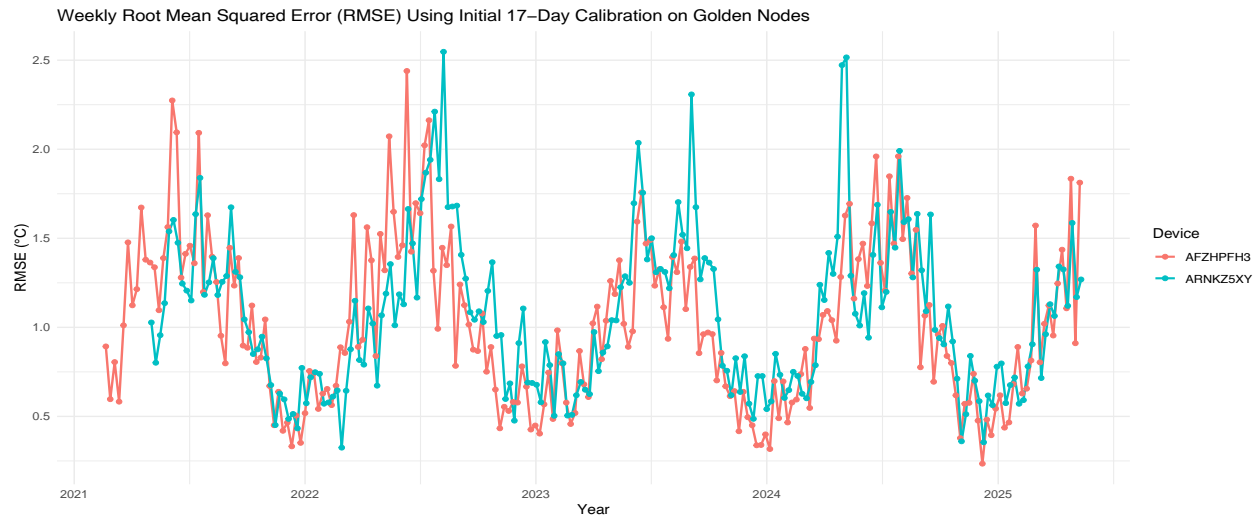


Figure 11: Weekly root mean squared error (RMSE) following initial 17-day calibration for each golden node. The RMSE values were calculated by applying the calibration model fitted on the first 17 days of co-location to successive non-overlapping weekly intervals across the deployment period.

A repeat first-stage calibration was performed during the summer months, using data from 1st July to 17th July 2021 for each golden node. For AFZHPFH3, this calibration resulted in an RMSE of 0.97°C, MAE of 0.77°C, and R^2 of 0.90. For ARNKZ5XY, the corresponding values were an RMSE of 0.95°C, MAE of 0.75°C, and R^2 of 0.90. The regression plots for these summer calibrations are presented in Supplementary Materials 8. Rolling weekly RMSE for this first stage calibration, in July 2021, are shown for each node in Figure 12. Over the full observation period, after calibration over summer, AFZHPFH3 exhibited an RMSE of 1.55°C and an MAE of 1.26°C, while ARNKZ5XY exhibited an RMSE of 1.29°C and an MAE of 1.02°C.

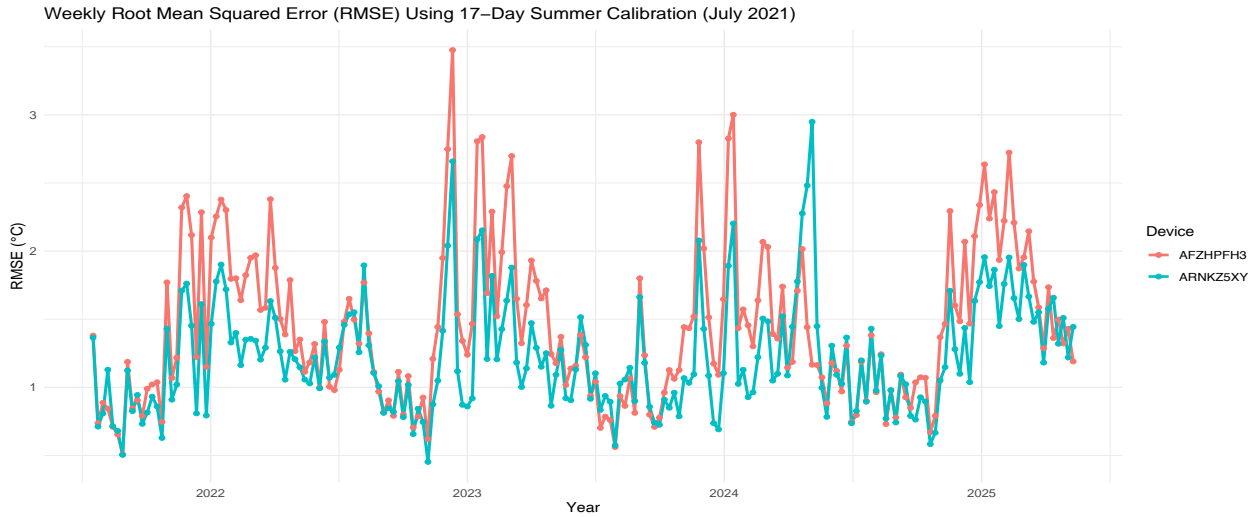


Figure 12: Weekly root mean squared error (RMSE) following first stage calibration for each golden node in July 2021. The RMSE values were calculated by applying the calibration model fitted in July 2021 to successive non-overlapping weekly intervals across the deployment period.

The distribution of temperature differences between AFZHPFH3 and ARNKZ5XY was examined, with results displayed as a histogram in Supplementary Material 9. Homoscedasticity was evaluated by plotting absolute temperature differences against mean temperature values with a fitted loess line and is shown in Supplementary Materials 10. Temporal dependence in the differences was investigated using autocorrelation functions at daily, weekly, and monthly aggregation levels and this is displayed Supplementary Materials 11. Following these checks, Bland–Altman analysis was performed on monthly aggregated temperature means between the two golden nodes. The resulting Bland–Altman plot is shown in Figure 13.

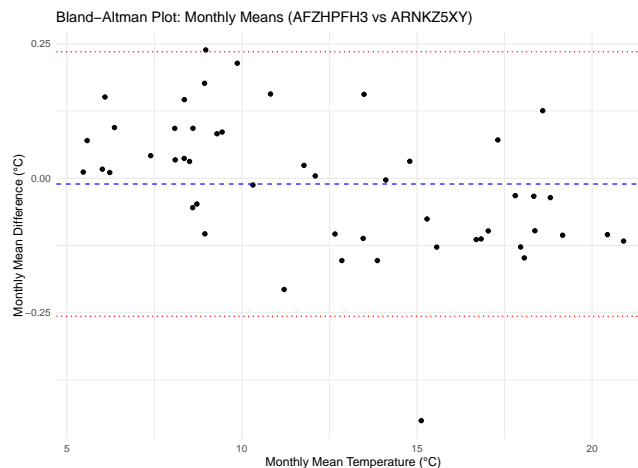


Figure 13: Bland–Altman plot of monthly mean temperatures comparing the two golden nodes. Each point represents the mean difference in temperature for a given month plotted against the corresponding monthly mean temperature. The dashed blue line indicates the overall mean difference, while the dotted red lines represent the 95% limits of agreement.

A linear mixed-effects model was fitted to the temperature differences between the two golden nodes, with a fixed intercept and a random intercept for month. The fixed intercept was estimated at -0.011 (SE = 0.018, t = -0.611). The random effect variance for month was 0.015 (SD = 0.124), and the residual variance was 0.225 (SD = 0.474). Based on these results, the two golden nodes were considered sufficiently consistent, and a decision was made to pool them for the second stage calibration.

Daily, weekly, and monthly second stage calibration models were fitted, and their performance was compared using error metrics summarised in Table 1. Of these, the weekly calibration model provided the best overall performance, with the lowest RMSE and MAE values. Weekly RMSE values were calculated for each golden node, comparing uncalibrated temperature measurements, first stage calibrated values, and second stage calibrated values against the reference station. The results are presented in Figure 14.

Table 1: Root mean squared error (RMSE) and mean absolute error (MAE) for daily, weekly, and monthly second stage calibration models across the two golden nodes, AFZHPFH3 (GN1) and ARNKZ5XY (GN2), including averages across nodes.

Period	GN1 RMSE (°C)	GN2 RMSE (°C)	Average RMSE (°C)	GN1 MAE (°C)	GN2 MAE (°C)	Average MAE (°C)
Daily	0.69	1.28	0.98	0.63	1.21	0.92
Weekly	0.94	0.95	0.95	0.74	0.78	0.76
Monthly	0.98	0.98	0.98	0.75	0.78	0.76

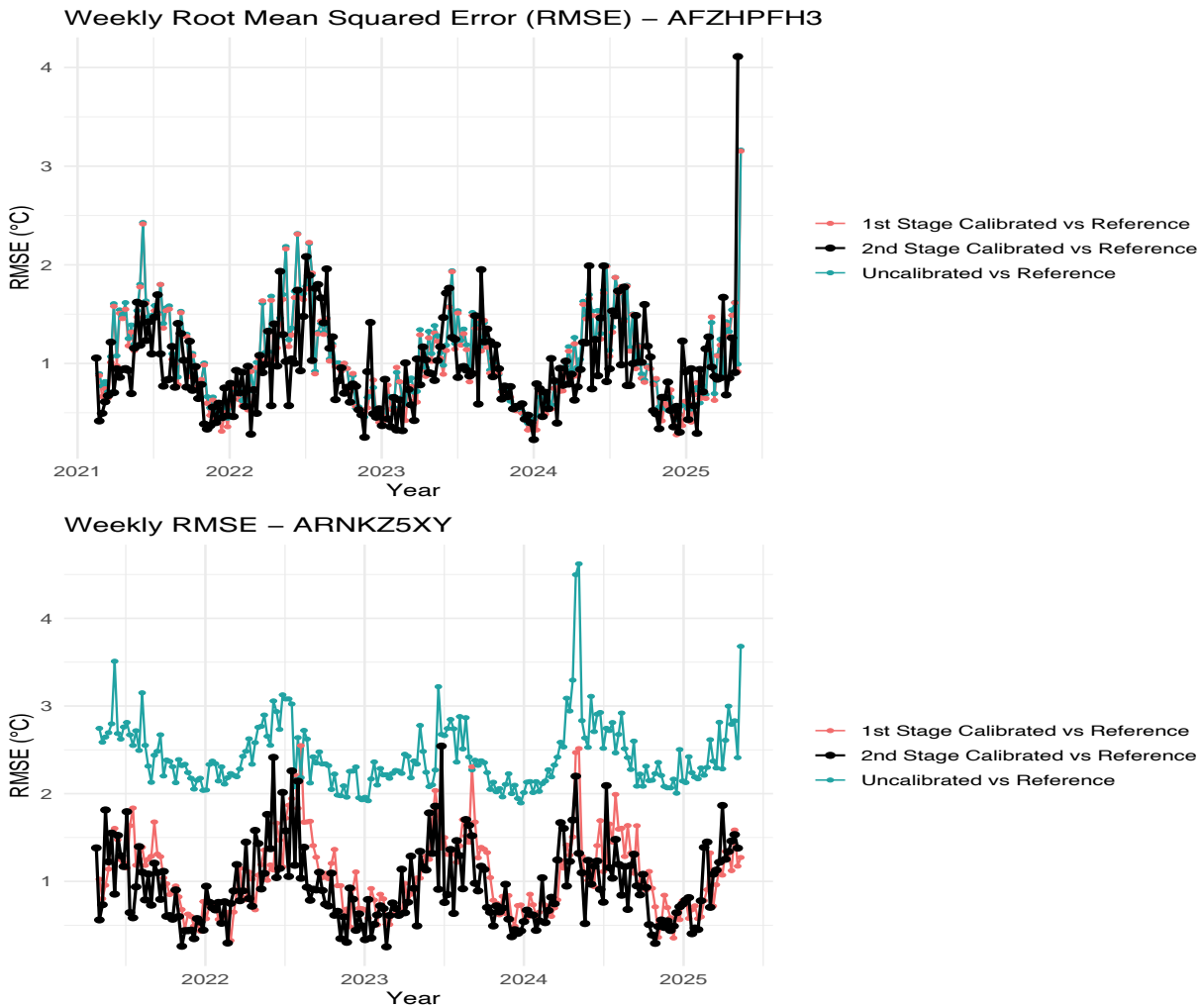


Figure 14: Each plot shows weekly root mean squared error for uncalibrated measurements, first stage calibrated measurements, and second stage calibrated measurements over the full deployment period.

4.5 External Validation

Three sensor nodes were found within 200m of a UKMO reference site (St James Park), as shown in Figure 15. These 3 devices were AFM334TS, AMLKW32G, and A9MBPGH5. Sensor node AFM334TS recorded data from 22 February 2021 at 12:00 until 13 December 2024 at 22:00. Sensor node AMLKW32G recorded data from 23 June 2022 at 12:00 until 11 May 2025 at 23:00. Sensor node A9MBPGH5 recorded data from 29 July 2023 at 03:00 until 12 May 2025 at 14:00. Their missing data by month can be visualised in Supplementary Materials 12. Missing data from St James Park between January 2021 and July 2025 can be visualised in Supplementary Materials 13. Performance metrics are calculated for each node, comparing uncalibrated temperature values, first stage calibrated values, and second stage calibrated values against the UKMO reference data. The results

are summarised per node in Table 2. Weekly RMSE values were calculated for each node, comparing uncalibrated temperature measurements, first stage calibrated values, and second stage calibrated values against the reference station. The results are presented in Figure 16.

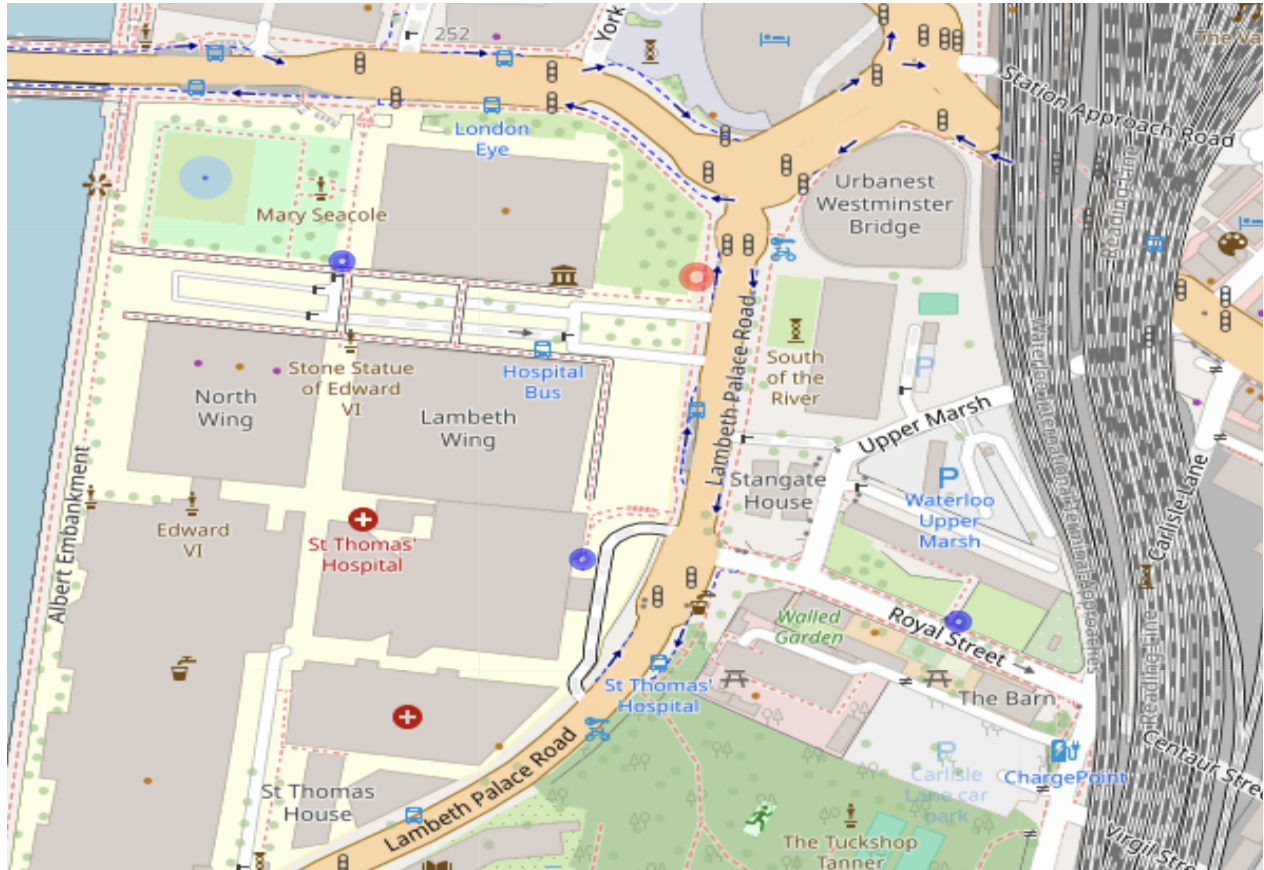


Figure 15: Map of an area within London, showing St James Park's reference site (red) and 3 deployed sensor nodes with 200m (blue). Created in R using the leaflet package.

Table 2: Overall root mean squared error (RMSE) and mean absolute error (MAE) for uncalibrated (U), first stage (1st), and second stage (2nd) calibration temperature values across three sensor nodes compared to St James Park's reference site.

Node	U RMSE (°C)	1st RMSE (°C)	2nd RMSE (°C)	U MAE (°C)	1st MAE (°C)	2nd MAE (°C)
AFM334TS	1.45	1.47	1.36	1.29	1.31	1.16
AMLKW32G	3.58	2.06	2.01	3.21	1.60	1.61
A9MBPGH5	1.63	1.28	1.32	1.47	1.07	1.00

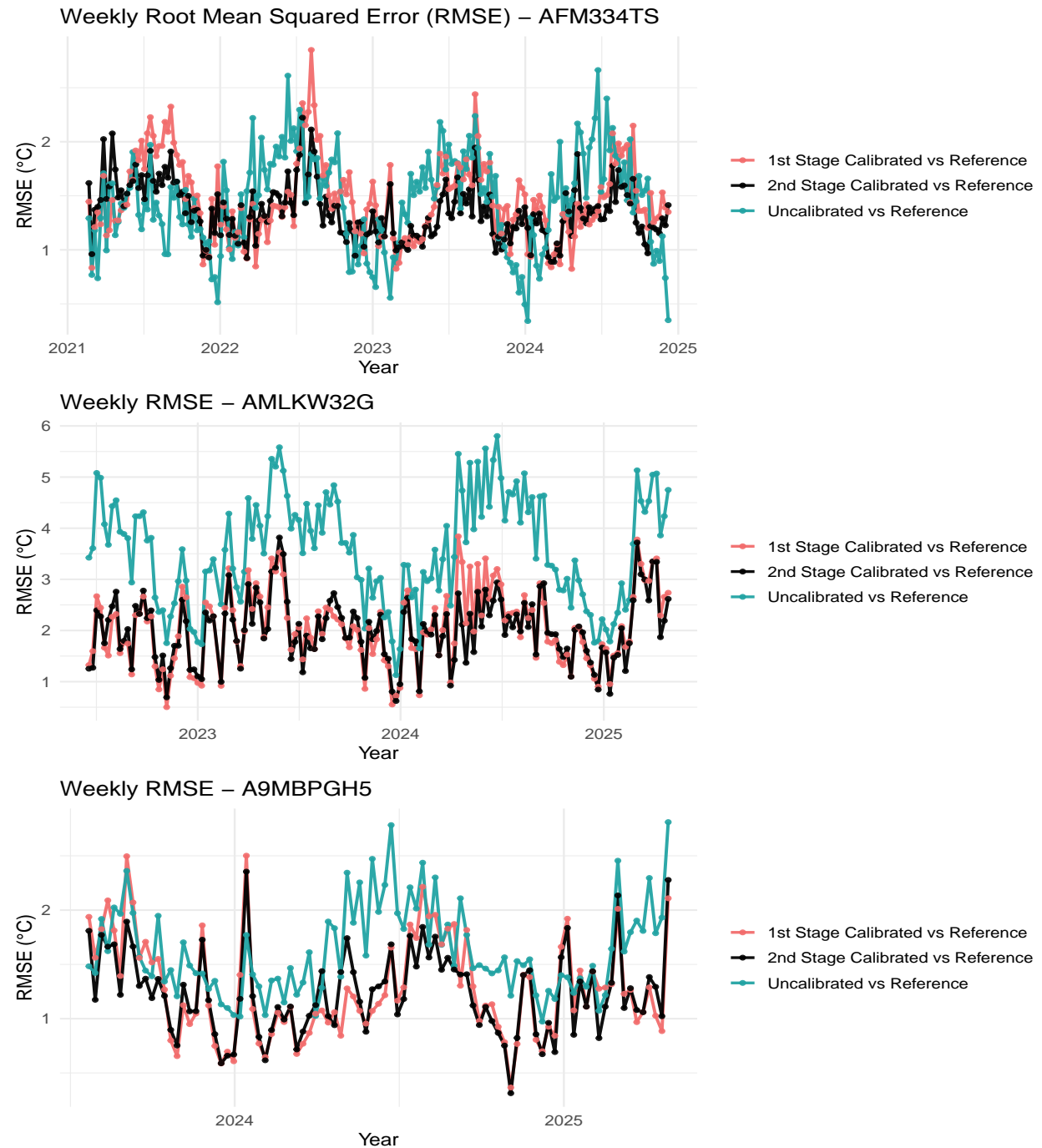


Figure 16: Weekly root mean squared error for three sensor nodes compared against the St James Park reference site. The plots compare uncalibrated, first stage calibrated, and second stage calibrated temperature errors.

4.6 Spatial Interpolation

Yearly averaged per node calibrated temperatures maps for 2021 to 2025 without interpolation are shown in the Supplementary Materials 14. In terms of Bayesian interpolation, PC priors were set directly from empirical features of the dataset. The prior for the spatial range (ρ) was anchored to the network's geometry by using the median nearest-neighbour spacing of the sensors in the densest year, 2023, rounded to the nearest 100 (400m), specifying $P(\rho < 400m) = 0.10$ (i.e., prior $\rho = c(400, 0.10)$). The prior for the marginal standard deviation (σ) was anchored to observed spatial variability by taking the 95th percentile of the daily cross-city standard deviation from 2023, which was 4.49°C . This value was used as σ_0 in a prior specifying $P(\sigma > 4.49^{\circ}\text{C}) = 0.01$ (i.e., prior $\sigma = c(4.49, 0.01)$). Prior–posterior distributions for ρ and σ are shown in Figure 17. Posterior predictive maps of yearly mean temperatures for 2022–2024 are shown in Figure 18. Posterior summaries of the hyperparameters are reported in Table 3, which presents posterior means and 95% credible intervals for ρ and σ across 2022 to 2024. Model evaluation metrics, WAIC and DIC, for 2022 to 2024 are reported in Supplementary Materials 15. Posterior standard deviation maps of interpolated yearly mean temperatures are provided in Supplementary Materials 16. The SPDE meshes used for each year are provided in Supplementary Materials 17.

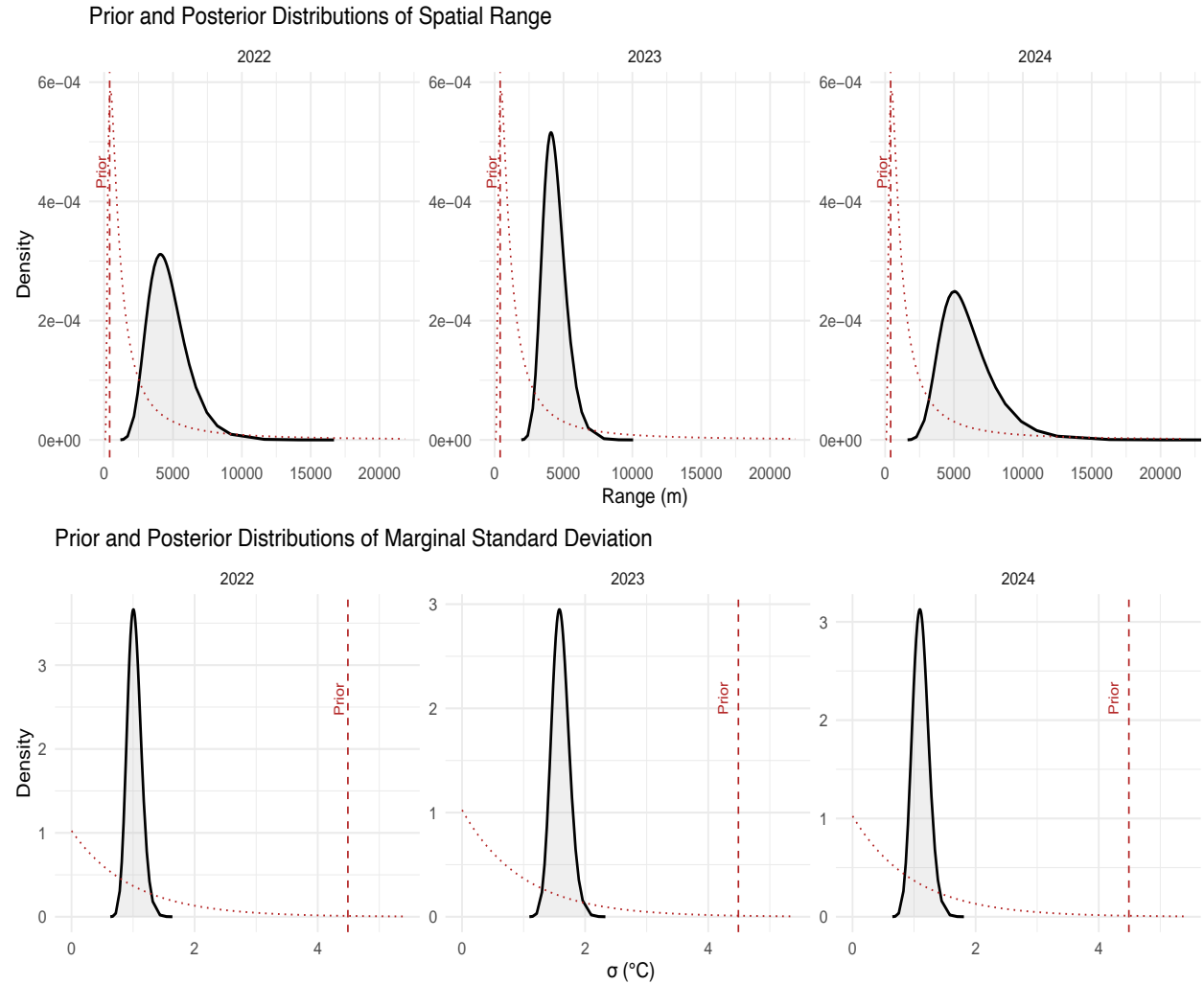


Figure 17: Red dashed lines indicate the penalised complexity prior anchors: spatial range $p_0 = 400\text{m}$ with $P(p < p_0) = 0.10$, and marginal standard deviation $\sigma_0 = 4.49C$ with $P(\sigma > \sigma_0) = 0.01$. Black curves show the posterior distributions for each year.

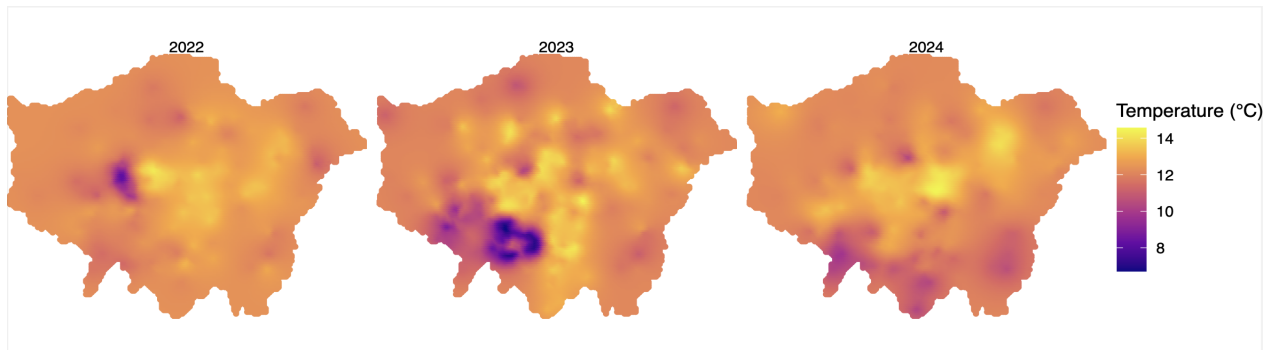


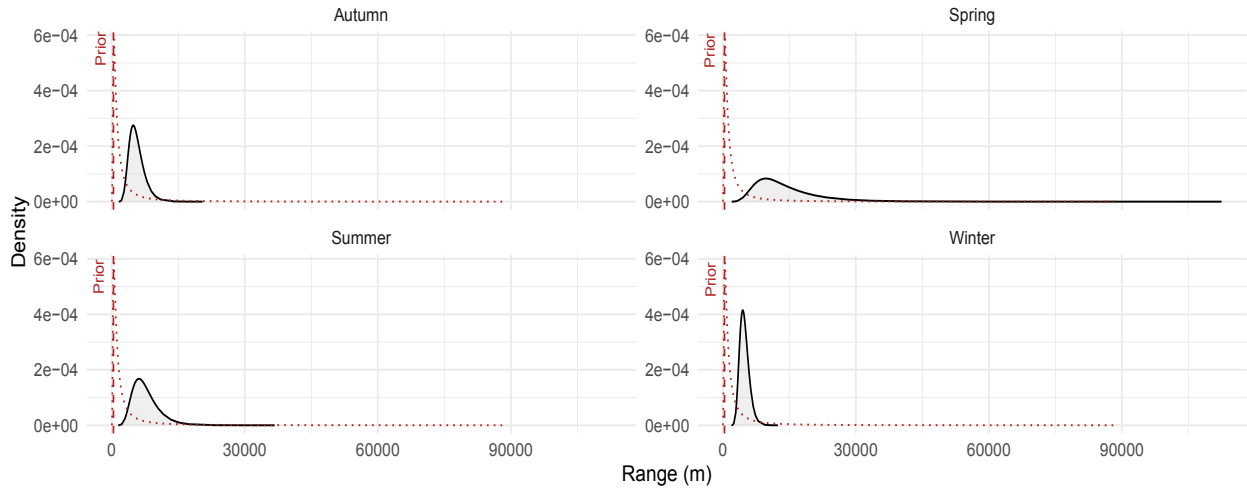
Figure 18: Posterior predictive maps of yearly mean temperatures across London for 2022 to 2024 created via Bayesian spatial interpolation.

Table 3: Posterior summaries of hyperparameters by year. Reported are posterior means and 95% credible intervals (CI) for the spatial range (ρ) and marginal standard deviation (σ).

Year	Range mean (m)	Range 95% CI (m)	σ mean ($^{\circ}$ C)	σ 95% CI ($^{\circ}$ C)
2022	4699	2431–8211	1.02	0.82–1.27
2023	4377	2965–6323	1.60	1.34–1.90
2024	6045	3160–11013	1.11	0.87–1.39

Prior–posterior distributions for seasonal spatial models for ρ and σ are shown in Figure 19. Posterior predictive maps of seasonal mean temperatures are shown in Figure 20. Normalised anomaly maps are provided in Figure 21 to highlight relative spatial deviations within each season. Posterior summaries of the hyperparameters are reported in Table 4, which presents posterior means and 95% credible intervals for ρ and σ across the four seasons. Model evaluation metrics, WAIC and DIC, for each season are reported in Supplementary Materials 18. Posterior standard deviation maps of interpolated seasonal mean temperatures are provided in Supplementary Materials 19. The SPDE meshes used for each season are provided in Supplementary Materials 20.

Prior and Posterior Distributions of Spatial Range



Prior and Posterior Distributions of Marginal Standard Deviation

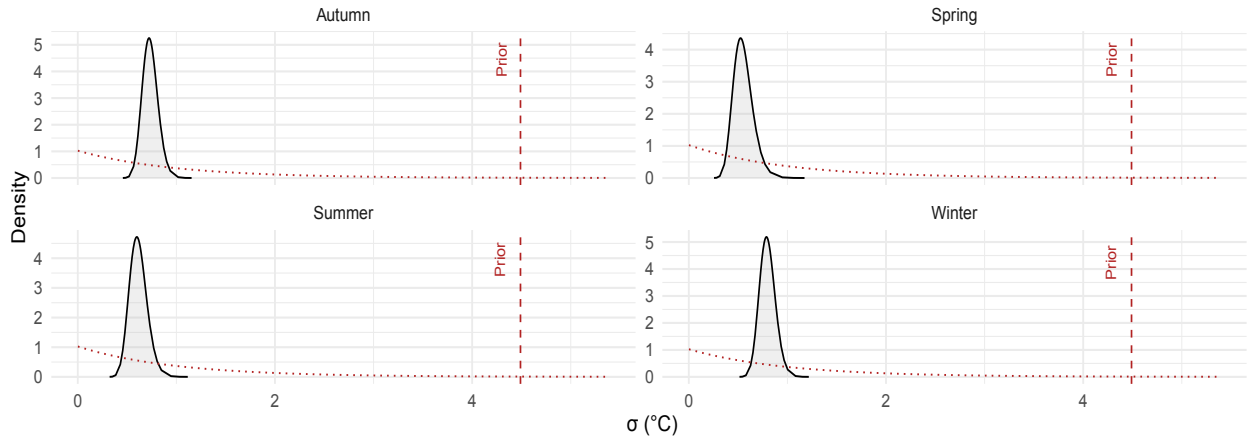


Figure 19: Red dashed lines indicate the penalised complexity prior anchors: spatial range $p_0 = 400\text{m}$ with $P(p < p_0) = 0.10$, and marginal standard deviation $\sigma_0 = 4.49\text{C}$ with $P(\sigma > \sigma_0) = 0.01$. Black curves show the posterior distributions for each season.

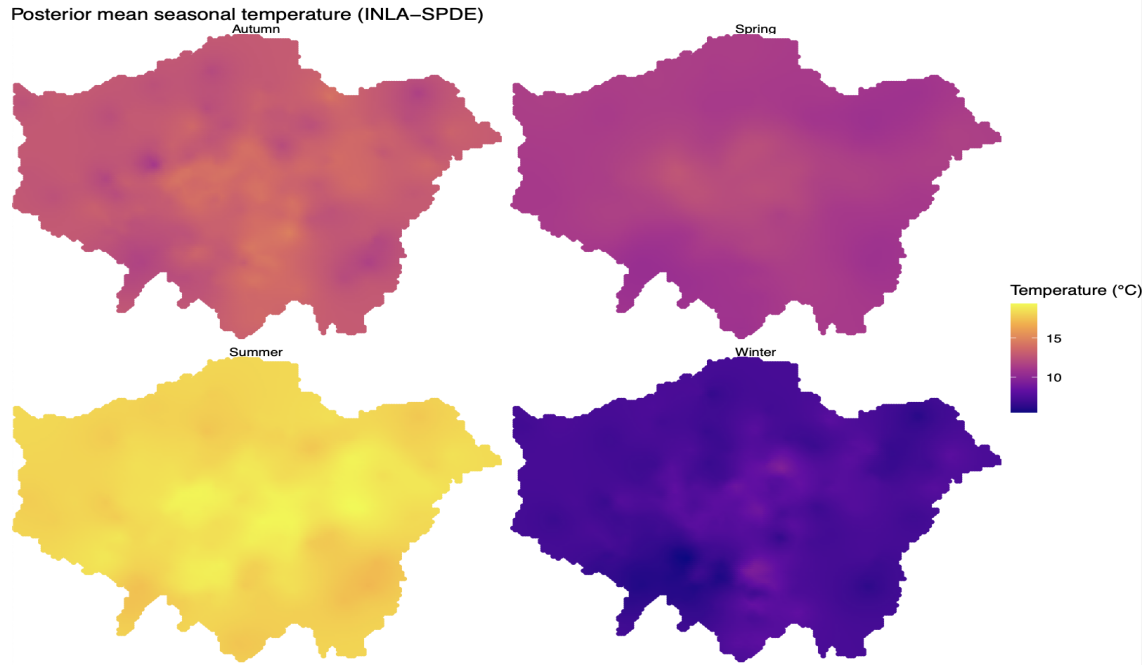


Figure 20: Posterior predictive maps of seasonal mean temperatures across London, grouped by seasons across 2021 to 2025, created via Bayesian spatial interpolation.

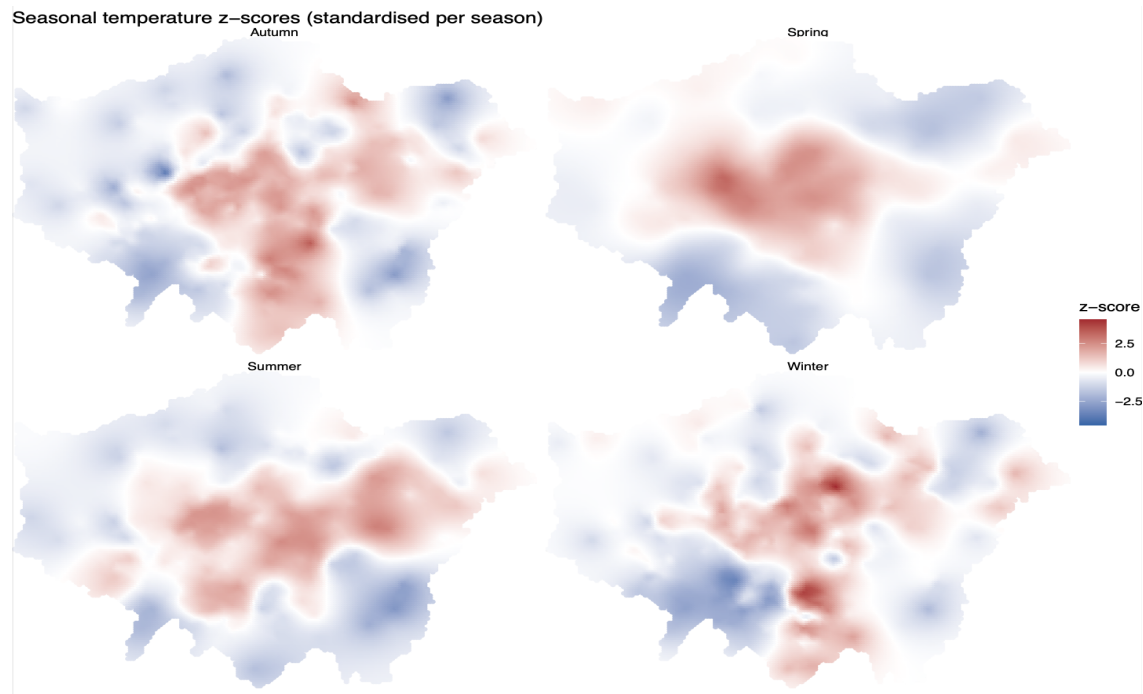


Figure 21: Normalised anomaly maps of seasonal mean temperatures across London, between 2021 to 2025, expressed as z-scores relative to each season's mean and standard deviation, generated using Bayesian spatial interpolation.

Season	Range mean (m)	Range 95% CI (m)	σ mean ($^{\circ}$ C)	σ 95% CI ($^{\circ}$ C)
Winter	4897	3153–7377	0.80	0.65–0.97
Spring	14175	5271–33476	0.55	0.38–0.77
Summer	7655	3440–15060	0.61	0.46–0.81
Autumn	5656	3060–9874	0.73	0.59–0.90

Table 4: Posterior means and 95% credible intervals for the range parameter (ρ) and spatial standard deviation (σ) across seasons, between 2021 and 2025.

Discussion

5.1 Summary of Findings

This study aimed to calibrate the Breathe London LCSN to produce accurate high-resolution air temperature data and to generate interpolated temperature maps illustrating spatial and temporal variability across London. A network-wide calibration was undertaken for 679 deployed nodes. First stage calibration, using co-location data from Honor Oak Park, achieved high in-sample fit with ground-truth measurements, with average R^2 greater than 0.9, and RMSE and MAE, both, less than 1°C. Quadratic regression provided only marginal gains, with both RMSE and MAE improving by 0.01 and no change being observed in R^2 . Consequently, linear regression was adopted for first stage calibration as the more interpretable approach. Temporal drift was addressed through second stage calibration with two permanently co-located golden nodes. Among the tested recalibration intervals, the weekly approach yielded the lowest average RMSE and MAE, marginally outperforming monthly recalibration. External validation against the reference site at St James Park demonstrated that calibration improved accuracy overall, although gains varied between sensors and calibration stages. First stage calibration generally produced the largest reduction in error relative to uncalibrated measurements, while second stage calibration yielded more modest but consistent additional improvements, particularly with MAE. Application of Bayesian spatial interpolation to the calibrated dataset revealed marked intra-urban temperature variability, highlighting the capacity of this LCSN to capture high resolution urban heat patterns.

5.2 Calibration Performance

First stage co-location calibration using linear regression provided strong agreement with reference measurements, reflected by consistently high overall R^2 values and the aggregated residual versus fitted plot which implied there was a broadly linear relationship without major systematic deviations (Figure 6; Figure 7). Moreover, all individual device models achieved R^2 values above 0.8, suggesting that every node in this LCSN behaves similarly. A review from 2025, identified 17 studies that applied linear regression for temperature sensor calibration, and among those reporting R^2 , all achieved R^2 values greater than 0.9.[18] The present results similarly indicate that this calibration approach can be effectively applied to the Breathe London LCSN.

Quadratic regression has been reported to outperform linear regression in calibrating soil moisture and pollutant sensors, but evidence for temperature calibration is limited.[42, 25] In the present study, quadratic regression resulted in small performance gains over linear regression, with improvements in RMSE and MAE of just 0.01°C and no change in R^2 . Given the already strong linear relationship with reference data and the greater interpretability of linear models, linear regression for first stage calibration was chosen as the final approach.

First stage calibration models were fitted using a median co-location period of 17 days. Previous work examining co-location periods for LCSN measuring air pollutants reported that while extended co-location periods of several months typically improved sensor accuracy, shorter calibration periods could also yield reliable models provided that the full range of environmental conditions expected during deployment was captured.[43] In the present study, excluding outliers, the co-location temperature period spanned approximately -2.5°C to 27.5°C, whereas deployed sensors experienced a wider range extending up to 32.5°C (Supplementary Materials 3; Supplementary Materials 4). This shortfall at the upper end indicates that sensors may have been underexposed to higher temperatures during calibration, potentially limiting their performance during warmer periods.

For the three nodes selected for external validation, the first stage calibration substantially reduced error for node AMLKW32G, where RMSE decreased from 3.58°C to 2.06°C and MAE from 3.21°C to 1.60°C (Table 2). This represents a dramatic improvement in accuracy and mirrors previous research where mean absolute error can be reduced by nearly half following calibration with linear regression.[13] In contrast, node AFM334TS did not exhibit improvement after the first stage calibration, with RMSE and MAE remaining essentially unchanged (Table 2). A likely explanation is that this sensor already exhibited relatively low error in its uncalibrated state, leaving limited scope for improvement. Additionally, first stage calibration was based on a relatively short co-location period, which may not have fully captured the range of temperatures encountered during this node's deployment period. This could have constrained the regression model's ability to refine performance for a device that was already well-aligned with reference values. Interestingly, AFM334TS did improve following the second stage calibration, suggesting that temporal recalibration using golden nodes corrected residual discrepancies not resolved during initial co-location calibration.

The trajectories of slope and intercept coefficients for first stage calibration on the golden nodes demonstrated that calibration parameters were not temporally stable, with both golden nodes showing fluctuations across the deployment period (Figure 9; Figure 10). Moreover, Repeating first stage calibration during a different co-location period resulted in different error values compared to the initial calibration, despite both being based on 17 days of data. This finding is consistent with previous reports in the literature that calibration accuracy is influenced by the surrounding environmental conditions during co-location.[44] These patterns highlight the limitations of relying on a single stage calibration. Due to the shifts observed with calibration coefficients, there is a requirement for a more dynamic approach to maintain measurement accuracy. As suggested by previous

work, dynamic recalibration models were implemented for second stage calibration using the two golden nodes in the Breathe London LCSN.[17, 25] Weekly calibration yielded the lowest average RMSE (0.95°C) and tied with monthly recalibration for the lowest average MAE (0.76°C), although the differences between weekly and monthly performance were relatively minor (Table 1). Daily recalibration did not provide additional benefit, and in the case of ARNKZ5XY introduced higher RMSE and MAE compared to weekly or monthly models.

For context, the uncalibrated measurements showed a clear baseline disparity between the two golden nodes. AFZHPFH3 recorded an RMSE of 1.14°C and an MAE of 0.78°C , while ARNKZ5XY recorded substantially higher errors with an RMSE of 2.46°C and an MAE of 2.26°C . First stage calibration reduced these errors across both nodes, with AFZHPFH3 improving to an RMSE of 0.99 and an MAE of 0.73, and ARNKZ5XY improving to an RMSE of 1.15 and an MAE of 0.90 over the full observation period. Second stage dynamic calibration provided only marginal additional improvements beyond these gains, with AFZHPFH3 remaining largely unchanged, while ARNKZ5XY exhibited further small reductions in both RMSE and MAE. These results suggest that the benefits of dynamic calibration are not uniform but dependent on the initial error structure of each node.

This is further supported by the results from external validation, which revealed heterogeneous responses to dynamic calibration (Table 2). AMLKW32G, which exhibited the highest uncalibrated errors, showed dramatic gains after first stage calibration but little further improvement with second stage calibration. By contrast, AFM334TS and A9MBPGH5 demonstrated modest but consistent additional reductions in error following the second stage, suggesting that dynamic calibration can still refine performance where initial alignment is already reasonably strong. These findings align with a previous study’s research in low-cost air pollution sensors, where it was reported that repeated monthly calibration improved model accuracy over static pre-deployment calibration.[45] However, their study did not evaluate finer-grained cycles. The present results therefore extend this evidence by demonstrating that weekly calibration can yield additional improvements in certain cases, while also underscoring that the magnitude of benefit is likely to be sensor-specific.

5.3 Spatial Interpolation

The purpose of the spatial interpolation in this study was not to deliver exact estimates of London’s temperature field, but to demonstrate the capability of a calibrated LCSN to reveal intra-urban temperature variability that would otherwise remain unresolved. Focusing first on the yearly models, the prior–posterior distributions showed that the data strongly updated the range (ρ), shifting from the conservative prior expectation of sub-kilometre correlation to several-kilometre scales, which is consistent with neighbourhood-level temperature structure (Figure 17; Table 3). By contrast, the marginal standard deviation (σ) remained between 1°C to 2°C across all years, which is within the prior bound, and suggests spatially consistent variability in London’s urban temperatures between the years of 2022 and 2024. Comparable values have been reported in long-term observational studies

of London. A recent analysis using a high-resolution gridded meteorological dataset for Europe, between 1990 and 2022, reported an average UHI intensity of around 1.4°C for London.[46, 47] This value is of the same order as the posterior σ estimates obtained in the present study, suggesting that the level of variability inferred by the model is consistent with independent estimates of London's UHI intensity, and thereby supporting the credibility of the calibrated network and Bayesian framework in reproducing realistic intra-urban temperature contrasts.

The posterior predictive maps illustrate how these yearly patterns manifest spatially across London, with coherent neighbourhood-level structures evident in each year (Figure 18). These maps reveal temperature contrasts of up to 4°C to 6°C across London, with warmer zones concentrated in denser central urban areas of London. These yearly averaged maps provide a baseline view of London's spatial temperature heterogeneity, though they inevitably smooth over shorter-term fluctuations.

The prior–posterior distributions for the seasonal models revealed that, as with the yearly models, the data strongly updated the range parameter (ρ) from the conservative prior, resulting in kilometre-level correlations across all seasons (Figure 19; Table 4). By contrast, the marginal standard deviation (σ) remained below 1°C , reflecting weaker variability within seasons. This is expected, since annual models aggregate across multiple seasons and therefore capture a broader spread of temperature contrasts. The seasonal posterior predictive maps highlight the expected seasonal cycle, with warmest conditions in summer and coldest in winter (Figure 20). The standardised anomaly maps further reveal that relative hot and cold areas are not random but reoccur in broadly similar locations across seasons, suggesting that neighbourhood characteristics exert a persistent influence on temperature even under differing meteorological conditions (Figure 21). It is important to note that these anomalies represent deviations from the seasonal mean rather than absolute temperatures, so positive anomalies in winter correspond to relatively mild temperatures within an otherwise cold season, while positive anomalies in summer indicate particularly high temperatures, as these temperatures are on top of an already elevated average temperature as seen during Summer.

Similar patterns of persistent spatial contrasts have been reported by the Greater London Authority, who produced borough-level heat hazard maps based on modelled summer air temperatures.[48] They identified hotspots of elevated heat risk in central and densely built areas of London, consistent with the anomalies observed in the present study (Figure 21). However, their approach relies on physics-based modelling of the surface energy balance rather than direct sensor observations, and as a result their findings are sensitive to assumptions about land cover and building characteristics, and fail to capture the fine-grained microclimatic variation detected by a dense sensor network. Moreover, because their outputs focus only on summer averages, they fail to capture temporal dynamics such as seasonal differences, which can be resolved through the use of a LCSN as described in the present study. By providing observational evidence of seasonal and neighbourhood-level variability, the present study reinforces the Greater London Authority's call for more fine-grained monitoring and targeted interventions.[48] In particular, the results from this study

complement the Greater London Authority's Cool Spaces initiative by offering an empirical basis for guiding residents to existing cool spaces and for prioritising where additional spaces should be built.[49]

5.4 Limitations

Several limitations should be considered when interpreting these findings. The second stage calibration step assumes that all deployed nodes behave in the same way as the golden nodes, however this assumption may not hold for all devices, introducing the possibility of calibration errors. External validation was limited to three sensors located near a reference site, which prevents systematic assessment of device-level errors across the wider network and reduces confidence in results at unvalidated sites. The evaluation of the second stage daily calibration models may also be biased, as the blocking time-series split method placed most test periods at night when temperature variability is lower.[28] This may have led to an overestimation of model performance in the daily case, although the weekly and monthly models, validated across entire days, are less affected. Spatial interpolation results are additionally constrained by the distribution of sensors, with posterior standard deviation maps showing greater uncertainty at the city's peripheries where coverage is sparse (Supplementary Materials 16; Supplementary Materials 19). Consequently, the interpolated surfaces represent modelled estimates rather than direct observations, and their reliability is reduced in poorly covered areas.

5.5 Conclusion

This study provides the first city-wide calibration of a dense low-cost temperature sensor network in London, combining initial co-location adjustments with a protocol for correcting long-term measurement drift. Furthermore, the results from external validation, which involved comparing a small subset of sensors with a nearby reference station, suggests that first and second stage calibrations may have resulted in an improvement of overall sensor accuracy across the entire LCSN. Using a Bayesian INLA-SPDE framework, the calibrated network revealed substantial intra-urban variation in air temperature, with neighbourhood-scale contrasts of several degrees and clear seasonal and annual patterns. These findings insinuate that a LCSN can capture fine-grained variability not captured by sparse reference-grade monitors, and can therefore offer valuable evidence to support urban climate adaptation. In particular, the ability to identify persistent hotspots provides a foundation for targeted interventions, such as cooling infrastructure and resilience planning in vulnerable neighbourhoods. Future research should extend external validation through additional reference sites in London and explore comparisons with other cities, thereby strengthening the generalisability of the described two step calibration approach used in this study. This in turn will advance the role of calibrated LCSN as a practical tool for managing the growing challenge of urban heat.

Acknowledgments

I would like to express my sincere gratitude to Professor Barratt and Dr Mead for their supervision and guidance throughout this project. I conducted the literature review, developed the methodology, interpreted the results, and wrote the conclusion independently. My supervisors provided the database used in this study, derived from their larger SQL repository, and advised me during regular meetings held approximately once every two weeks for the duration of the project. In these meetings, they offered critical feedback, helped ensure the study remained aligned with its overall objectives, and suggested potential statistical approaches that I considered when developing the analyses.

Bibliography

- [1] Nazarian N, Krayenhoff ES, Bechtel B, Hondula DM, Paolini R, Vanos J, et al. Integrated Assessment of Urban Overheating Impacts on Human Life. *Earth's Future*. 2022;10(8):e2022EF002682.
- [2] Pelling M, Garschagen M. Put equity first in climate adaptation. *Nature*. 2019;569(7756):327-9.
- [3] Yang L, Qian F, Song DX, Zheng KJ. Research on Urban Heat-Island Effect. *Procedia Engineering*. 2016;169(2016):11-8.
- [4] Mishra V, Ganguly AR, Nijssen B, Lettenmaier DP. Changes in observed climate extremes in global urban areas. *Environmental Research Letters*. 2015;10(2).
- [5] Ao X, Wang L, Zhi X, Gu W, Yang H, Li D. Observed Synergies between Urban Heat Islands and Heat Waves and Their Controlling Factors in Shanghai, China. *Journal of Applied Meteorology and Climatology*. 2019;58(9):1955-72.
- [6] Heaviside C, Macintyre H, Vardoulakis S. The Urban Heat Island: Implications for Health in a Changing Environment. *Current Environmental Health Reports*. 2017;4:296-305.
- [7] Cao J, Zhou W, Zheng Z, Ren T, Wang W. Within-city spatial and temporal heterogeneity of air temperature and its relationship with land surface temperature Author links open overlay panel. *Landscape and Urban Planning*. 2021;206:103979.
- [8] C40 Cities Climate Leadership Group and C40 Knowledge Hub. How to adapt your city to extreme heat. C40 Knowledge; 2021. Available from: https://www.c40knowledgehub.org/s/article/How-to-adapt-your-city-to-extreme-heat?language=en_US.
- [9] Guo Y, Unger J, Khabibolla A, Tian T, He R, Li H, et al. Modeling urban air temperature using satellite-derived surface temperature, meteorological data, and local climate zone pattern—a case study in Szeged, Hungary. *Theoretical and Applied Climatology*. 2024;115:3841-59.

- [10] Centre for Environmental Data Analysis. Met Office Integrated Data Archive System (MIDAS) station search; 2025. Available from: https://utils.ceda.ac.uk/cgi-bin/midas_stations/search_by_county.cgi.py?county=GREATERTHANLONDON&minyear=&maxyear=¤t=y.
- [11] White-Newsome JL, Brines SJ, Brown DG, Dvonch JT, Gronlund CJ, Zhang K, et al. Validating Satellite-Derived Land Surface Temperature with in Situ Measurements: A Public Health Perspective. *Environmental Health Perspectives*. 2013;121(8):925-31.
- [12] Mao F, Khamis K, Krause S, Clark J, Hannah DM. Low-Cost Environmental Sensor Networks: Recent Advances and Future Directions. *Frontiers in Earth Science*. 2019;7.
- [13] Yamamoto K, Togami T, Yamaguchi N, Ninomiya S. Machine Learning-Based Calibration of Low-Cost Air Temperature Sensors Using Environmental Data. *Sensors (Basel)*. 2017;17(6):1290.
- [14] Alfano B, Barretta L, Guidice AD, Vito SD, Francia GD, Esposito E, et al. A Review of Low-Cost Particulate Matter Sensors from the Developers' Perspectives. *Sensors (Basel)*. 2020;20(23):6819.
- [15] Chapman CL L and Muller, Young DT, Warren EL, Grimmond CSB, Cai XM, Ferranti EJS. The Birmingham Urban Climate Laboratory: An Open Meteorological Test Bed and Challenges of the Smart City. *Bulletin of the American Meteorological Society*. 2015;96(9):1545-60.
- [16] Liang L. Calibrating low-cost sensors for ambient air monitoring: Techniques, trends, and challenges. *Environmental Research*. 2021;197:111163.
- [17] Kizel F, Etzion Y, Shafran-Nathan R, Levy I, Fishbain B, Bartonova A, et al. Node-to-node field calibration of wireless distributed air pollution sensor network. *Environmental Pollution*. 2018;233:900-9.
- [18] Abdinoor JA, Hashim ZK, Horvath B, Zsebo S, Stencinger D, Hegedus G, et al. Performance of Low-Cost Air Temperature Sensors and Applied Calibration Techniques—A Systematic Review. *Atmosphere*. 2025;16(7):842.
- [19] Simpson CH, Brousse O, Heaviside C. Estimated mortality attributable to the urban heat island during the record-breaking 2022 heatwave in London. *Environmental Research Letters*. 2024;19(9):094047.
- [20] Yu T, Sützl BS, van Reeuwijk M. Urban neighbourhood classification and multi-scale heterogeneity analysis of Greater London. *Environment and Planning B: Urban Analytics and City Science*,. 2022;50(6):1534-58.
- [21] Taylor J, Simpson C, Brousse O, Viitanen AK, Heaviside C. The potential of urban trees to reduce heat-related mortality in London. *Environmental Research Letters*. 2024;19(5):054004.

- [22] Clarity Movement Co . Breathe London releases first air quality data analysis, demonstrating high accuracy for air quality sensors; 2024. Available from: <https://www.clarity.io/blog/breathe-london-air-pollution-monitoring-network-releases-first-comprehensive-analysis-of-air-quality-data-demonstrating-that-air-quality-sensors-can-achieve-high-data-accuracy>.
- [23] Clarity Movement Co . Node-S Air Sensor; 2025. Available from: <https://www.clarity.io/products/clarity-node-s>.
- [24] London Air. LAQN Monitoring Sites; 2025. Available from: <https://londonair.org.uk/london/asp/publicdetails.asp>.
- [25] Malings C, Tanzer R, Hauryliuk A, N KSP, Zimmerman N, Kara LB, et al. Development of a general calibration model and long-term performance evaluation of low-cost sensors for air pollutant gas monitoring. *Atmospheric Measurement Techniques*. 2019;12(2):903-20.
- [26] openair-project. GitHub Repository. GitHub; 2025. Available from: <https://github.com/openair-project>.
- [27] Schmidt AF, Finan C. Linear regression and the normality assumption. *Journal of Clinical Epidemiology*. 2018;98:146-51.
- [28] Shrivastava S. Cross Validation in Time Series. Medium; 2020. Available from: <https://medium.com/@soumyachess1496/cross-validation-in-time-series-566ae4981ce4>.
- [29] Dong J, Goodman N, Carre A, Rajagopalan P. Calibration and validation-based assessment of low-cost air quality sensors. *Science of The Total Environment*. 2025;977:179364.
- [30] Yan H, Fan S, Guo C, Hu J, Dong L. Quantifying the Impact of Land Cover Composition on Intra-Urban Air Temperature Variations at a Mid-Latitude City. *Plos One*. 2014;9(7):e102124.
- [31] Office of Geomatics. World Geodetic System 1984 (WGS 84); 2025. Available from: <https://earth-info.nga.mil/index.php?dir=wgs84&action=wgs84>.
- [32] Greater London Authority. Statistical GIS Boundary Files for London. London Data-store; 2025. Available from: <https://data.london.gov.uk/dataset/statistical-gis-boundary-files-london/>.
- [33] Rue H, Martino S, Chopin N. Approximate Bayesian inference for latent Gaussian models using integrated nested Laplace approximations (with discussion). *Journal of the Royal Statistical Society*. 2009;71(2):319-92.
- [34] Martins TG, Simpson D, Lindgren F, Rue H. Bayesian computing with INLA: new features; 2012. Available from: www.r-inla.org.

- [35] Lindgren F, Rue H, Lindstrom J. An explicit link between Gaussian fields and Gaussian Markov random fields: The SPDE approach (with discussion). *Journal of the Royal Statistical Society*. 2011;73(4):423-98.
- [36] Huang J, Malone BP, Minasny B, B MA, Triantafilis J. Evaluating a Bayesian modelling approach (INLA-SPDE) for environmental mapping. *Science of The Total Environment*. 2017;609:621-32.
- [37] Simpson D, Rue H, Riebler A, Martins TG, Sørbye SH. Penalising Model Component Complexity: A Principled, Practical Approach to Constructing Priors. *Statistical Science*. 2017;32(1):1-28.
- [38] Bolarinwa OA, Odimegwu C, Mohammed A, Gayawan E. Spatial modelling of the shared impact of sexual health knowledge and modern contraceptive use among women with disabilities in Africa. *Contraception and Reproductive Medicine*. 2025;28(10):16.
- [39] Lindgren F. Matern SPDE model object with PC prior for INLA. rdrr.io; 2019. Available from: https://rdrr.io/github/INBO-BMK/INLA/man/inla.spde2.pcmatern.html?utm_source=chatgpt.com.
- [40] Du H, Keller B, Alacam E, Enders C. Comparing DIC and WAIC for multilevel models with missing data. *Behaviour Research Methods*. 2024;56(4):2731-50.
- [41] Met Office. Our seasons. Met Office;. Available from: <https://weather.metoffice.gov.uk/learn-about/met-office-for-schools/other-content/other-resources/our-seasons>.
- [42] Hidayat MN, Hazarika H, Kanaya H. Calibration and Performance Evaluation of Cost-Effective Capacitive Moisture Sensor in Slope Model Experiments. *Sensors (Basel)*. 2024;24(24):8156.
- [43] Zamora ML, Buehler C, Datta A, Gentner DR, Koehler K. Identifying optimal co-location calibration periods for low-cost sensors. *Atmospheric Measurement Techniques*. 2023;16(1):169-79.
- [44] Ratingen SV, Vonk J, Blokhuis C, Wesseling J, Tielemans E, Weijers E. Seasonal Influence on the Performance of Low-Cost NO₂ Sensor Calibrations. *Sensors (Basel)*. 2021;21(23):7919.
- [45] Gabel P, Hertig E. Recalibration of low-cost air pollution sensors: Is it worth it? *EGU Sphere*. 2025:2677.
- [46] Perez IA, Garcia MA, Rasekhi S, Pazoki F, Fernandez-Duque B. Extension and trend of the London urban heat island under Lamb weather types. *Sustainable Cities and Society*. 2024;114:105743.
- [47] Thiemig V, Gomes GN, Skøien JO, Ziese M, Rauthe-Schöch A, Rustemeier E, et al. EMO-5: a high-resolution multi-variable gridded meteorological dataset for Europe. *Earth Systems Science Data*. 2022;14(7):3249-72.

- [48] Figueiredo A, Smith H. Properties Vulnerable to Heat Impacts in London. Greater London Authority; 2024. Available from: https://www.london.gov.uk/sites/default/files/2024-01/24-01-16%20GLA%20Properties%20Vulnerable%20to%20Heat%20Impacts%20in%20London.pdf?utm_source=chatgpt.com.
- [49] Allen T. Invitation – The Greater London Authority invites you to register sites for Cool Spaces – Summer 2022. Council for Voluntary Service; 2022. Available from: <https://thcvs.org.uk/news/invitation-the-greater-london-authority-invites-you-to-register-sites-for-cool-spaces-summer-2022/>.

Supplementary Materials

Supplementary Materials 1. The full device-level summary table of co-location periods, alongside quantification of missing data during those periods per node. Number of Matching Observations is the number of temperature data points from a node where a reference measurement is also available.

Supplementary Materials 1 - Device Summaries

	Device ID	Co-location Start	Co-location End	Expected No. of Observations	Percentage Missing (%)	Number of Matching Observations
1	A02P3MMN	2021-10-13 17:00:00	2021-10-27 14:00:00	334	0.6	332
2	A03197WZ	2021-10-13 16:00:00	2021-10-27 14:00:00	335	0.6	333
3	A06V5FQY	2021-10-27 13:00:00	2021-11-10 13:00:00	337	0	337
4	A0CW72T5	2020-12-18 07:00:00	2021-02-18 15:00:00	1497	11.29	1328
5	A0FVVFV3	2023-07-07 11:00:00	2023-10-03 00:00:00	2102	0	2102
6	A0GKTRKF	2021-10-01 14:00:00	2021-10-20 12:00:00	455	0	455
7	A0LY7PX8	2021-10-14 11:00:00	2021-10-27 14:00:00	316	0.63	314
8	A0P5RYM6	2022-03-08 16:00:00	2022-03-30 15:00:00	528	10.04	475
9	A0VPQ6ZQ	2022-03-08 16:00:00	2022-05-12 10:00:00	1555	3.54	1500
10	A0WCGYXY	2021-05-11 14:00:00	2021-06-07 16:00:00	651	0.15	650
11	A136KTH8	2021-04-16 13:00:00	2021-06-28 13:00:00	1753	0.06	1752
12	A15JMZ5K	2021-10-14 11:00:00	2021-10-27 14:00:00	316	0.63	314
13	A1BYHS2K	2021-08-24 13:00:00	2021-09-06 15:00:00	630	0	630
14	A1C8LWF7	2022-03-08 13:00:00	2022-03-30 15:00:00	531	9.98	478
15	A1GZKRQG	2021-10-01 14:00:00	2021-10-13 13:00:00	288	0	288
16	A1K92FFK	2021-10-01 17:00:00	2021-10-13 13:00:00	285	0	285
17	A1MZQNTM	2021-10-01 16:00:00	2021-10-13 13:00:00	572	0	572
18	A1WBQPR3	2021-03-24 14:00:00	2021-06-30 17:00:00	2356	0.04	2355
19	A20KSGXX	2021-04-29 15:00:00	2021-06-10 06:00:00	1000	0.1	999
20	A246B3NS	2021-02-10 14:00:00	2021-06-05 00:00:00	2747	9.54	2485
21	A25W9VTP	2022-02-04 15:00:00	2022-03-08 11:00:00	765	0	765
22	A28GQNKV	2021-10-01 13:00:00	2021-10-13 13:00:00	289	0	289
23	A2BRCQP1	2021-10-27 13:00:00	2021-11-10 13:00:00	337	0	337
24	A2GY6B2R	2021-04-29 13:00:00	2021-05-24 17:00:00	605	0	605
25	A2HGRKBL	2021-08-24 13:00:00	2021-09-06 15:00:00	315	0	315
26	A2KKHJN4	2021-10-13 16:00:00	2021-10-27 14:00:00	335	0.6	333
27	A2NRYWB6	2021-10-01 13:00:00	2021-10-13 13:00:00	289	0	289
28	A2P121Q5	2022-03-30 15:00:00	2022-05-12 10:00:00	1028	0.19	1026
29	A2RBMLV3	2021-04-29 15:00:00	2021-06-11 05:00:00	1023	0.1	1022
30	A30RL2YP	2021-03-24 14:00:00	2021-06-05 00:00:00	1739	0.06	1738
31	A33QC3XV	2023-07-25 12:00:00	2023-08-11 12:00:00	409	0	409
32	A346F4QH	2022-11-10 12:00:00	2022-11-28 12:00:00	433	0	433
33	A36R8B5N	2021-02-09 13:00:00	2021-06-05 00:00:00	2772	9.45	2510
34	A3743L80	2021-02-10 13:00:00	2021-06-05 00:00:00	2748	9.53	2486
35	A37DKBQS	2021-10-13 18:00:00	2021-10-27 14:00:00	333	0.6	331
36	A37FW3XL	2022-11-10 12:00:00	2022-11-28 12:00:00	433	0	433
37	A38Q1N13	2022-02-04 16:00:00	2022-03-08 11:00:00	764	0	764
38	A3CQ3XXY	2024-11-08 19:00:00	2024-12-09 14:00:00	740	0	740
39	A3DMR7DP	2022-03-10 23:00:00	2022-03-30 15:00:00	473	11.21	420
40	A3DT6KPG	2021-03-24 14:00:00	2021-06-05 00:00:00	1739	0.06	1738
41	A3FLFC3C	2024-02-28 13:00:00	2024-05-15 12:00:00	1848	0	1848
42	A3G8C9P4	2021-10-01 17:00:00	2021-10-13 13:00:00	570	0	570
43	A3H21B53	2021-04-29 13:00:00	2021-06-09 05:00:00	977	0.1	976
44	A3HL7PCV	2023-07-07 17:00:00	2023-07-25 12:00:00	428	0	428
45	A3HYWR97	2024-02-28 13:00:00	2024-05-15 12:00:00	1848	0	1848
46	A3J7HL31	2021-02-10 13:00:00	2021-06-05 00:00:00	2748	9.53	2486
47	A3JKCHL4	2022-10-19 14:00:00	2022-11-10 12:00:00	527	0.19	526
48	A3JML6KR	2022-12-22 15:00:00	2023-01-05 11:00:00	333	0	333
49	A3KH2QPB	2021-10-01 16:00:00	2021-10-13 13:00:00	572	0	572
50	A3M329GS	2021-04-16 13:00:00	2021-06-05 00:00:00	1188	0.08	1187
51	A3NXNTG3	2022-08-04 15:00:00	2022-08-24 11:00:00	477	0	477
52	A3PJWV3X	2022-12-22 13:00:00	2023-01-05 11:00:00	335	0	335
53	A3Q3GW9W	2024-11-08 18:00:00	2024-12-09 14:00:00	741	0	741
54	A3QJ3JVN	2023-11-24 12:00:00	2024-02-27 11:00:00	4566	0	4566
55	A3TY3Q03	2020-12-18 07:00:00	2021-01-28 23:00:00	1037	0	1037

56	A3TZV7XD	2021-04-29 16:00:00	2021-05-24 17:00:00	602	0	602
57	A3WVG6W4	2022-12-22 13:00:00	2023-01-05 11:00:00	335	0	335
58	A3XD4G3M	2022-02-04 14:00:00	2022-03-08 11:00:00	766	0	766
59	A3XGGXYP	2024-11-08 19:00:00	2024-12-09 14:00:00	740	0	740
60	A3XKMKN7	2022-12-22 13:00:00	2023-01-05 11:00:00	335	0	335
61	A3YS3GGN	2021-04-16 16:00:00	2021-06-05 00:00:00	1185	0.08	1184
62	A3ZKYBXJ	2021-04-16 16:00:00	2021-06-05 00:00:00	1185	0.08	1184
63	A46VY215	2021-04-29 13:00:00	2021-05-24 17:00:00	605	0	605
64	A4906BNR	2021-10-13 17:00:00	2021-10-27 14:00:00	334	0.6	332
65	A49RVQ3L	2023-01-05 13:00:00	2023-01-19 13:00:00	337	0	337
66	A4BZTZNQ	2021-04-16 13:00:00	2021-06-28 14:00:00	1754	0.06	1753
67	A4CQ64RP	2022-02-04 16:00:00	2022-03-08 11:00:00	764	0	764
68	A4F4R3FV	2023-01-05 13:00:00	2023-02-02 16:00:00	676	0	676
69	A4FKH4GF	2022-11-10 13:00:00	2022-11-28 12:00:00	432	0	432
70	A4FP7CRF	2023-01-05 13:00:00	2023-01-19 13:00:00	337	0	337
71	A4GHRP73	2023-07-07 14:00:00	2023-07-25 12:00:00	431	0	431
72	A4HCPHQ9	2023-01-05 13:00:00	2023-01-19 13:00:00	337	0	337
73	A4HJ6LYM	2023-07-07 17:00:00	2023-07-25 12:00:00	428	0	428
74	A4JKGFLG	2024-11-08 19:00:00	2024-12-09 14:00:00	740	0	740
75	A4KGRMYQ	2022-10-19 14:00:00	2022-11-10 12:00:00	527	0.19	526
76	A4KLG4PM	2023-01-05 13:00:00	2023-01-19 13:00:00	337	0	337
77	A4KVG7J6	2024-05-15 13:00:00	2024-06-26 11:00:00	1007	0	1007
78	A4LTX3QM	2024-02-28 13:00:00	2024-05-15 12:00:00	1848	0	1848
79	A4MBTCFZ	2021-01-27 14:00:00	2021-02-15 19:00:00	462	21.86	361
80	A4MNMHLF	2022-12-22 13:00:00	2023-01-05 11:00:00	335	0	335
81	A4N3XTQ	2022-10-19 13:00:00	2022-11-10 12:00:00	528	0.19	527
82	A4NK73XK	2023-07-25 12:00:00	2023-08-11 12:00:00	409	0	409
83	A4NP3XJR	2023-08-11 16:00:00	2023-09-05 12:00:00	597	0	597
84	A4NRKT3Y	2024-02-28 12:00:00	2024-05-15 12:00:00	1849	0	1849
85	A4QJ7YYX	2022-03-08 16:00:00	2022-03-30 15:00:00	528	10.04	475
86	A4R67DLC	2021-04-16 15:00:00	2021-06-05 00:00:00	1186	0.08	1185
87	A4SJ326S	2021-04-29 14:00:00	2021-06-07 16:00:00	939	0.11	938
88	A4V9TYLY	2022-11-10 13:00:00	2022-11-28 12:00:00	432	0	432
89	A4VGVFMQ	2023-01-05 14:00:00	2023-01-19 13:00:00	336	0	336
90	A4XNCWTP	2022-11-10 14:00:00	2022-11-28 12:00:00	431	0	431
91	A4Y5T1N4	2021-01-27 14:00:00	2021-02-18 12:00:00	527	31.5	361
92	A4YRYKHW	2023-08-11 16:00:00	2023-09-05 12:00:00	597	0	597
93	A4ZH9PDW	2021-04-16 13:00:00	2021-06-28 13:00:00	1753	0.06	1752
94	A51L01SS	2021-01-27 14:00:00	2021-02-15 19:00:00	462	21.86	361
95	A520Y11R	2022-02-04 17:00:00	2022-03-08 11:00:00	763	0	763
96	A55LX3JK	2021-10-01 14:00:00	2022-05-12 10:00:00	5349	1.07	5292
97	A56WSKQK	2022-03-08 13:00:00	2022-03-30 15:00:00	531	9.98	478
98	A58MYYZG	2022-02-04 17:00:00	2022-03-08 11:00:00	763	0	763
99	A59H491W	2022-03-30 16:00:00	2022-05-12 10:00:00	1027	0.19	1025
100	A5BY6XCB	2021-10-13 17:00:00	2021-10-27 14:00:00	334	0.6	332
101	A5DMJD25	2021-02-10 15:00:00	2021-06-05 00:00:00	2746	9.54	2484
102	A5DN1GBC	2021-05-11 14:00:00	2021-07-12 12:00:00	1487	0.07	1486
103	A5FH8VYK	2022-02-04 15:00:00	2022-03-08 11:00:00	765	0	765
104	A5L38R9F	2022-02-04 17:00:00	2022-03-08 11:00:00	763	0	763
105	A5LRB358	2021-10-13 15:00:00	2021-10-27 14:00:00	336	0.6	334
106	A5PJ3YS5	2022-02-04 14:00:00	2022-03-08 11:00:00	766	0	766
107	A5X60912	2021-10-01 16:00:00	2021-10-13 13:00:00	286	0	286
108	A5XRYSYD	2021-10-01 15:00:00	2021-10-13 13:00:00	287	0	287
109	A61DSG0C	2021-02-10 14:00:00	2021-06-05 00:00:00	2747	9.54	2485
110	A63GRYRR	2023-07-07 12:00:00	2023-07-25 12:00:00	433	0	433
111	A63KCWGJ	2023-01-05 15:00:00	2023-02-02 14:00:00	672	0	672
112	A640BNCD	2020-12-18 07:00:00	2021-01-23 10:00:00	868	0	868

113	A64LMNF4	2023-07-07 12:00:00	2023-07-25 12:00:00	433	0	433
114	A66CL7Q3	2024-02-28 13:00:00	2024-05-15 12:00:00	1848	0	1848
115	A66JF74Y	2023-07-07 14:00:00	2023-07-25 12:00:00	431	0	431
116	A66MVJVJ	2023-07-07 12:00:00	2023-07-25 12:00:00	433	0	433
117	A67PMT6T	2022-10-19 16:00:00	2022-11-10 12:00:00	525	0.19	524
118	A6CYLXY6	2023-07-25 12:00:00	2023-08-11 12:00:00	409	0	409
119	A6GQYNOK	2021-02-10 12:00:00	2021-06-30 17:00:00	3366	7.78	3104
120	A6GQYPB5	2021-02-10 12:00:00	2021-05-14 11:00:00	4464	11.69	3942
121	A6HC48H8	2021-10-13 16:00:00	2021-10-27 14:00:00	335	0.6	333
122	A6JF3J66	2022-11-10 13:00:00	2022-11-28 12:00:00	432	0	432
123	A6Q4BM26	2021-01-27 15:00:00	2021-02-18 12:00:00	526	31.56	360
124	A6QB5NMJ	2023-03-31 00:00:00	2023-07-07 10:00:00	2363	0	2363
125	A6RW5RM2	2022-02-04 16:00:00	2022-03-08 11:00:00	764	0	764
126	A6RZYOST	2021-03-24 16:00:00	2021-06-29 09:00:00	2322	0.04	2321
127	A6WG76WH	2021-05-11 14:00:00	2021-07-12 12:00:00	1487	0.07	1486
128	A6XGDF2C	2022-03-08 16:00:00	2022-03-30 15:00:00	528	10.04	475
129	A6XR1V8N	2021-11-10 14:00:00	2021-11-24 15:00:00	338	0	338
130	A6ZKPGHJ	2021-01-27 14:00:00	2021-02-15 19:00:00	462	21.86	361
131	A71R6VK1	2021-10-01 13:00:00	2021-10-13 13:00:00	578	0	578
132	A73F94NH	2023-07-07 17:00:00	2023-07-25 12:00:00	428	0	428
133	A73KXWPM	2023-01-05 13:00:00	2023-02-02 14:00:00	674	0	674
134	A7682FDJ	2021-05-11 15:00:00	2021-06-08 22:00:00	680	0.15	679
135	A7834S3T	2023-03-31 00:00:00	2023-07-07 10:00:00	2363	0	2363
136	A7C6RNYW	2023-07-07 17:00:00	2023-07-25 12:00:00	428	0	428
137	A7FPHG7V	2023-11-24 19:00:00	2024-02-27 11:00:00	2273	0	2273
138	A7G4HP73	2022-12-22 12:00:00	2023-01-05 11:00:00	336	0	336
139	A7GB59JG	2021-10-27 14:00:00	2021-11-10 13:00:00	672	0	672
140	A7GF9WN7	2023-07-07 12:00:00	2023-07-25 12:00:00	433	0	433
141	A7K3337L	2022-10-19 14:00:00	2022-11-10 12:00:00	527	0.19	526
142	A7K7RL6R	2024-02-28 12:00:00	2024-05-15 12:00:00	1849	0	1849
143	A7NQ5D5Y	2021-10-27 12:00:00	2021-11-10 13:00:00	676	0	676
144	A7NTRNNH	2022-10-19 12:00:00	2022-11-10 12:00:00	529	0.19	528
145	A7PBD8ZR	2021-10-01 16:00:00	2021-10-13 13:00:00	286	0	286
146	A7R0844Q	2021-02-10 13:00:00	2021-06-05 00:00:00	2748	9.53	2486
147	A7R2JL8S	2021-02-10 15:00:00	2021-06-03 11:00:00	2709	9.67	2447
148	A7TQVG79	2021-05-11 14:00:00	2021-06-18 00:00:00	899	0.11	898
149	A7TS84C4	2022-03-08 16:00:00	2022-03-30 15:00:00	528	10.04	475
150	A7WLFVHN	2023-07-07 14:00:00	2023-07-25 12:00:00	431	0	431
151	A7X3JWNM	2023-07-07 12:00:00	2023-07-25 12:00:00	433	0	433
152	A7XCQ764	2023-07-25 11:00:00	2023-08-11 12:00:00	410	0	410
153	A7Y7PQ49	2023-01-05 12:00:00	2023-01-19 13:00:00	338	0	338
154	A7Y9WHYD	2020-12-18 07:00:00	2021-01-22 09:00:00	843	0	843
155	A87F54RP	2022-02-04 14:00:00	2022-03-08 11:00:00	766	0	766
156	A89B69WZ	2021-11-24 19:00:00	2021-12-08 11:00:00	658	0	658
157	A8FT4H8N	2022-02-04 17:00:00	2022-03-08 11:00:00	763	0	763
158	A8HZ08D0	2021-08-24 12:00:00	2021-09-06 15:00:00	316	0	316
159	A8K1L5DF	2022-02-04 14:00:00	2022-03-08 11:00:00	766	0	766
160	A8THQR6Z	2020-12-18 06:00:00	2021-01-28 23:00:00	1002	0	1002
161	A8V2YFM6	2021-10-01 13:00:00	2021-10-13 13:00:00	289	0	289
162	A8XTXZFW	2021-04-29 12:00:00	2021-05-24 17:00:00	606	0	606
163	A8YJ320G	2021-04-29 12:00:00	2021-05-24 17:00:00	606	0	606
164	A900M97B	2021-11-24 16:00:00	2021-12-08 11:00:00	332	0	332
165	A91GZMQV	2022-03-08 16:00:00	2022-03-30 15:00:00	528	10.04	475
166	A91M6XL5	2021-08-24 11:00:00	2021-09-06 15:00:00	634	0	634
167	A93PWKHN	2022-08-05 10:00:00	2022-08-24 11:00:00	458	0	458
168	A9449MRR	2022-08-04 15:00:00	2022-08-24 11:00:00	477	0	477
169	A974NKKY	2023-07-07 12:00:00	2023-07-25 12:00:00	433	0	433

170	A9793KLJ	2023-01-05 14:00:00	2023-02-02 16:00:00	675	0	675
171	A97XNTKD	2021-10-27 16:00:00	2021-11-10 13:00:00	334	0	334
172	A98VZ3Z1	2021-10-01 16:00:00	2021-10-13 13:00:00	286	0	286
173	A9CHL9KS	2021-10-27 14:00:00	2021-11-10 13:00:00	336	0	336
174	A9CL7XVN	2022-11-10 13:00:00	2022-11-28 12:00:00	432	0	432
175	A9DWKPVP	2021-08-24 12:00:00	2021-09-06 15:00:00	632	0	632
176	A9G7TH00	2021-04-16 14:00:00	2021-06-28 14:00:00	1753	0.06	1752
177	A9GH0PR7	2021-10-01 15:00:00	2021-10-13 13:00:00	574	0	574
178	A9HRX1MC	2021-11-10 16:00:00	2021-11-24 15:00:00	336	0	336
179	A9JWGN76	2023-08-11 12:00:00	2023-09-05 12:00:00	601	0	601
180	A9JYHMCV	2023-01-05 12:00:00	2023-01-19 13:00:00	338	0	338
181	A9LPNMMPH	2022-12-22 13:00:00	2023-01-05 11:00:00	335	0	335
182	A9LTNYNC	2022-11-10 12:00:00	2022-11-28 12:00:00	433	0	433
183	A9MBPGH5	2022-03-08 15:00:00	2022-03-30 15:00:00	529	10.02	476
184	A9MTPKNG	2022-10-19 14:00:00	2022-11-10 12:00:00	527	0.19	526
185	A9MXQ5X	2021-10-27 14:00:00	2021-11-10 13:00:00	336	0	336
186	A9N3VY12	2021-12-08 15:00:00	2022-02-04 12:00:00	1390	0	1390
187	A9NGLD97	2021-04-16 15:00:00	2021-06-05 00:00:00	1186	0.08	1185
188	A9PFPKRK	2022-10-19 13:00:00	2022-11-10 12:00:00	528	0.19	527
189	A9QTM6HL	2024-11-08 19:00:00	2024-12-09 14:00:00	740	0	740
190	A9RNFBHT	2022-03-08 16:00:00	2022-03-30 15:00:00	528	10.04	475
191	A9RZ5BZP	2021-04-29 14:00:00	2021-06-10 06:00:00	1001	0.1	1000
192	A9T3NKKWW	2022-10-19 16:00:00	2022-11-10 12:00:00	525	0.19	524
193	A9VDNLFN	2022-02-04 17:00:00	2022-03-08 11:00:00	763	0	763
194	A9WVLXK3	2023-01-05 15:00:00	2023-02-02 14:00:00	672	0	672
195	A9XRXVFQ	2022-12-22 12:00:00	2023-01-05 11:00:00	336	0	336
196	A9XTHCMJ	2022-10-19 13:00:00	2022-11-10 12:00:00	528	0.19	527
197	A9XXF9C	2023-07-07 12:00:00	2023-07-25 12:00:00	433	0	433
198	A9YVVZSW	2021-04-16 14:00:00	2021-06-28 13:00:00	1752	0.06	1751
199	ABOLX8JC	2021-12-08 12:00:00	2022-02-04 12:00:00	1393	0	1393
200	ABOR2Y6J	2021-10-27 16:00:00	2021-11-10 13:00:00	334	0	334
201	AB2H6G26	2021-02-10 14:00:00	2021-06-05 00:00:00	2747	9.54	2485
202	AB7B00LQ	2021-10-27 14:00:00	2021-11-10 13:00:00	336	0	336
203	ABBCHEVM	2022-03-10 23:00:00	2022-03-30 15:00:00	473	11.21	420
204	ABDD0LWT	2020-12-18 07:00:00	2021-01-22 09:00:00	843	0	843
205	ABF970MZ	2022-02-04 15:00:00	2022-03-08 11:00:00	765	0	765
206	ABGZG9TW	2021-04-16 13:00:00	2021-06-28 13:00:00	1753	0.06	1752
207	ABKK8C6R	2021-05-04 16:00:00	2021-06-07 16:00:00	817	0.12	816
208	ABMKW4RK	2021-10-27 14:00:00	2021-11-10 13:00:00	336	0	336
209	ABNFXQ6Q	2021-10-14 11:00:00	2021-10-27 14:00:00	316	0.63	314
210	ABQ8SW3J	2021-11-10 11:00:00	2021-12-14 14:00:00	820	0	820
211	ABRRWPRN	2022-02-04 15:00:00	2022-03-08 11:00:00	765	0	765
212	ABS2JHGS	2021-05-11 15:00:00	2021-06-05 00:00:00	586	0.17	585
213	ABXVYGPW	2021-04-29 13:00:00	2021-06-10 06:00:00	1002	0.1	1001
214	ABZ4Z89V	2021-05-11 14:00:00	2021-07-12 12:00:00	1487	0.07	1486
215	ABZPKJ6Y	2020-12-18 07:00:00	2021-01-22 09:00:00	843	0	843
216	AC125XBV	2021-11-10 16:00:00	2021-11-24 15:00:00	336	0	336
217	AC3HX41B	2021-05-11 15:00:00	2021-06-05 00:00:00	586	0.17	585
218	AC49Y4P7	2022-08-04 15:00:00	2022-08-24 11:00:00	477	0	477
219	AC4D64KS	2021-10-13 15:00:00	2021-10-27 14:00:00	336	0.6	334
220	AC4GLLNK	2023-08-11 12:00:00	2023-09-05 12:00:00	601	0	601
221	AC4XCF67	2023-07-07 12:00:00	2023-07-25 12:00:00	433	0	433
222	AC65RNX3	2022-03-08 16:00:00	2022-03-30 15:00:00	528	10.04	475
223	AC78CBKY	2021-03-24 14:00:00	2021-06-05 00:00:00	3478	0.06	3476
224	AC8THC26	2021-10-27 14:00:00	2021-11-10 13:00:00	672	0	672
225	AC94PN3Q	2023-07-25 12:00:00	2023-08-11 12:00:00	409	0	409
226	ACBB22RZ	2021-10-13 18:00:00	2021-10-27 14:00:00	333	0.6	331

227	ACCCPMQ9	2023-01-05 13:00:00	2023-01-19 13:00:00	337	0	337
228	ACGTQMHM	2023-01-05 14:00:00	2023-02-02 14:00:00	673	0	673
229	ACMQ6NMP	2024-02-28 12:00:00	2024-05-15 12:00:00	1849	0	1849
230	ACNS6P37	2021-08-24 12:00:00	2021-09-06 15:00:00	316	0	316
231	ACNTMYKY	2024-05-15 13:00:00	2024-06-26 11:00:00	1007	0	1007
232	ACPXC6RP	2022-10-19 12:00:00	2022-11-10 12:00:00	529	0.19	528
233	ACQ6YT9T	2022-10-19 14:00:00	2022-11-10 12:00:00	527	0.19	526
234	ACQHV37K	2023-11-24 19:00:00	2024-02-27 11:00:00	2273	0	2273
235	ACQWP7Q7	2023-07-07 12:00:00	2023-07-25 12:00:00	433	0	433
236	ACV4N9JP	2022-08-04 15:00:00	2022-08-24 11:00:00	477	0	477
237	ACX36H9G	2022-12-22 13:00:00	2023-01-05 11:00:00	335	0	335
238	ACXLFXJL	2024-02-28 12:00:00	2024-05-15 12:00:00	1849	0	1849
239	AD2VQS57	2021-10-13 18:00:00	2021-10-27 14:00:00	333	0.6	331
240	AD38TWW5	2021-10-27 14:00:00	2021-11-10 13:00:00	672	0	672
241	AD608SZP	2021-08-24 13:00:00	2021-09-06 15:00:00	315	0	315
242	ADC57JPN	2021-03-24 14:00:00	2021-06-05 00:00:00	1739	0.06	1738
243	ADCX87FP	2021-04-29 14:00:00	2021-05-24 17:00:00	604	0	604
244	ADS13WQG	2022-03-08 13:00:00	2022-03-30 15:00:00	531	9.98	478
245	ADVX0D1W	2022-02-04 15:00:00	2022-03-08 11:00:00	765	0	765
246	ADXP0P15	2021-11-24 16:00:00	2022-03-08 11:00:00	2492	0	2492
247	ADY153L4	2021-10-13 17:00:00	2021-10-27 14:00:00	334	0.6	332
248	ADZJ1CQV	2021-10-27 16:00:00	2021-11-10 13:00:00	334	0	334
249	AF3386RN	2021-04-29 12:00:00	2021-05-24 17:00:00	606	0	606
250	AF671XJ6	2021-04-29 12:00:00	2021-05-24 17:00:00	606	0	606
251	AF6QMYCG	2022-12-22 13:00:00	2023-01-05 11:00:00	335	0	335
252	AF7MMMTY	2024-02-28 13:00:00	2024-05-15 12:00:00	1848	0	1848
253	AF8SDT8G	2022-03-30 15:00:00	2022-05-12 10:00:00	1028	0.19	1026
254	AF99JQLF	2023-07-25 13:00:00	2023-08-11 12:00:00	408	0	408
255	AFCPNQT3	2023-07-25 17:00:00	2023-08-11 12:00:00	404	0	404
256	AFCY809L	2021-10-01 14:00:00	2021-10-13 13:00:00	288	0	288
257	AFJ2WC8T	2021-10-01 15:00:00	2021-10-13 13:00:00	574	0	574
258	AFJ8DL5G	2022-03-08 15:00:00	2022-03-30 15:00:00	529	10.02	476
259	AFJD2TT0	2021-07-12 12:00:00	2021-09-30 16:00:00	1925	0	1925
260	AFL82W0Z	2021-10-01 15:00:00	2021-10-13 13:00:00	287	0	287
261	AFM334TS	2020-12-18 07:00:00	2021-01-28 23:00:00	1001	0	1001
262	AFM3RV9X	2022-10-19 16:00:00	2022-11-10 12:00:00	525	0.19	524
263	AFM7BS07	2021-01-27 14:00:00	2021-02-15 19:00:00	462	21.86	361
264	AFMC9TRV	2023-01-05 15:00:00	2023-02-02 16:00:00	1348	0	1348
265	AFN6QH4F	2023-08-11 12:00:00	2023-09-05 12:00:00	601	0	601
266	AFRPTLMP	2022-10-19 13:00:00	2022-11-10 12:00:00	528	0.19	527
267	AFTN3XTG	2023-08-11 17:00:00	2023-09-05 12:00:00	596	0	596
268	AFX3G7V4	2023-07-07 12:00:00	2023-07-25 12:00:00	433	0	433
269	AFXG7YMK	2023-07-25 12:00:00	2023-08-11 12:00:00	409	0	409
270	AFZH4TTD	2021-10-13 17:00:00	2021-10-27 14:00:00	668	0.6	664
271	AG3YLG7K	2023-07-07 15:00:00	2023-07-25 12:00:00	430	0	430
272	AG4PMJRL	2024-05-15 13:00:00	2024-06-26 11:00:00	1007	0	1007
273	AG4WNXXF	2023-11-24 20:00:00	2024-02-27 11:00:00	2272	0	2272
274	AG5R906F	2022-02-04 14:00:00	2022-03-08 11:00:00	766	0	766
275	AG6MNG4R	2022-12-22 15:00:00	2023-01-05 11:00:00	333	0	333
276	AG6VCJJG	2024-11-08 19:00:00	2024-12-09 14:00:00	740	0	740
277	AG7WFZL1	2021-01-27 13:00:00	2021-06-05 08:00:00	3092	8.47	2830
278	AG9Q64FR	2022-11-10 13:00:00	2022-11-28 12:00:00	432	0	432
279	AGFX6FLM	2022-12-22 15:00:00	2023-01-05 11:00:00	333	0	333
280	AGH6P1GM	2021-05-11 14:00:00	2021-06-09 18:00:00	701	0.14	700
281	AGHKT9NG	2023-01-05 13:00:00	2023-01-19 13:00:00	337	0	337
282	AGJ477F7	2023-11-25 00:00:00	2024-02-27 11:00:00	2268	0	2268
283	AGJKJNCT	2023-07-07 12:00:00	2023-07-25 12:00:00	433	0	433

284	AGJPW6WM	2023-08-11 12:00:00	2023-09-05 12:00:00	601	0	601
285	AGJY5BD1	2021-02-10 15:00:00	2021-06-05 00:00:00	2746	9.54	2484
286	AGLCXGYN	2023-01-05 13:00:00	2023-01-19 13:00:00	674	0	674
287	AGNKM6HL	2023-07-25 14:00:00	2023-08-11 12:00:00	407	0	407
288	AGNN4QMG	2022-10-19 13:00:00	2022-11-10 12:00:00	528	0.19	527
289	AGR43YMK	2023-01-05 15:00:00	2023-02-02 16:00:00	674	0	674
290	AGR9CMTR	2023-08-11 17:00:00	2023-09-05 12:00:00	596	0	596
291	AGRX3HC4	2023-07-07 15:00:00	2023-07-25 12:00:00	430	0	430
292	AGTWG4P4	2022-10-19 14:00:00	2022-11-10 12:00:00	527	0.19	526
293	AGW3DV5P	2021-03-24 14:00:00	2021-06-05 00:00:00	1739	0.06	1738
294	AGWX7P	2022-03-08 16:00:00	2022-03-30 15:00:00	528	10.04	475
295	AGWHMYCN	2022-10-19 13:00:00	2022-11-10 12:00:00	528	0.19	527
296	AGYCPJDB	2020-12-18 07:00:00	2021-01-23 10:00:00	1736	0	1736
297	AGYP9708	2021-11-10 11:00:00	2021-12-14 14:00:00	1640	0	1640
298	AHDCCSQN	2022-03-08 13:00:00	2022-03-30 15:00:00	531	9.98	478
299	AH1RL98J	2022-03-08 16:00:00	2022-03-30 15:00:00	528	10.04	475
300	AH4GKWW7	2024-05-15 13:00:00	2024-06-26 11:00:00	1007	0	1007
301	AH67C79G	2023-07-25 14:00:00	2023-08-11 12:00:00	407	0	407
302	AH67QGC3	2022-12-22 15:00:00	2023-01-05 11:00:00	333	0	333
303	AH77XTQF	2021-05-04 17:00:00	2021-06-05 00:00:00	752	0.13	751
304	AHD1RTJ6	2021-10-13 15:00:00	2021-10-27 14:00:00	336	0.6	334
305	AHFGTVTG	2023-07-25 17:00:00	2023-08-11 12:00:00	404	0	404
306	AHGK4Q9L	2024-05-15 13:00:00	2024-06-26 11:00:00	1007	0	1007
307	AHGTCPCT	2022-08-04 15:00:00	2022-08-24 11:00:00	477	0	477
308	AHPXP1JB	2021-02-14 12:00:00	2021-06-05 00:00:00	2653	7.27	2460
309	AHQ7YHWX	2023-07-25 12:00:00	2023-08-11 12:00:00	409	0	409
310	AHQNVLH4	2023-07-07 15:00:00	2023-07-25 12:00:00	430	0	430
311	AHQQR8XG2	2022-02-04 16:00:00	2022-03-08 11:00:00	764	0	764
312	AHQTVKVMV	2023-01-05 15:00:00	2023-02-02 16:00:00	674	0	674
313	AHRYFRTG	2023-01-05 13:00:00	2023-01-19 13:00:00	337	0	337
314	AHSFF4P8	2022-02-04 16:00:00	2022-03-08 11:00:00	764	0	764
315	AHTTQ7M7	2023-07-07 18:00:00	2023-07-25 12:00:00	427	0	427
316	AHVVKWHGQ	2023-08-11 17:00:00	2023-09-05 12:00:00	596	0	596
317	AHWXLSZ9	2021-04-16 14:00:00	2021-06-05 00:00:00	1187	0.08	1186
318	AHX79QHW	2023-07-25 11:00:00	2023-08-11 12:00:00	410	0	410
319	AHYPNGCH	2023-08-11 12:00:00	2023-09-05 12:00:00	601	0	601
320	AHZ6LG4H	2021-10-27 13:00:00	2021-11-10 13:00:00	674	0	674
321	AHZ7100Q	2021-10-13 15:00:00	2021-10-27 14:00:00	336	0.6	334
322	AHZCR5VJ	2021-10-13 17:00:00	2021-10-27 14:00:00	334	0.6	332
323	AHZPHD60	2022-03-08 16:00:00	2022-03-30 15:00:00	528	10.04	475
324	AJ0BCSSD	2021-10-14 11:00:00	2021-10-27 14:00:00	316	0.63	314
325	AJ0TC8ZG	2022-03-08 13:00:00	2022-03-30 15:00:00	531	9.98	478
326	AJ1085D4	2021-01-27 15:00:00	2021-02-12 09:00:00	379	5.01	360
327	AJ49HCGN	2022-08-04 15:00:00	2022-08-24 11:00:00	477	0	477
328	AJ71T3GP	2021-04-16 13:00:00	2021-06-28 13:00:00	1753	0.06	1752
329	AJGBLH7M	2021-10-27 15:00:00	2021-11-24 15:00:00	673	0	673
330	AJGMPCPJ	2023-01-05 15:00:00	2023-01-19 13:00:00	335	0	335
331	AJJ078T0	2022-02-04 15:00:00	2022-03-08 11:00:00	765	0	765
332	AJJV67LC	2024-11-08 19:00:00	2024-12-09 14:00:00	740	0	740
333	AJJXKHR3	2023-01-05 15:00:00	2023-02-02 14:00:00	672	0	672
334	AJK2V2MX	2021-04-16 16:00:00	2021-06-29 09:00:00	1770	0.06	1769
335	AJM0P0HB	2021-02-10 14:00:00	2021-06-05 00:00:00	2747	9.54	2485
336	AJMHR6VY	2021-04-29 12:00:00	2021-05-24 17:00:00	606	0	606
337	AJNGKKP9	2023-01-05 13:00:00	2023-01-19 13:00:00	337	0	337
338	AJRGGFTW	2022-10-19 14:00:00	2022-11-10 12:00:00	527	0.19	526
339	AJS4R98L	2021-10-13 16:00:00	2021-10-27 14:00:00	335	0.6	333
340	AJTPF7QN	2022-11-10 13:00:00	2022-11-28 12:00:00	432	0	432

341	AJTQT666	2023-11-24 19:00:00	2024-02-27 11:00:00	2273	0	2273
342	AJTWFKVC	2022-10-19 12:00:00	2022-11-10 12:00:00	529	0.19	528
343	AJV35PYC	2021-04-16 13:00:00	2021-06-05 00:00:00	1188	0.08	1187
344	AJVCN6VR	2024-02-28 13:00:00	2024-05-15 12:00:00	1848	0	1848
345	AJVFX57	2021-10-13 17:00:00	2021-10-27 14:00:00	334	0.6	332
346	AJVJLFX7	2023-08-11 14:00:00	2023-09-05 12:00:00	599	0	599
347	AJVN3VM7	2024-05-15 12:00:00	2024-06-26 11:00:00	1011	0	1011
348	AJYPMNH3	2022-08-05 10:00:00	2022-08-24 11:00:00	458	0	458
349	AJZP5VRL	2021-02-10 15:00:00	2021-06-29 09:00:00	3331	7.87	3069
350	AK1J9WNF	2021-10-27 14:00:00	2021-11-10 13:00:00	672	0	672
351	AK3NQ8HY	2022-03-30 15:00:00	2022-05-12 10:00:00	1028	0.19	1026
352	AK44N3RN	2023-07-25 17:00:00	2023-08-11 12:00:00	404	0	404
353	AK6890PH	2021-10-13 15:00:00	2021-10-27 14:00:00	336	0.6	334
354	AK6H84M9	2021-10-27 13:00:00	2021-11-10 13:00:00	674	0	674
355	AK7YQRDK	2021-10-01 13:00:00	2021-10-13 13:00:00	578	0	578
356	AK947TVJ	2024-11-08 19:00:00	2024-12-09 14:00:00	740	0	740
357	AKB5MCTS	2021-04-16 14:00:00	2021-06-25 16:00:00	1683	0.06	1682
358	AKCCK47P9	2023-11-25 01:00:00	2024-02-27 11:00:00	2267	0	2267
359	AKCQ897B	2021-04-29 12:00:00	2021-05-24 17:00:00	606	0	606
360	AKCVJY4J	2022-11-10 13:00:00	2022-11-28 12:00:00	432	0	432
361	AKCX3LFC	2023-01-05 13:00:00	2023-01-19 13:00:00	337	0	337
362	AKFJ7F4N	2022-12-22 13:00:00	2023-01-05 11:00:00	335	0	335
363	AKG6JFQH	2022-10-19 13:00:00	2022-11-10 12:00:00	528	0.19	527
364	AKGYGQQ	2024-02-28 12:00:00	2024-05-15 12:00:00	1849	0	1849
365	AKHHGNMC	2022-11-10 12:00:00	2022-11-28 12:00:00	433	0	433
366	AKHNJ65X	2021-01-27 14:00:00	2021-02-15 19:00:00	462	21.86	361
367	AKJ97THK	2023-08-11 17:00:00	2023-09-05 12:00:00	596	0	596
368	AKLCDY9Z	2021-10-13 16:00:00	2021-10-27 14:00:00	335	0.6	333
369	AKNW43NG	2022-12-22 13:00:00	2023-01-05 11:00:00	335	0	335
370	AKPCX63V	2023-07-07 18:00:00	2023-07-25 12:00:00	427	0	427
371	AKPQ6WXH	2021-01-27 14:00:00	2021-02-12 09:00:00	380	5	361
372	AKPYHRJW	2024-05-15 13:00:00	2024-06-26 11:00:00	1007	0	1007
373	AKQSLMCO	2021-04-29 14:00:00	2021-06-09 05:00:00	976	0.1	975
374	AKV51LB8	2022-02-04 16:00:00	2022-03-08 11:00:00	764	0	764
375	AKV9FQXT	2023-07-07 18:00:00	2023-07-25 12:00:00	427	0	427
376	AKVGBNJR	2021-11-10 15:00:00	2021-11-24 12:00:00	334	0	334
377	AKVM4XKJ	2023-01-05 15:00:00	2023-02-02 14:00:00	672	0	672
378	AKXQRGFP	2023-07-07 15:00:00	2023-07-25 12:00:00	430	0	430
379	AKXYN3CW	2021-03-24 14:00:00	2021-06-05 00:00:00	1739	0.06	1738
380	AKZ75N0S	2021-10-27 13:00:00	2021-11-10 13:00:00	337	0	337
381	AL19S6YZ	2021-03-24 13:00:00	2021-07-30 14:00:00	3074	0.03	3073
382	AL1GYP52	2021-01-27 13:00:00	2021-02-10 11:00:00	335	0	335
383	AL35LGPR	2021-04-29 14:00:00	2021-06-05 00:00:00	875	0.11	874
384	AL3N7T4H	2021-10-27 13:00:00	2021-11-10 13:00:00	674	0	674
385	AL4Y7KGQ	2023-08-11 14:00:00	2023-09-05 12:00:00	599	0	599
386	AL66R7M9	2023-08-11 14:00:00	2023-09-05 12:00:00	599	0	599
387	AL6K6YL8	2022-03-08 16:00:00	2022-03-30 15:00:00	528	10.04	475
388	AL6T3MYP	2023-07-25 13:00:00	2023-08-11 12:00:00	408	0	408
389	AL70BB72	2021-10-27 13:00:00	2021-11-10 13:00:00	674	0	674
390	AL9H4QKC	2023-11-24 19:00:00	2024-02-27 11:00:00	4546	0	4546
391	ALF3QLGQ	2023-07-07 15:00:00	2023-07-25 12:00:00	430	0	430
392	ALG4G6ML	2022-12-22 12:00:00	2023-01-05 11:00:00	336	0	336
393	ALGDM8PL	2021-10-14 11:00:00	2021-10-27 14:00:00	316	0.63	314
394	ALJGMDHK	2022-03-08 15:00:00	2022-03-30 15:00:00	529	10.02	476
395	ALJXJFLF	2023-07-07 12:00:00	2023-07-25 12:00:00	433	0	433
396	ALKW77W7	2022-03-30 16:00:00	2022-05-12 10:00:00	1027	0.19	1025
397	ALL64YFL	2023-07-25 17:00:00	2023-08-11 12:00:00	404	0	404

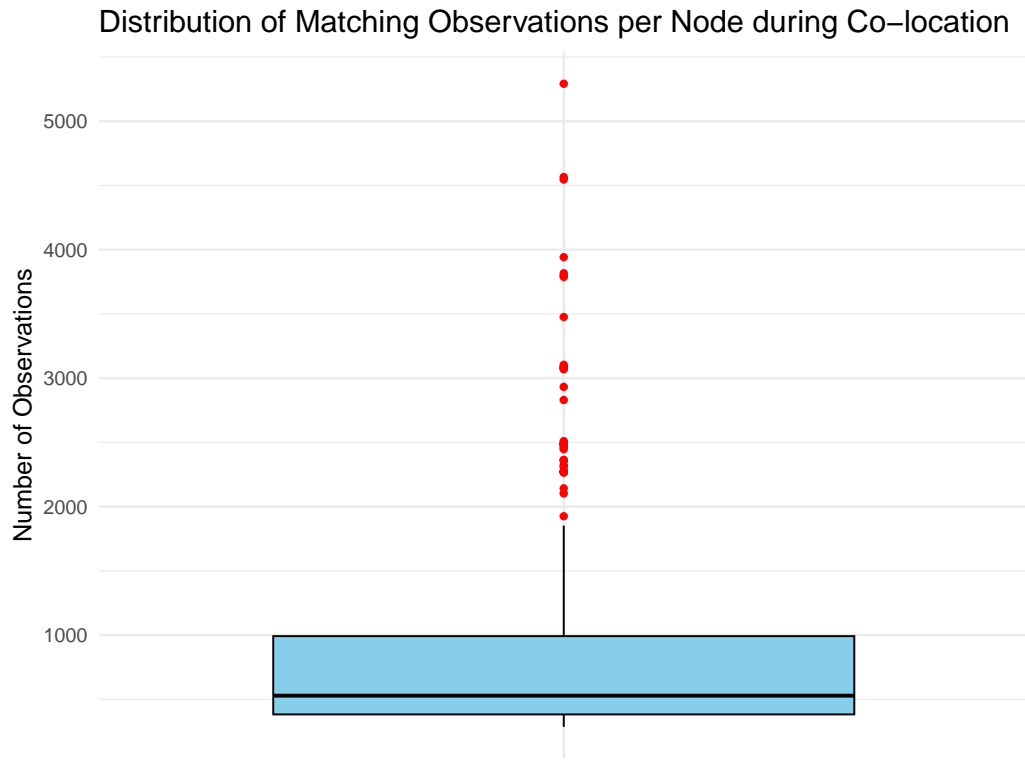
398	ALNJWLLJ	2023-01-05 15:00:00	2023-02-02 14:00:00	672	0	672
399	ALPYC8ZL	2020-12-18 07:00:00	2021-06-05 00:00:00	4050	6.47	3788
400	ALQ2MZ40	2021-02-10 16:00:00	2021-07-30 14:00:00	4079	6.42	3817
401	ALQ6D53S	2021-10-27 14:00:00	2021-11-10 13:00:00	336	0	336
402	ALQVX9CT	2023-11-25 01:00:00	2024-02-27 11:00:00	2267	0	2267
403	ALS35W89	2021-04-29 16:00:00	2021-05-24 17:00:00	602	0	602
404	ALSVJRT7	2021-04-16 15:00:00	2021-06-28 13:00:00	1751	0.06	1750
405	ALVQVGRP	2021-11-10 15:00:00	2021-11-24 12:00:00	668	0	668
406	ALYHTVVC	2022-11-10 12:00:00	2022-11-28 12:00:00	433	0	433
407	ALYLPH6X	2022-03-08 15:00:00	2022-03-30 15:00:00	529	10.02	476
408	AM06S5MV	2021-02-10 13:00:00	2021-06-05 00:00:00	2748	9.53	2486
409	AM198N4N	2021-11-24 16:00:00	2021-12-08 11:00:00	332	0	332
410	AM1Q4C3P	2021-02-10 15:00:00	2021-06-05 00:00:00	2746	9.54	2484
411	AM5T4RFC	2022-03-08 16:00:00	2022-03-30 15:00:00	528	10.04	475
412	AM6M7FJW	2023-11-25 01:00:00	2024-02-27 11:00:00	2267	0	2267
413	AM79N4KZ	2021-11-24 16:00:00	2022-02-04 12:00:00	1725	0	1725
414	AM86S1FB	2021-04-29 13:00:00	2021-06-03 22:00:00	850	0.12	849
415	AMHFLVM9	2022-12-22 13:00:00	2023-01-05 11:00:00	335	0	335
416	AMLH4MWX	2022-12-22 13:00:00	2023-01-05 11:00:00	335	0	335
417	AMLKW32G	2022-02-04 17:00:00	2022-03-08 11:00:00	763	0	763
418	AMLKWXLQ	2024-02-28 13:00:00	2024-05-15 12:00:00	1848	0	1848
419	AMML44RH	2023-11-24 19:00:00	2024-02-27 11:00:00	2273	0	2273
420	AMRVYTMY	2022-11-10 13:00:00	2022-11-28 12:00:00	432	0	432
421	AMVQRGC6	2023-11-24 19:00:00	2024-05-01 00:00:00	3798	0	3798
422	AMYQNRPW	2022-08-05 10:00:00	2022-08-24 11:00:00	458	0	458
423	AN18W133	2021-02-10 13:00:00	2021-06-05 00:00:00	2748	9.53	2486
424	AN2GM079	2021-05-11 14:00:00	2021-06-23 07:00:00	1026	0.1	1025
425	AN3GTRJY	2024-11-08 19:00:00	2024-12-09 14:00:00	740	0	740
426	AN3Y39L4	2022-12-22 13:00:00	2023-01-05 11:00:00	335	0	335
427	AN58KQ8Q	2022-02-04 17:00:00	2022-03-08 11:00:00	763	0	763
428	AN69F9C6	2024-11-08 18:00:00	2024-12-09 14:00:00	741	0	741
429	AN757QF8	2022-02-04 17:00:00	2022-03-08 11:00:00	763	0	763
430	AN7FL4FX	2022-10-19 14:00:00	2022-11-10 12:00:00	527	0.19	526
431	AN7GG79F	2024-11-08 19:00:00	2024-12-09 14:00:00	740	0	740
432	AN7P7N7G	2023-11-24 19:00:00	2024-02-27 11:00:00	2273	0	2273
433	AN7TPXPW6	2023-08-11 12:00:00	2023-09-05 12:00:00	601	0	601
434	AN937CLQ	2023-07-25 13:00:00	2023-08-11 12:00:00	408	0	408
435	AN94KMCX	2023-07-07 15:00:00	2023-07-25 12:00:00	430	0	430
436	AN9GCJ62	2021-10-27 14:00:00	2021-11-10 13:00:00	672	0	672
437	AN9JPM7W	2023-08-11 13:00:00	2023-09-05 12:00:00	1200	0	1200
438	ANB427YP	2022-03-08 15:00:00	2022-03-30 15:00:00	529	10.02	476
439	ANCTVWLR	2023-11-24 18:00:00	2024-02-27 11:00:00	2274	0	2274
440	ANDWDJJZ	2022-03-08 16:00:00	2022-03-30 15:00:00	528	10.04	475
441	ANJNQMM7	2023-07-07 15:00:00	2023-07-25 12:00:00	430	0	430
442	ANK1W6Y5	2021-10-27 13:00:00	2021-11-10 13:00:00	674	0	674
443	ANMQY861	2020-12-18 06:00:00	2021-02-10 11:00:00	1302	0	1302
444	ANNZ9H0K	2021-08-24 12:00:00	2021-09-06 15:00:00	948	0	948
445	ANPCG993	2023-07-07 12:00:00	2023-07-25 12:00:00	433	0	433
446	ANQQKMY3	2022-12-22 15:00:00	2023-01-05 11:00:00	334	0	334
447	ANQY9PPR	2021-11-10 15:00:00	2021-11-24 12:00:00	334	0	334
448	ANR9CRN3	2023-01-05 15:00:00	2023-02-02 16:00:00	1348	0	1348
449	ANRRX430	2022-02-04 17:00:00	2022-03-30 15:00:00	1295	4.09	1242
450	ANTLJ53X	2021-03-24 14:00:00	2021-06-05 00:00:00	1739	0.06	1738
451	ANW7RN4M	2023-07-25 17:00:00	2023-08-11 12:00:00	404	0	404
452	ANWF7CCY	2024-05-15 13:00:00	2024-06-26 11:00:00	1007	0	1007
453	ANX6NMT6	2022-08-04 15:00:00	2022-08-24 11:00:00	477	0	477
454	ANXNLK37	2022-12-22 13:00:00	2023-01-05 11:00:00	335	0	335

455	ANXWMX6J	2024-11-08 19:00:00	2024-12-09 14:00:00	740	0	740
456	ANYN43V3	2022-12-22 13:00:00	2023-01-05 11:00:00	335	0	335
457	ANZ0CBLJ	2021-02-10 15:00:00	2021-06-05 00:00:00	2746	9.54	2484
458	AP2GNB15	2021-04-29 13:00:00	2021-06-09 05:00:00	977	0.1	976
459	AP34CQX7	2021-10-13 16:00:00	2021-10-27 14:00:00	335	0.6	333
460	AP43DQGX	2021-10-01 15:00:00	2021-10-13 13:00:00	287	0	287
461	AP6NPNG3	2023-07-25 18:00:00	2023-08-11 12:00:00	403	0	403
462	AP94SLZ4	2021-10-13 15:00:00	2021-10-27 14:00:00	336	0.6	334
463	AP96K4JY	2022-10-19 13:00:00	2022-11-10 12:00:00	528	0.19	527
464	AP977TK9	2024-05-15 12:00:00	2024-06-26 11:00:00	1008	0	1008
465	APF23JMJ	2021-03-24 14:00:00	2021-06-05 00:00:00	1739	0.06	1738
466	APFTJNKH	2023-01-05 13:00:00	2023-01-19 13:00:00	337	0	337
467	APG9NJLT	2024-11-08 18:00:00	2024-12-09 14:00:00	741	0	741
468	APGTVQH0	2022-03-08 16:00:00	2022-03-30 15:00:00	528	10.04	475
469	APGVT5WBT	2021-10-14 11:00:00	2021-10-27 14:00:00	316	0.63	314
470	APJHP47R	2021-11-24 19:00:00	2021-12-08 11:00:00	329	0	329
471	APJMKVF6	2024-11-08 19:00:00	2024-12-09 14:00:00	740	0	740
472	APKXXVX6	2023-07-07 18:00:00	2023-07-25 12:00:00	427	0	427
473	APM2HW6P	2021-11-10 14:00:00	2021-11-24 13:00:00	336	0	336
474	APMLPGWL	2023-01-05 13:00:00	2023-02-02 14:00:00	674	0	674
475	APP20K6Y	2021-04-29 13:00:00	2021-06-09 05:00:00	977	0.1	976
476	APR8W2KS	2021-10-01 14:00:00	2021-10-13 13:00:00	288	0	288
477	APRFKXLT	2023-07-07 15:00:00	2023-07-25 12:00:00	430	0	430
478	APRV79WL	2023-08-11 17:00:00	2023-09-05 12:00:00	596	0	596
479	APV46KGH	2023-01-05 13:00:00	2023-01-19 13:00:00	337	0	337
480	APV9CV9L	2022-10-19 13:00:00	2022-11-10 12:00:00	528	0.19	527
481	APW556XZ	2020-12-18 06:00:00	2021-02-12 13:00:00	1352	1.7	1329
482	APWY5WWD	2021-10-27 12:00:00	2021-11-10 13:00:00	676	0	676
483	APY74G8X	2021-04-29 15:00:00	2021-06-10 06:00:00	1000	0.1	999
484	APZDLCWL	2021-02-10 11:00:00	2021-03-24 13:00:00	1011	25.82	750
485	AQN272X	2021-10-01 15:00:00	2021-10-13 13:00:00	287	0	287
486	AQ2XM3JF	2021-04-29 15:00:00	2021-06-23 12:00:00	1318	0.08	1317
487	AQ37XYM2	2021-02-10 15:00:00	2021-06-05 00:00:00	2746	9.54	2484
488	AQ3JQ6DH	2021-11-15 17:00:00	2021-12-08 11:00:00	547	0	547
489	AQ77WPFF	2022-08-05 10:00:00	2022-08-24 11:00:00	458	0	458
490	AQ7JLRMN	2022-10-19 12:00:00	2022-11-10 12:00:00	529	0.19	528
491	AQ93NVYR	2024-11-08 19:00:00	2024-12-09 14:00:00	740	0	740
492	AQCJ92MP	2021-05-11 14:00:00	2021-06-05 00:00:00	587	0.17	586
493	AQCP6PRW	2023-07-25 18:00:00	2023-08-11 12:00:00	403	0	403
494	AQG9CGCT	2024-11-08 19:00:00	2024-12-09 14:00:00	740	0	740
495	AQGZH3C5	2021-10-01 13:00:00	2021-12-17 18:00:00	1854	0.11	1852
496	AQH0R1R5	2021-10-27 15:00:00	2021-11-10 13:00:00	335	0	335
497	AQH4K9RP	2022-08-04 15:00:00	2022-08-24 11:00:00	477	0	477
498	AQLK7MXK	2022-10-19 16:00:00	2022-11-10 12:00:00	525	0.19	524
499	AQLNLXKF	2023-01-05 13:00:00	2023-02-02 16:00:00	676	0	676
500	AQM6BTT8	2021-11-10 16:00:00	2021-11-24 12:00:00	333	0	333
501	AQM8WX0J	2021-10-27 14:00:00	2021-11-10 13:00:00	336	0	336
502	AQMN49F4	2024-05-15 11:00:00	2024-08-12 16:00:00	2142	0	2142
503	AQMWMQ9X	2022-12-22 15:00:00	2023-01-05 11:00:00	333	0	333
504	AQPNP33R	2022-10-19 12:00:00	2022-11-10 12:00:00	529	0.19	528
505	AQPZX0ZB	2021-08-24 12:00:00	2021-09-06 15:00:00	316	0	316
506	AQQ4MDXH	2021-11-24 16:00:00	2021-12-08 11:00:00	332	0	332
507	AQRTKRXH	2023-11-24 12:00:00	2024-04-01 00:00:00	3085	0	3085
508	AQS3FPLG	2022-03-30 15:00:00	2022-05-12 10:00:00	1028	0.19	1026
509	AQWCWGQM	2022-08-05 10:00:00	2022-08-24 11:00:00	916	0	916
510	AQYQWJ3X	2022-08-05 10:00:00	2022-08-24 11:00:00	458	0	458
511	AR3XFKF4	2022-08-04 15:00:00	2022-08-24 11:00:00	477	0	477

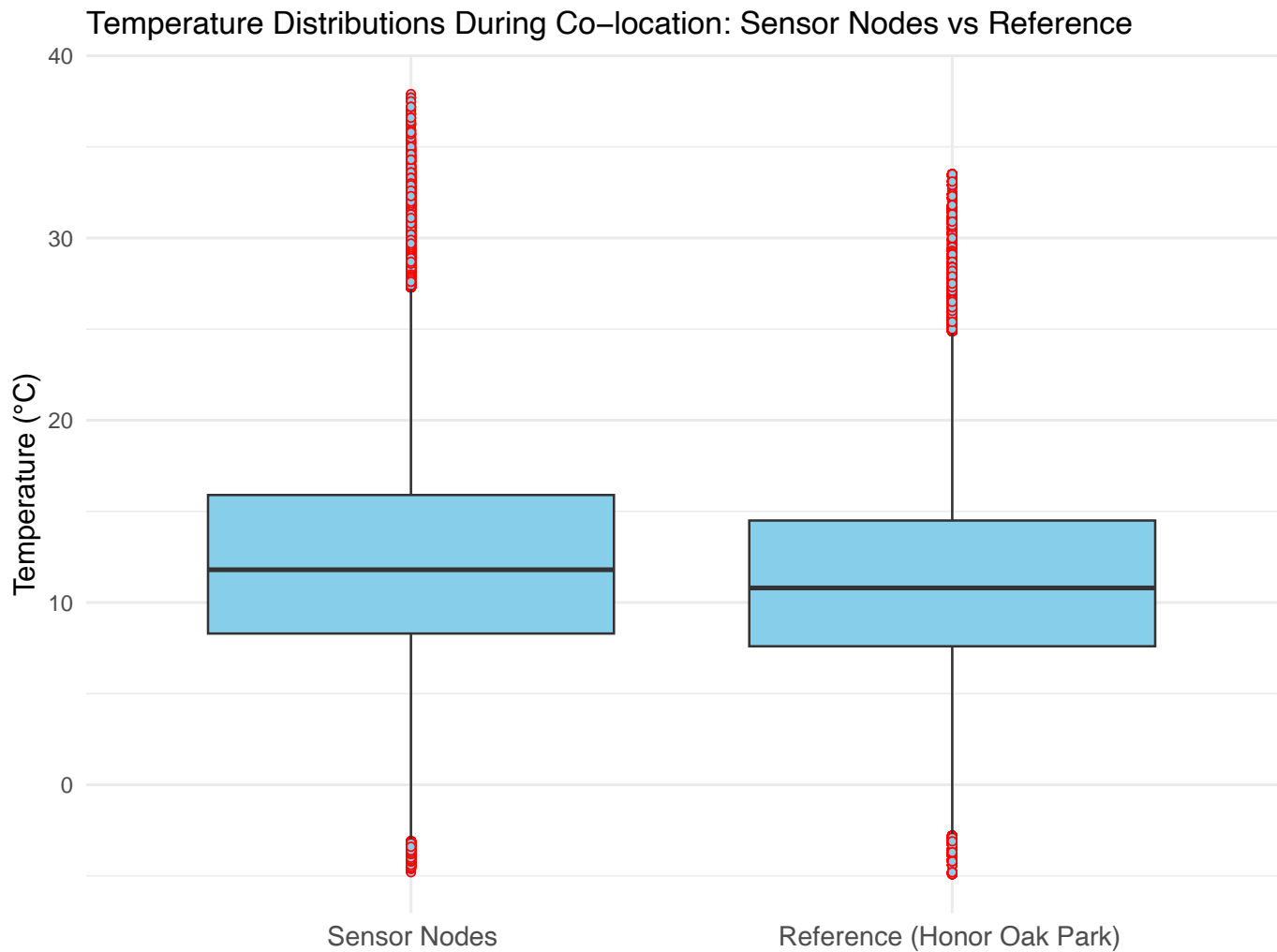
512	AR3YN796	2023-07-07 18:00:00	2023-07-25 12:00:00	427	0	427
513	AR6FL66F	2022-11-10 13:00:00	2022-11-28 12:00:00	432	0	432
514	AR6XFYVV	2024-11-08 19:00:00	2024-12-09 14:00:00	740	0	740
515	AR8J9CKL	2021-05-11 14:00:00	2021-06-23 12:00:00	1031	0.1	1030
516	AR9XTCKF	2022-12-22 15:00:00	2023-01-05 11:00:00	333	0	333
517	ARCXB36L	2021-08-24 12:00:00	2021-09-06 15:00:00	632	0	632
518	ARGRFFTH	2024-11-08 19:00:00	2024-12-09 14:00:00	740	0	740
519	ARHRPCF4	2022-12-22 13:00:00	2023-01-05 11:00:00	335	0	335
520	ARJPTY52	2022-03-08 16:00:00	2022-03-30 15:00:00	528	10.04	475
521	ARJZSSBZ	2021-02-10 13:00:00	2021-06-05 00:00:00	2748	9.53	2486
522	ARLHPK7N	2023-07-07 18:00:00	2023-07-25 12:00:00	427	0	427
523	ARLNHH6C	2022-08-04 15:00:00	2022-08-24 11:00:00	477	0	477
524	ARLVQ3FY	2021-04-16 14:00:00	2021-06-28 14:00:00	1753	0.06	1752
525	ARMK7VQV	2022-12-22 13:00:00	2023-01-05 11:00:00	335	0	335
526	ARMMMVY4X	2022-11-10 12:00:00	2022-11-28 12:00:00	433	0	433
527	ARMT3HVF	2023-01-05 16:00:00	2023-01-19 13:00:00	334	0	334
528	ARNC37XL	2022-08-04 15:00:00	2022-08-24 11:00:00	477	0	477
529	ARNCNJ7T	2023-01-05 13:00:00	2023-01-19 13:00:00	337	0	337
530	ARNP9HMK	2022-12-22 16:00:00	2023-01-05 11:00:00	332	0	332
531	AROCWY6W	2023-07-07 14:00:00	2023-07-25 12:00:00	431	0	431
532	ARQLJWFF	2023-08-11 18:00:00	2023-09-04 12:00:00	595	0	595
533	ARTLT64C	2022-12-22 13:00:00	2023-01-05 11:00:00	335	0	335
534	ARVN4402	2021-11-10 15:00:00	2021-11-24 12:00:00	668	0	668
535	ARVNNX64	2024-02-28 13:00:00	2024-05-15 12:00:00	1848	0	1848
536	ARWMCHVM	2024-11-08 19:00:00	2024-12-09 14:00:00	740	0	740
537	ARXJKG7S	2021-10-01 15:00:00	2021-10-13 13:00:00	287	0	287
538	ARY39ZDQ	2022-02-04 13:00:00	2022-03-08 11:00:00	767	0	767
539	AS7M2WNZ	2021-08-24 13:00:00	2021-09-08 15:00:00	315	0	315
540	AS87QWLB	2021-11-10 14:00:00	2021-11-24 12:00:00	335	0	335
541	AS8C020M	2021-03-26 13:00:00	2021-06-05 00:00:00	1692	0.06	1691
542	AS9SXGRD	2021-05-11 14:00:00	2021-07-12 12:00:00	1487	0.07	1486
543	ASFHV9FQ	2022-03-08 16:00:00	2022-03-30 15:00:00	528	10.04	475
544	ASFQTKJ1	2021-04-16 13:00:00	2021-06-05 00:00:00	1188	0.08	1187
545	ASKCV14G	2022-02-04 14:00:00	2022-03-08 11:00:00	766	0	766
546	ASN66MZC	2022-02-04 17:00:00	2022-03-08 11:00:00	763	0	763
547	ASYGC6ST	2021-03-26 13:00:00	2021-06-05 00:00:00	1692	0.06	1691
548	ATOVGXQK	2022-03-08 13:00:00	2022-03-30 15:00:00	531	9.98	478
549	AT4HQ3LW	2023-07-25 15:00:00	2023-08-11 12:00:00	406	0	406
550	AT5WBWQG	2021-01-27 14:00:00	2021-02-15 19:00:00	462	21.86	361
551	AT7G8FKK	2021-10-13 15:00:00	2021-10-27 14:00:00	336	0.6	334
552	AT9FHYNXN	2022-10-19 13:00:00	2022-11-10 12:00:00	528	0.19	527
553	AT9GB7LJ	2021-02-10 15:00:00	2021-05-28 15:00:00	2569	10.16	2308
554	AT9GNXQ	2022-12-22 14:00:00	2023-01-05 11:00:00	334	0	334
555	ATCYDDH5	2021-10-13 17:00:00	2021-10-27 14:00:00	334	0.6	332
556	ATFPWVMP	2022-03-30 16:00:00	2022-05-12 10:00:00	1027	0.19	1025
557	ATG2LNX2	2021-04-16 16:00:00	2021-06-29 14:00:00	1775	0.06	1774
558	ATJ4G3MW	2022-12-22 12:00:00	2023-01-05 11:00:00	336	0	336
559	ATK6YRXJ	2020-12-22 07:00:00	2021-02-12 13:00:00	1255	1.83	1232
560	ATKT6Y7H	2024-11-08 19:00:00	2024-12-09 14:00:00	740	0	740
561	ATLZD29K	2021-11-10 14:00:00	2021-12-14 13:00:00	816	0	816
562	ATNGMQKJ	2023-01-05 14:00:00	2023-01-19 13:00:00	336	0	336
563	ATP66LMB	2022-02-04 16:00:00	2022-03-08 11:00:00	764	0	764
564	ATQRX81P	2021-04-16 13:00:00	2021-04-29 11:00:00	311	0	311
565	ATVPLGMH	2022-12-22 16:00:00	2023-01-05 11:00:00	332	0	332
566	ATWQPKVL	2022-08-04 15:00:00	2022-08-24 11:00:00	477	0	477
567	ATXXJ33N	2022-10-19 13:00:00	2022-11-10 12:00:00	528	0.19	527
568	ATXYJ3XW	2022-12-22 12:00:00	2023-01-05 11:00:00	336	0	336

569	ATY3N3D1	2022-02-04 17:00:00	2022-03-08 11:00:00	763	0	763
570	ATYKZCJ2	2021-11-10 15:00:00	2021-11-24 12:00:00	334	0	334
571	AV0RFJMP	2021-10-27 14:00:00	2021-11-10 13:00:00	336	0	336
572	AV332V37	2021-04-16 16:00:00	2021-06-05 00:00:00	1185	0.08	1184
573	AV3RR0Z3	2022-03-08 16:00:00	2022-03-30 15:00:00	528	10.04	475
574	AV6HGQNM	2023-08-11 18:00:00	2023-09-05 12:00:00	595	0	595
575	AV6K61W9	2022-03-08 16:00:00	2022-03-30 15:00:00	531	9.98	478
576	AV7WP379	2022-12-22 12:00:00	2023-01-05 11:00:00	336	0	336
577	AV9N9QCC	2024-11-08 19:00:00	2024-12-09 14:00:00	740	0	740
578	AVBSWHR5	2021-10-14 11:00:00	2021-12-14 14:00:00	2936	0.14	2932
579	AVCRX42Z	2021-03-25 18:00:00	2021-06-05 00:00:00	1711	0.06	1710
580	AVDJXR6T	2021-10-01 14:00:00	2021-10-13 13:00:00	288	0	288
581	AVDS0L1T	2022-03-08 13:00:00	2022-03-30 15:00:00	531	9.98	478
582	AVFXBYL1	2022-03-08 16:00:00	2022-03-30 15:00:00	528	10.04	475
583	AVG1P63Y	2020-12-18 07:00:00	2021-01-22 09:00:00	843	0	843
584	AVG6JFNT	2023-11-24 19:00:00	2024-02-27 11:00:00	2273	0	2273
585	AVG7CHRF	2023-11-24 19:00:00	2024-02-27 11:00:00	2273	0	2273
586	AVGT7Q7V	2024-02-28 12:00:00	2024-05-15 12:00:00	1849	0	1849
587	AVHCHXHT	2021-10-01 14:00:00	2021-10-13 13:00:00	288	0	288
588	AVKQXW9R	2023-07-07 12:00:00	2023-07-25 12:00:00	433	0	433
589	AVM2VSZG	2021-10-13 17:00:00	2021-10-27 14:00:00	334	0.6	332
590	AVM9Q74X	2022-11-10 12:00:00	2022-11-28 12:00:00	433	0	433
591	AVMCM749	2024-02-28 12:00:00	2024-05-15 12:00:00	1849	0	1849
592	AVN9LFXL	2022-12-22 16:00:00	2023-01-05 11:00:00	332	0	332
593	AVNP9KCQ	2024-02-28 12:00:00	2024-05-15 12:00:00	1849	0	1849
594	AVPN29JP	2020-12-18 07:00:00	2021-02-10 11:00:00	1301	0	1301
595	AVT36GP6	2022-12-22 12:00:00	2023-01-05 11:00:00	336	0	336
596	AVTX5XOC	2021-10-01 16:00:00	2021-10-13 13:00:00	286	0	286
597	AVW49VY4	2023-07-25 13:00:00	2023-08-11 12:00:00	408	0	408
598	AVWSJTQV	2021-10-13 17:00:00	2021-10-27 14:00:00	334	0.6	332
599	AVYRL6C6	2023-01-05 12:00:00	2023-01-19 13:00:00	338	0	338
600	AW2SZ3QV	2021-12-08 15:00:00	2022-02-04 12:00:00	1390	0	1390
601	AW3XY7YX	2022-11-10 12:00:00	2022-11-28 12:00:00	433	0	433
602	AW4M9YQ6	2023-07-25 12:00:00	2023-08-11 12:00:00	409	0	409
603	AW4RKNGN	2024-05-15 13:00:00	2024-06-26 11:00:00	1007	0	1007
604	AW4XQ66Y	2023-07-07 12:00:00	2023-07-25 12:00:00	433	0	433
605	AW6H6N9F	2022-10-19 17:00:00	2022-11-10 12:00:00	524	0.19	523
606	AW6HPPPR	2023-08-11 18:00:00	2023-09-05 12:00:00	595	0	595
607	AWC8LH4P	2022-02-04 13:00:00	2022-03-08 11:00:00	767	0	767
608	AWFJBQMS	2021-10-27 14:00:00	2021-11-10 13:00:00	336	0	336
609	AWHHV79C	2023-07-25 13:00:00	2023-08-11 12:00:00	408	0	408
610	AWJD9PVN	2022-02-04 16:00:00	2022-03-08 11:00:00	764	0	764
611	AWJZD9YQ	2022-08-04 15:00:00	2022-08-24 11:00:00	477	0	477
612	AWKJL7Y3	2023-08-11 18:00:00	2023-09-05 12:00:00	595	0	595
613	AWL6CVPT	2022-10-19 12:00:00	2022-11-10 12:00:00	529	0.19	528
614	AWM4179Y	2021-10-01 13:00:00	2021-10-13 13:00:00	289	0	289
615	AWIMGJ99F	2022-12-22 13:00:00	2023-01-05 11:00:00	335	0	335
616	AWQ8G2W4	2022-03-08 15:00:00	2022-03-30 15:00:00	529	10.02	476
617	AWR1PSML	2021-08-24 12:00:00	2021-09-06 15:00:00	316	0	316
618	AWTYCYJK	2021-04-16 14:00:00	2021-06-17 08:00:00	1483	0.07	1482
619	AX031PPQ	2021-04-16 13:00:00	2021-06-28 13:00:00	1753	0.06	1752
620	AX2HL288	2021-08-27 05:00:00	2021-09-30 16:00:00	828	0	828
621	AX3083FB	2021-08-24 14:00:00	2021-09-06 15:00:00	314	0	314
622	AX3PPGTC	2023-07-07 12:00:00	2023-07-25 12:00:00	433	0	433
623	AX58XMS7	2021-02-10 14:00:00	2021-06-05 00:00:00	2747	9.54	2485
624	AX944KZY	2021-04-16 14:00:00	2021-06-28 13:00:00	1752	0.06	1751
625	AXCK5M62	2022-03-08 15:00:00	2022-03-30 15:00:00	529	10.02	476

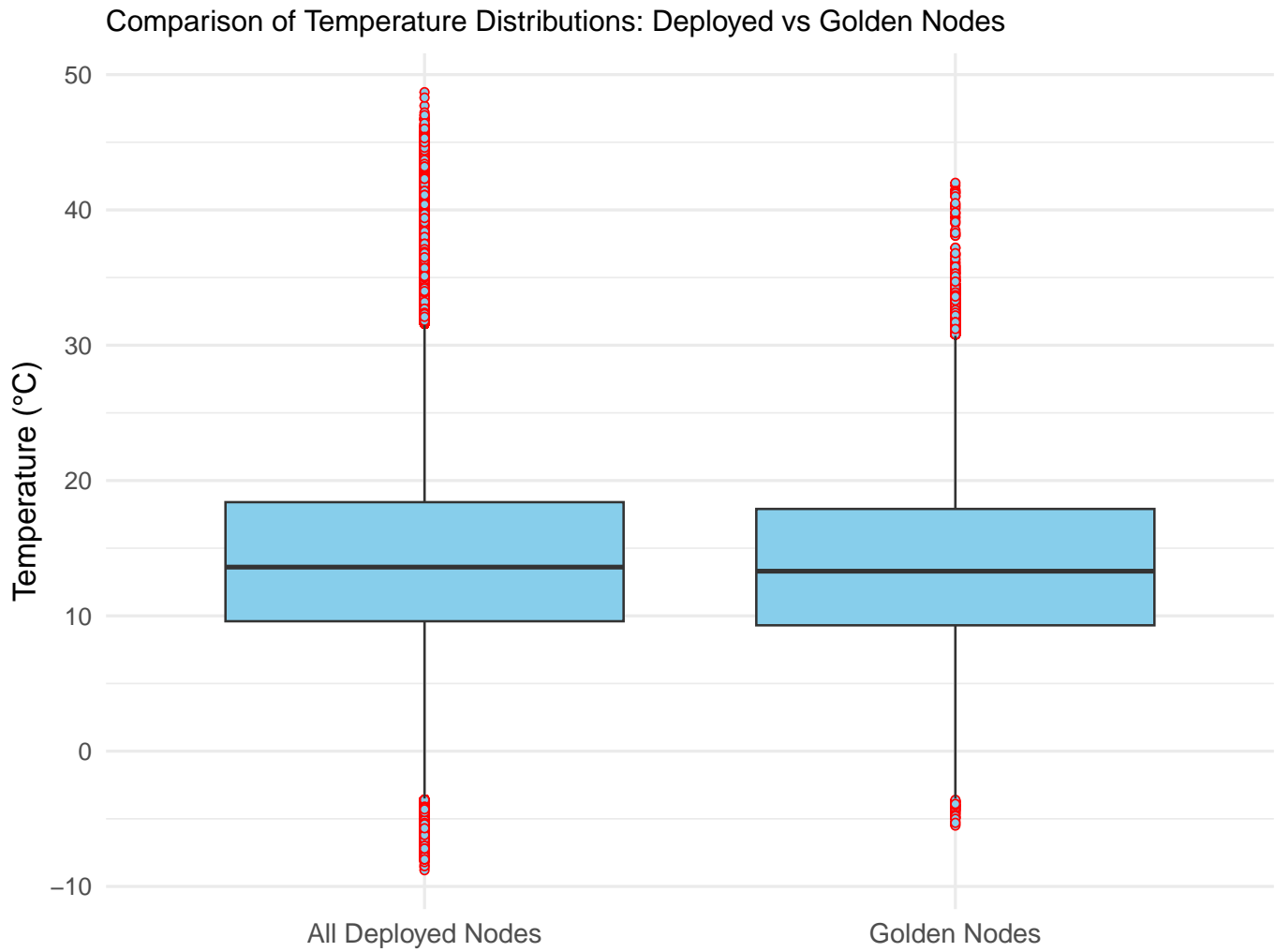
626	AXFPRRG4	2023-07-07 16:00:00	2023-07-25 12:00:00	429	0	429
627	AXGVNVWL	2022-12-22 16:00:00	2023-01-05 11:00:00	332	0	332
628	AXH9MYYQ	2023-07-25 12:00:00	2023-08-11 12:00:00	409	0	409
629	AXJFVKHR	2023-11-24 12:00:00	2024-04-01 00:00:00	3085	0	3085
630	AXLFQQLH	2022-12-22 14:00:00	2023-01-05 11:00:00	334	0	334
631	AXLVRPML	2022-08-05 10:00:00	2022-08-24 11:00:00	458	0	458
632	AXQGZCGM	2021-04-29 13:00:00	2021-05-24 17:00:00	605	0	605
633	AXR7TGKK	2021-05-11 15:00:00	2021-06-05 00:00:00	586	0.17	585
634	AXRJBZFR	2021-02-10 13:00:00	2021-06-05 00:00:00	2748	9.53	2486
635	AXSB57ZB	2021-10-13 17:00:00	2021-10-27 14:00:00	334	0.6	332
636	AXTQJYMN	2023-07-25 13:00:00	2023-08-11 12:00:00	408	0	408
637	AXTX9P7Y	2024-05-15 12:00:00	2024-06-26 11:00:00	1009	0	1009
638	AXX6C6RK	2022-12-22 14:00:00	2023-01-05 11:00:00	334	0	334
639	AXXFGMQH	2024-05-15 13:00:00	2024-06-26 11:00:00	1007	0	1007
640	AXXM3MGP	2023-08-11 18:00:00	2023-09-05 12:00:00	595	0	595
641	AY4JNFF7	2021-10-27 13:00:00	2021-11-10 13:00:00	674	0	674
642	AY57Z6BB	2021-10-27 14:00:00	2021-11-10 13:00:00	336	0	336
643	AY72DXZF	2023-11-24 12:00:00	2024-04-01 00:00:00	3085	0	3085
644	AY7R7FHK	2022-10-19 15:00:00	2022-11-10 12:00:00	526	0.19	525
645	AY9PGKC4	2022-10-19 15:00:00	2022-11-10 12:00:00	526	0.19	525
646	AYBQS9BS	2021-04-16 16:00:00	2021-06-01 00:00:00	1185	0.08	1184
647	AYFYZ07C	2021-02-10 12:00:00	2021-06-05 00:00:00	2749	9.53	2487
648	AYHMFY7F	2022-12-22 13:00:00	2023-01-05 11:00:00	335	0	335
649	AYJ3W4JH	2023-07-25 15:00:00	2023-08-11 12:00:00	406	0	406
650	AYJ7BKMD	2021-01-27 14:00:00	2021-02-18 15:00:00	530	31.89	361
651	AYJNYT97	2021-04-16 16:00:00	2021-06-05 00:00:00	1185	0.08	1184
652	AYJWH21M	2021-10-13 16:00:00	2021-10-27 14:00:00	335	0.6	333
653	AYKP6PFQ	2023-08-11 12:00:00	2023-09-05 12:00:00	601	0	601
654	AYM6LQ7Y	2022-08-05 10:00:00	2022-08-24 11:00:00	458	0	458
655	AYNZZT1P	2021-10-27 13:00:00	2021-11-10 13:00:00	337	0	337
656	AYP1BBCX	2021-01-27 14:00:00	2021-02-15 19:00:00	462	21.86	361
657	AYP3MKLN	2023-07-07 19:00:00	2023-07-25 12:00:00	426	0	426
658	AYQD3N97	2021-04-16 16:00:00	2021-06-05 00:00:00	1185	0.08	1184
659	AYR5C2BH	2022-02-04 16:00:00	2022-03-08 11:00:00	764	0	764
660	AYWC6QNH	2024-05-15 12:00:00	2024-06-26 11:00:00	1008	0	1008
661	AYWR6907	2022-03-08 16:00:00	2022-03-30 15:00:00	528	10.04	475
662	AYX0GP8K	2021-04-29 12:00:00	2021-05-24 17:00:00	606	0	606
663	AYXM0D4R	2021-04-16 14:00:00	2021-06-25 16:00:00	1683	0.06	1682
664	AYXMCMNX	2022-10-19 12:00:00	2022-11-10 12:00:00	529	0.19	528
665	AYYD87P4	2021-02-10 14:00:00	2021-06-05 00:00:00	2747	9.54	2485
666	AZ28QML0	2021-04-29 13:00:00	2021-06-09 20:00:00	992	0.1	991
667	AZ7SFYDD	2021-11-10 15:00:00	2021-11-24 12:00:00	334	0	334
668	AZDN7DL8	2021-04-29 12:00:00	2021-05-24 17:00:00	606	0	606
669	AZFP8PN2K	2021-10-27 13:00:00	2021-11-10 13:00:00	337	0	337
670	AZL3QS7L	2021-10-01 15:00:00	2021-10-13 13:00:00	287	0	287
671	AZLN7YLV	2021-07-12 12:00:00	2021-08-24 13:00:00	1034	0	1034
672	AZNVQGSZ	2021-03-24 14:00:00	2021-06-05 00:00:00	1739	0.06	1738
673	AZQ36BDH	2021-04-16 15:00:00	2021-06-05 00:00:00	1186	0.08	1185
674	AZRHPXZT	2021-10-13 16:00:00	2021-10-27 14:00:00	335	0.6	333
675	AZSH19QB	2021-10-27 13:00:00	2021-11-10 13:00:00	337	0	337
676	AZT4NLJ4	2021-10-01 14:00:00	2021-10-13 13:00:00	288	0	288
677	AZTJ378M	2021-05-11 14:00:00	2021-06-05 00:00:00	587	0.17	586
678	AZVV18KY	2021-08-24 15:00:00	2021-09-06 15:00:00	313	0	313
679	AZX1NK85	2021-04-29 12:00:00	2021-06-09 20:00:00	993	0.1	992



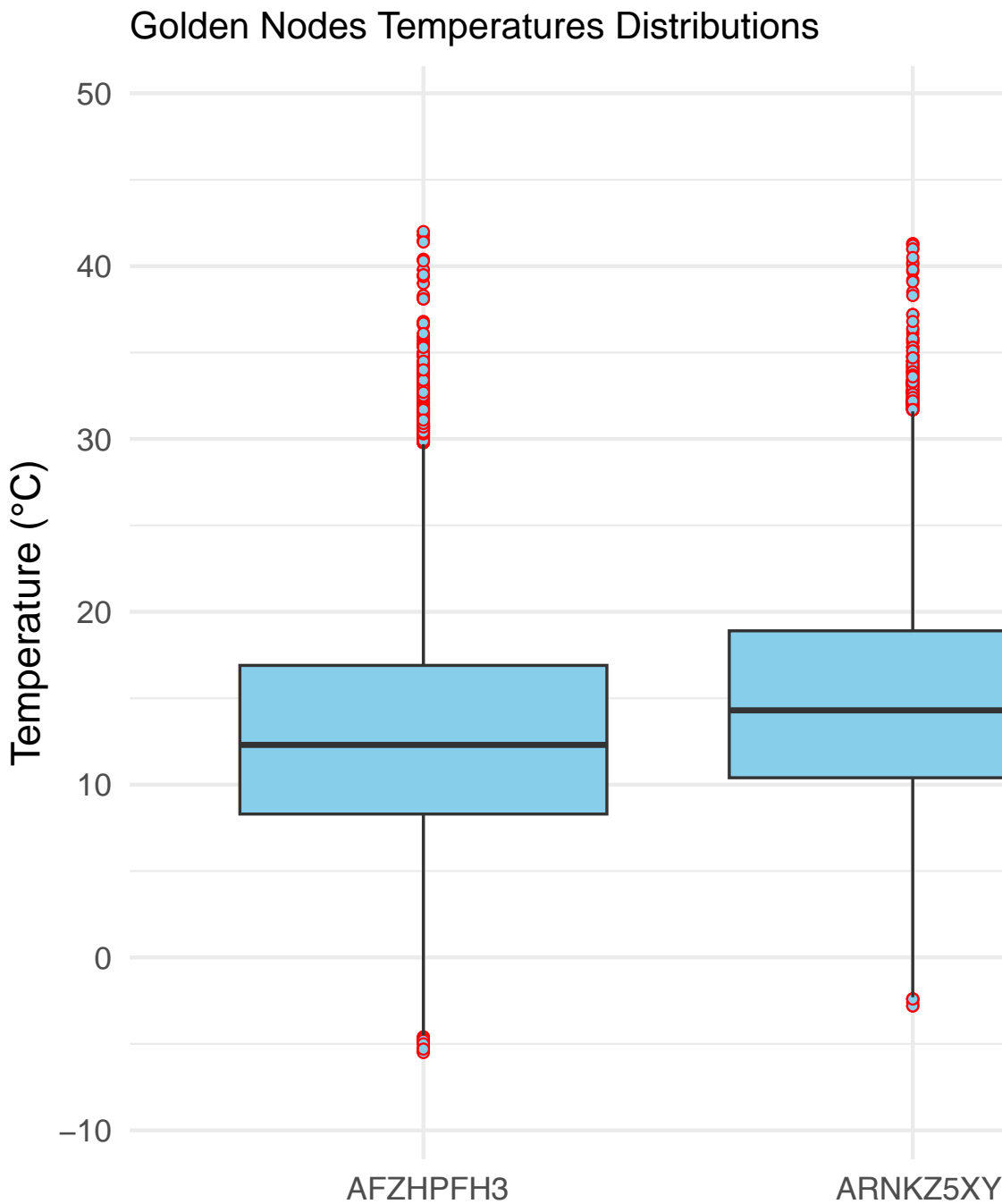
Supplementary Material 2. Boxplot showing the distribution of the number of sensor-recorded temperature observations per node that had a corresponding reference temperature measurement during the co-location period.



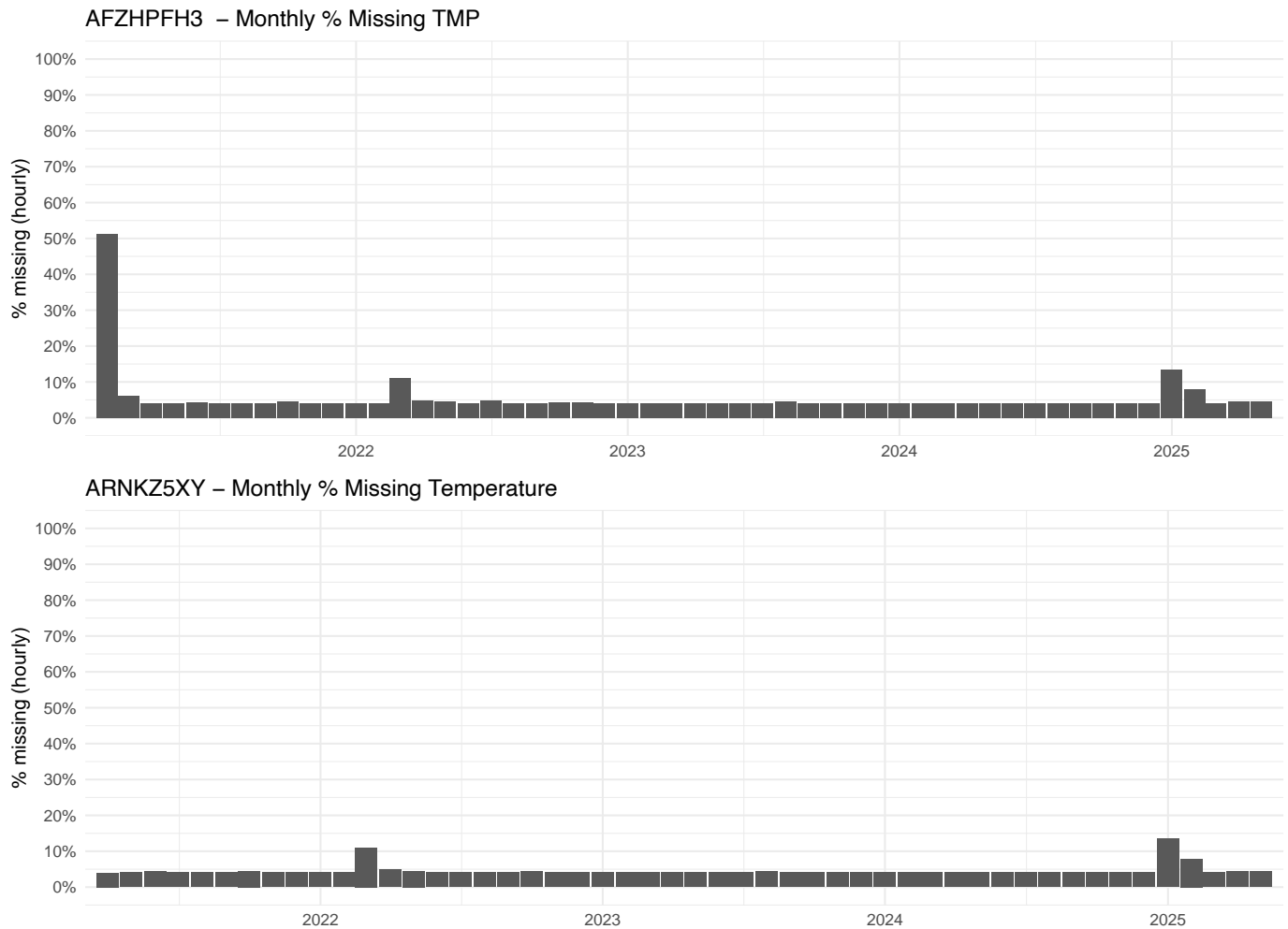
Supplementary Material 3. Boxplot comparing the distribution of sensor-recorded temperatures with reference temperatures from Honor Oak Park during co-location periods.



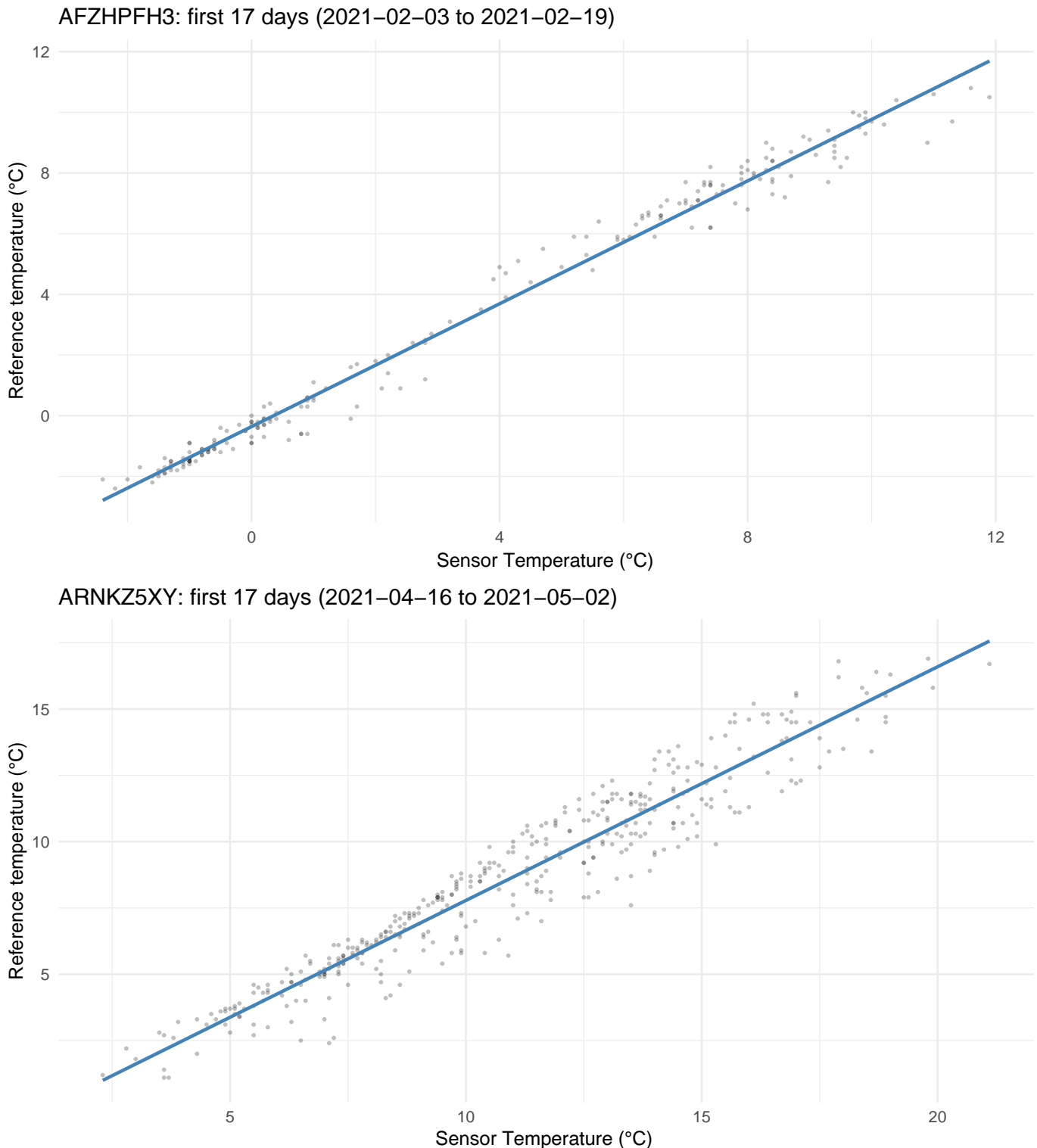
Supplementary Material 4. Boxplots comparing the distribution of sensor node temperatures across all deployed nodes and for the two golden nodes between 2021 and 2025.



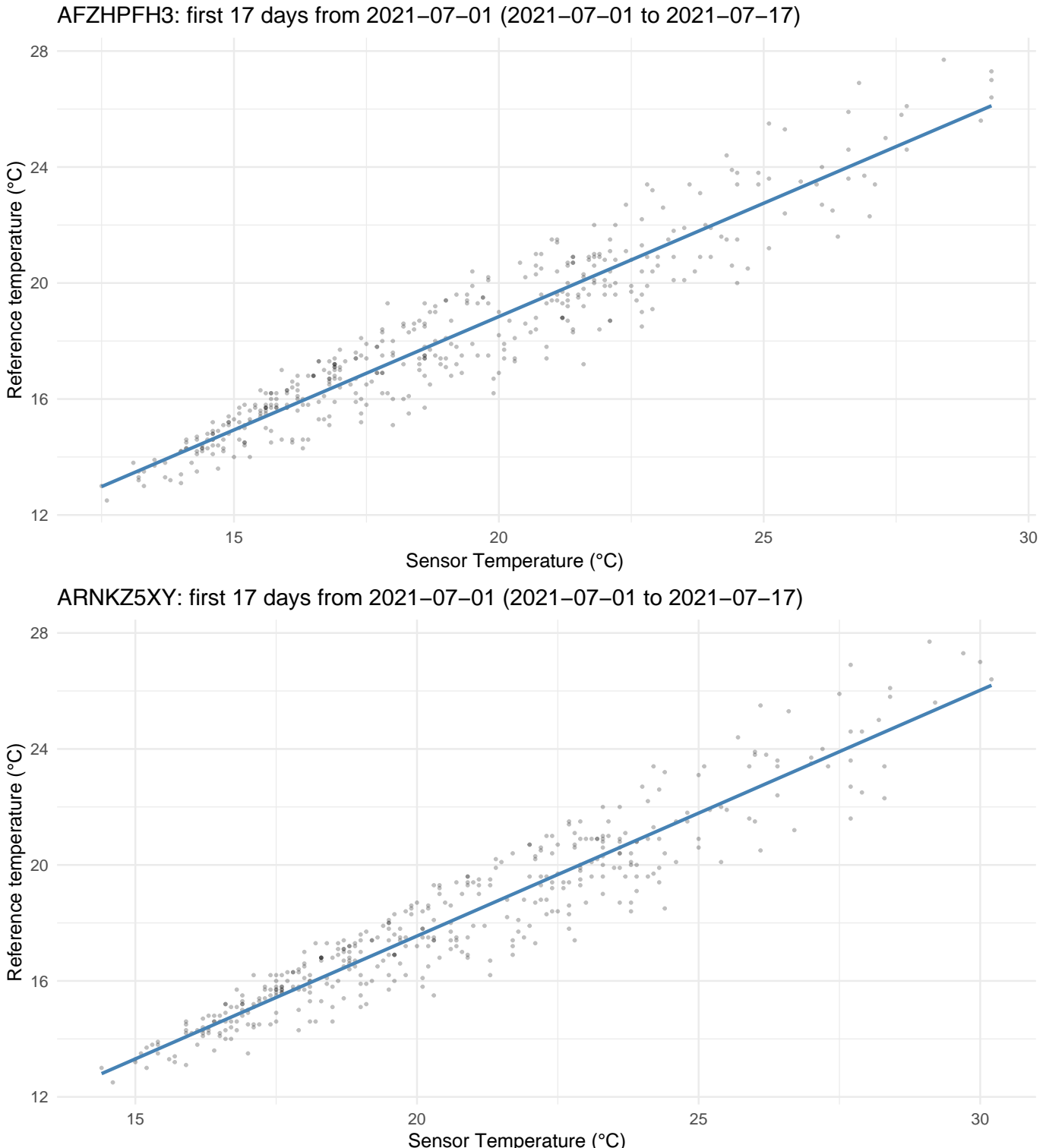
Supplementary Material 5. Boxplots comparing the temperature distributions of each golden node throughout the study period between 2021 and 2025.



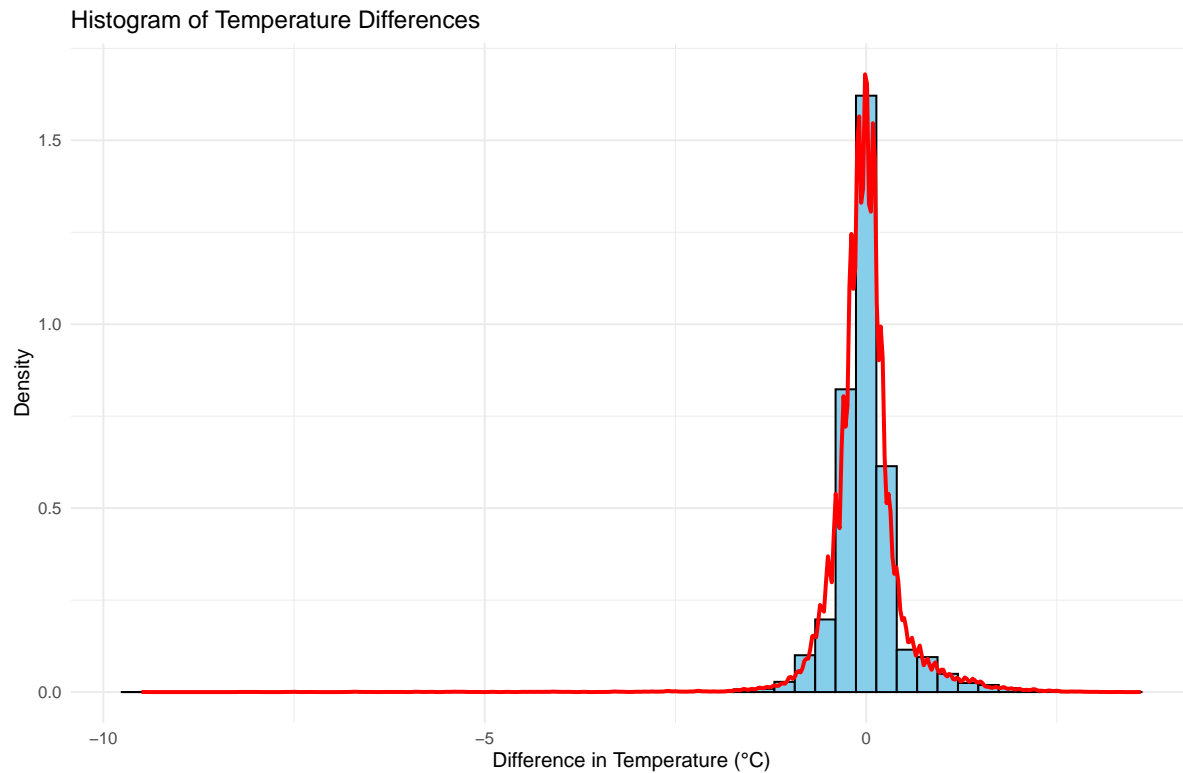
Supplementary Material 6. Monthly percentage of missing hourly temperature observations for the two golden nodes, AFZHPFH3 and ARNKZ5XY, over their deployment periods.



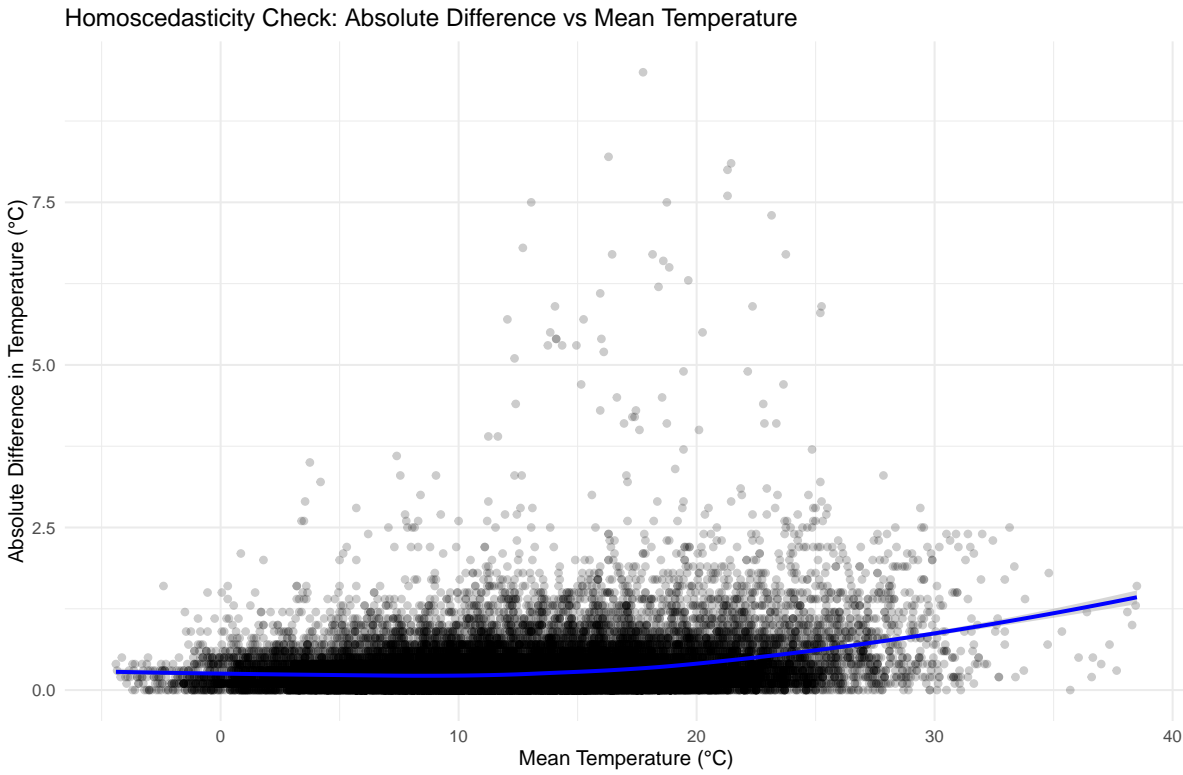
Supplementary Material 7: Scatter plots of sensor temperature against reference temperature from Honor Oak Park for the first 17 days of the co-location period for each golden node. Linear regression lines fitted to the data are shown.



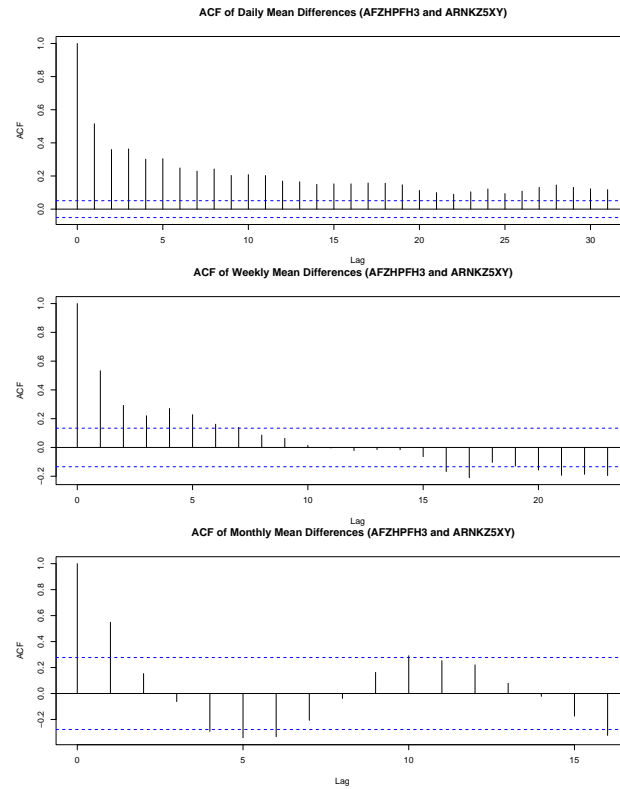
Supplementary Material 8: Scatter plots of sensor temperature against reference temperature from Honor Oak Park from the 1st of July to the 17th of July 2021 for each golden node. Linear regression lines fitted to the data are shown.



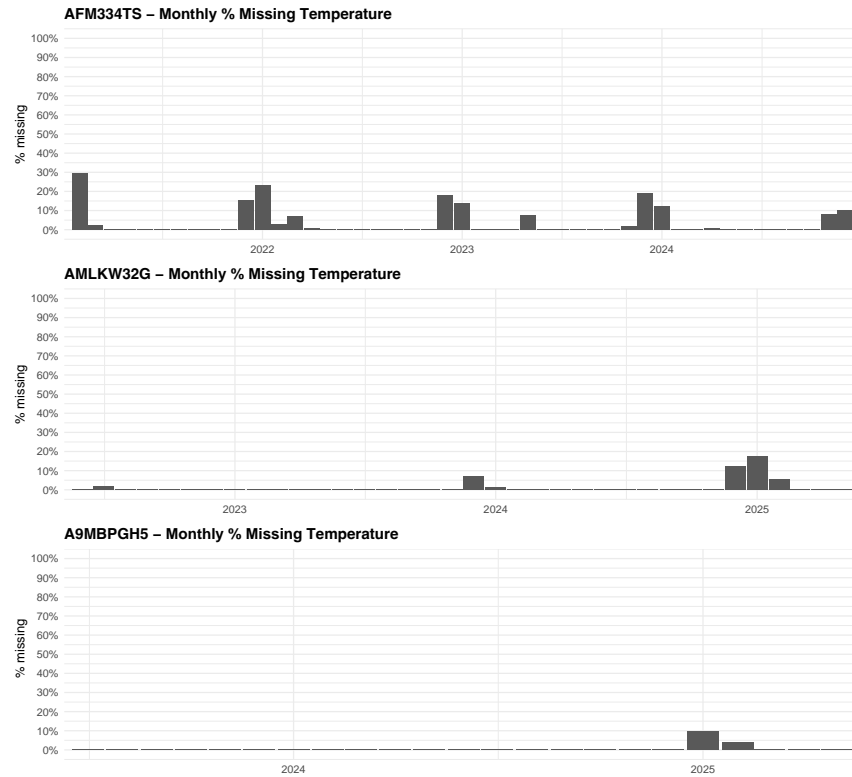
Supplementary Material 9: Histogram displaying the difference in temperature between the two golden nodes, AFZHPFH3 and ARNKZ5XY.



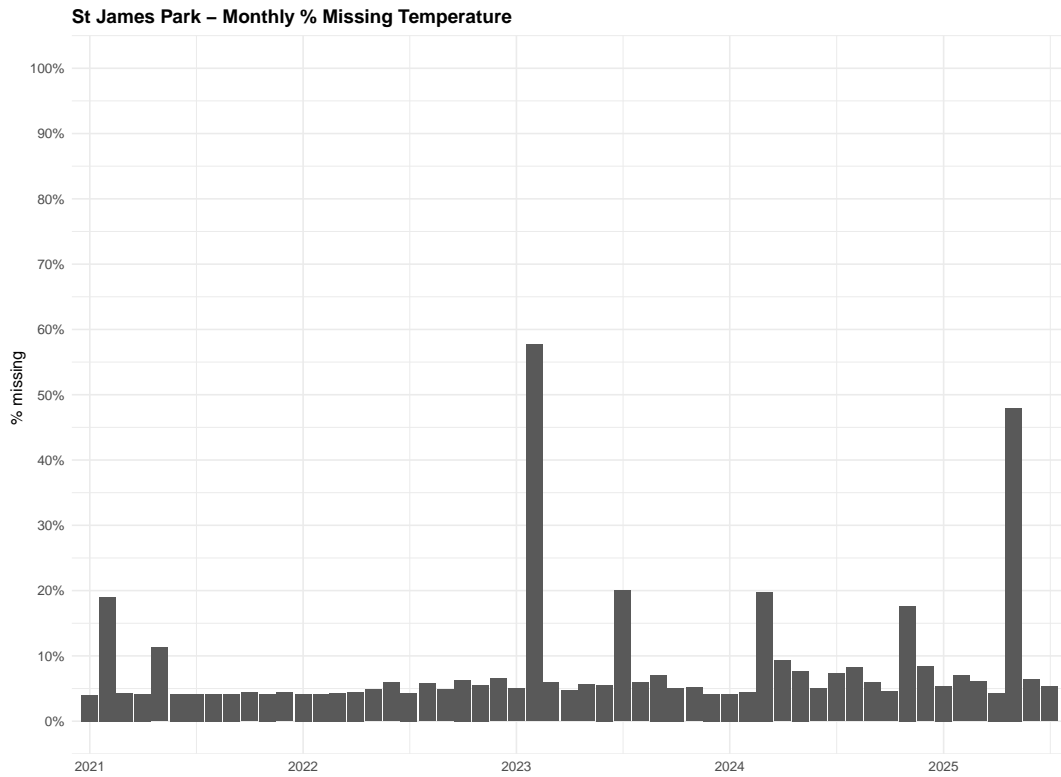
Supplementary Material 10: Homoscedasticity check for agreement between two golden nodes, AFZHPFH3 and ARNKZ5XY. Absolute temperature differences between the two golden nodes are plotted against their mean temperature, with a fitted loess smoothing line (blue) to visualise patterns in variance across the temperature range.



Supplementary Material 11: Autocorrelation Function (ACF) of mean temperature differences between golden nodes at daily, weekly, and monthly aggregation levels.

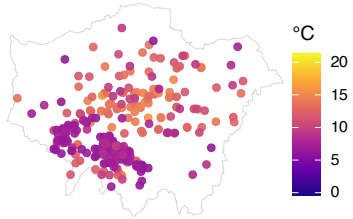


Supplementary Material 12: Monthly percentage of missing hourly temperature observations for the three sensor nodes (AFM334TS, AMLKW32G, and A9MBPGH5) used in external validation, across their respective deployment periods.

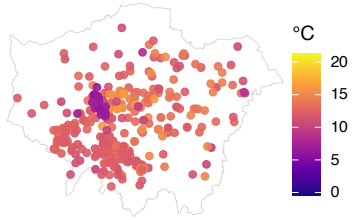


Supplementary Material 13: Monthly percentage of missing hourly temperature data for the St James Park reference site.

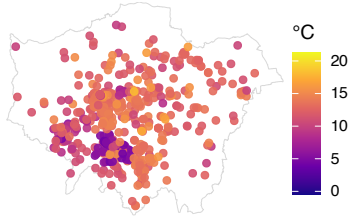
Yearly Average Temperature — 2021



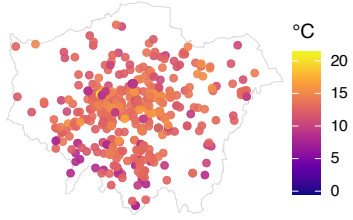
Yearly Average Temperature — 2022



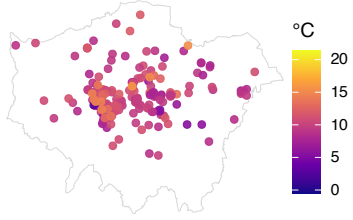
Yearly Average Temperature — 2023



Yearly Average Temperature — 2024



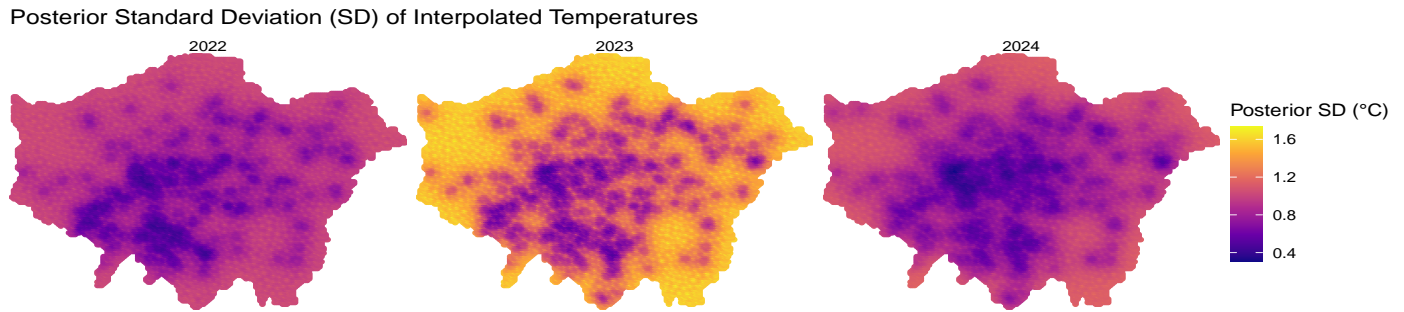
Yearly Average Temperature — 2025



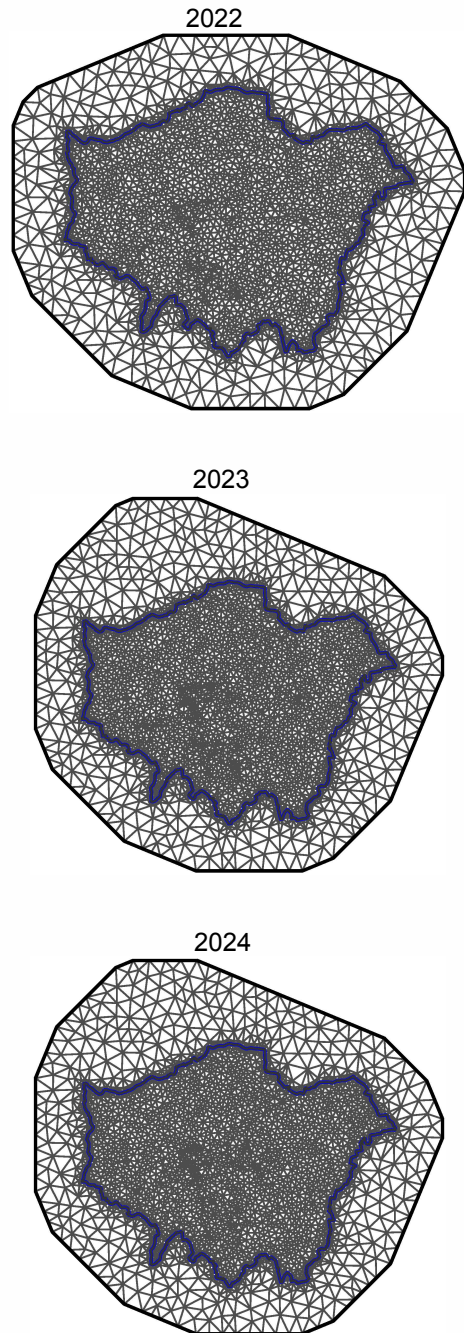
Supplementary Material 14: Yearly averaged per node calibrated temperatures maps between 2021 and 2025 without interpolation.

Supplementary Material 15: Deviance Information Criterion (DIC) and Watanabe-Akaike Information Criterion (WAIC), for the yearly SPDE models, between 2022 and 2024.

Year	DIC	WAIC
2022	1318	1321
2023	2170	2165
2024	1802	1930



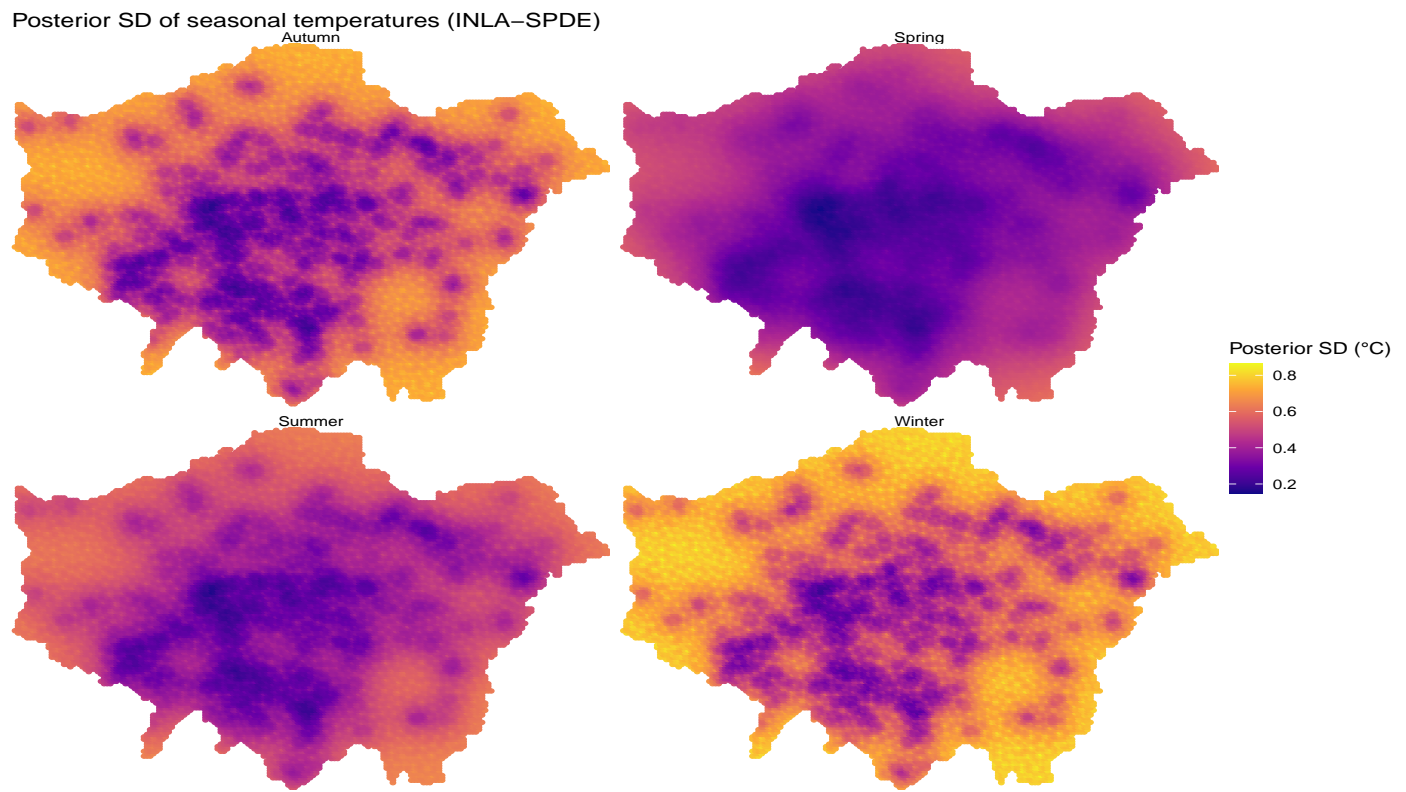
Supplementary Material 16: Posterior standard deviation maps of interpolated yearly mean temperatures between 2022 and 2024. Warmer colours indicate higher posterior uncertainty in the temperature estimates, reflecting areas with lower sensor density or greater variability in the underlying field.



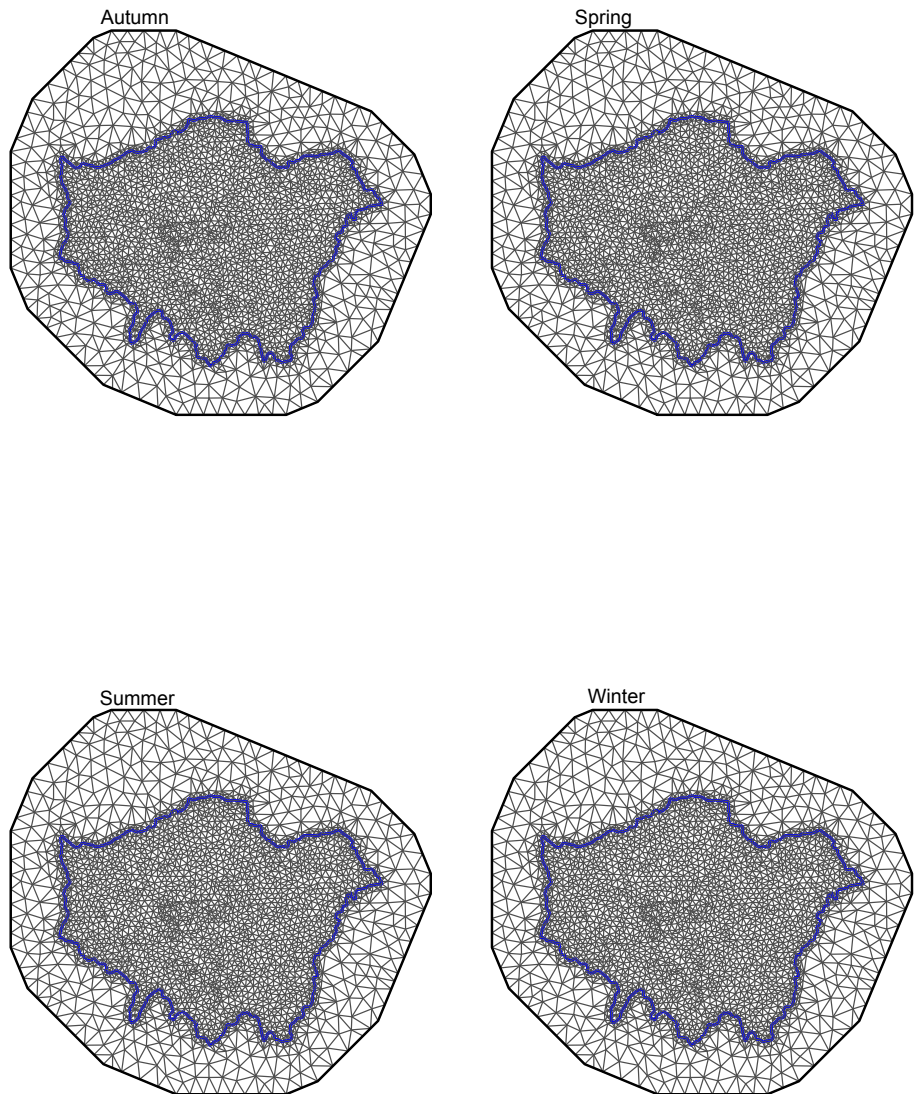
Supplementary Material 17: Stochastic Partial Differential Equation meshes constructed for 2022, 2023, and 2024, showing the triangulated representation of the spatial domain used in Bayesian interpolation.

Supplementary Material 18: Deviance Information Criterion (DIC) and Watanabe-Akaike Information Criterion (WAIC), for seasonal spatial models, between 2021 and 2025.

Season	DIC	WAIC
Winter	1712	1715
Spring	1785	1792
Summer	1519	1532
Autumn	1417	1435



Supplementary Material 19: Posterior standard deviation maps of interpolated seasonal temperatures between 2021 and 2025. Warmer colours indicate higher posterior uncertainty in the temperature estimates, reflecting areas with lower sensor density or greater variability in the underlying field.



Supplementary Material 20: Stochastic Partial Differential Equation meshes constructed for each season between 2021 and 2025, showing the triangulated representation of the spatial domain used in Bayesian interpolation.